DESIGN OF EFFICIENT ALGORITHMS FOR BRAIN DISEASE IDENTIFICATION AND CLASSIFICATION

A Thesis Submitted
in Partial Fulfillment of the Requirements
for the Degree of

DOCTOR OF PHILOSOPHY

in

Electronics and Communication Engineering

by

Kavita Bhatt

(Roll No. 2K20/PHDEC/510)

Under the Supervision of

Dr. N. Jayanthi and Dr. Manjeet Kumar

Delhi Technological University

DELHI TECHNOLOGICAL UNIVERSITY

(Formerly Delhi College of Engineering)

Shahbad Daulatpur, Main Bawana Road, Delhi 110042, India.

February, 2026

DELHI TECHNOLOGICAL UNIVERSITY
(Formerly Delhi College of Engineering)
Shahbad Daulatpur, Main Bawana Road, Delhi-42

CANDIDATE'S DECLARATION

I **Kavita Bhatt** hereby certify that the work which is being presented in the thesis entitled **"Design of Efficient Algorithms for Brain Disease Identification and Classification"** in partial fulfillment of the requirements for the award of the Degree of Doctor of Philosophy, submitted in the Department of Electronics and Communication Engineering, Delhi Technological University, is an authentic record of my own work carried out during the period from January 2021 to September 2025 under the supervision of **Dr. N. Jayanthi**, Associate Professor in the Department of Electronics and Communication Engineering, Delhi Technological University, Delhi, India, and **Dr. Manjeet Kumar**, Assistant Professor in the Department of Electronics and Communication Engineering, Delhi Technological University, Delhi, India. The matter presented in the thesis has not been submitted by me for the award of any other degree of this or any other institute.

Candidate's Signature
Kavita Bhatt

This is to certify that the student has incorporated all the corrections suggested by the examiner in the thesis, and the statement made by the student is correct to the best of our knowledge.

Signature of Supervisor(s) **Signature of External Examiner**

DELHI TECHNOLOGICAL UNIVERSITY
(Formerly Delhi College of Engineering)
Shahbad Daulatpur, Main Bawana Road, Delhi-42

CERTIFICATE BY THE SUPERVISOR

Certified that **Kavita Bhatt** (2K20/PHDEC/510) has carried out her research work presented in this thesis entitled **"Design of Efficient Algorithms for Brain Disease Identification and Classification"** for the award of Doctor of Philosophy from Department of Electronics and Communication Engineering, Delhi Technological University, Delhi, under my supervision. The thesis embodies results of original work, and studies are carried out by the student herself and the contents of the synopsis do not form the basis for the award of any other degree to the candidate or to anybody else from this or any other University/Institution.

Dr. N. Jayanthi
Associate Professor
Department of ECE
Delhi Technological University

Dr. Manjeet Kumar
Assistant Professor
Department of ECE
Delhi Technological University

Date:

Acknowledgement

I supremely thank the Almighty God for the opportunities and abilities he has endowed in me that have enabled me to come this far.

I take the opportunity to humbly submit my heartfelt appreciation to my supervisors **Dr. N. Jayanthi** and **Dr. Manjeet Kumar** from the Department of Electronics and Communication Engineering, Delhi Technological University, Delhi, for steering me this far in the scholarly research work. Their immense contribution and rare dedication in providing much-needed guidance are worth much honor. They are my continual source of inspiration in the face of monumental challenges in research. They are academic giants under whose watch I am molded into a seasoned research scholar. They have been of great help in the successful completion of my research work. I extend my sincere regards to **Prof. Neeta Pandey**, HOD ECE department, for her constant support. I wish to express my gratitude towards the DRC chairperson and the esteemed faculty members for their valuable time and efforts throughout this journey.

My appreciation also goes to my colleagues and lab mates in the Department of Electronics and Communication Engineering, Delhi Technological University, Delhi, for their constant encouragement and motivation. I also thank my family for their continual prayers, encouragement, and support throughout this research period.

Kavita Bhatt

ABSTRACT

Brain diseases encompass a wide range of disorders, such as neurodegenerative disorders, cerebrovascular disorders, neurodevelopmental disorders, seizure disorders, and brain tumors that impair cognitive, motor, and behavioral functions of human beings. Among these disorders, neurodegenerative disorders are considered the most prominent brain disorders due to their progressive nature, which leads to a continuous decline in cognitive, motor, and behavioral functions. Unlike other brain disorders, these disorders worsen over time and currently have no definitive cure, which makes them a major challenge for healthcare systems worldwide.

Alzheimer's Disease (AD) and Parkinson's Disease (PD) are the two most prevalent neurodegenerative disorders, affecting millions of people worldwide and imposing substantial social and economic burdens. AD primarily causes progressive memory loss and cognitive decline due to amyloid plaques and tau tangles, while PD mainly leads to motor and non-motor symptoms like tremor, rigidity, and bradykinesia due to dopaminergic neuron loss and Lewy bodies. Both AD and PD are irreversible, progressive neurodegenerative disorders with no particular cure, leading to a gradual decline in cognitive and motor functions and a significant deterioration in patients' quality of life. Although the progression of these disorders can be slowed with certain medications and therapies. Early and accurate diagnosis is essential to provide timely and effective interventions. Therefore, early detection is crucial for ensuring the much-needed care and support for patients.

This thesis aims to develop optimized, automated frameworks for early and accurate identification of these brain diseases using biomedical signal analysis and advanced machine learning (ML) and deep learning (DL) techniques. Biosignaling modalities such as electroencephalography (EEG), gait analysis, and speech pattern assessment are cost-efficient and non-invasive in nature. These signals capture essential physiological and behavioral markers reflecting neurological impairments. These

modalities enable the detection of subtle abnormalities in brain activity, motor function, and communication, providing valuable insights into the onset and progression of neurodegenerative disorders without the need for invasive or expensive clinical procedures.

Biomedical signals are typically high-dimensional and contain redundant or irrelevant information. Identifying the most informative and discriminative features is crucial to improving classification accuracy and computational efficiency. Hence, feature selection-driven optimization models are developed for brain disease detection. For PD, EEG datasets obtained from OpenNeuro are analyzed using statistical and ensemble-based feature selection methods. The Kruskal–Wallis test and Extra tree classifier (ETC) are used to select the most discriminative EEG features. Additionally, a two-stage PD detection framework is developed to enhance diagnostic accuracy and computational efficiency. Initially, an ETC-based feature selection is employed to obtain the most relevant and discriminative speech features while eliminating redundant or non-informative ones. These optimal feature subsets effectively reduced dimensionality and improved the model's ability to capture meaningful variations associated with PD. To address the issue of class imbalance commonly observed in biomedical datasets, the synthetic minority oversampling technique is applied to generate synthetic samples for the minority class. This ensured balanced training data and prevented bias toward the majority class. Then, a stacked ensemble model is employed for classification, which leverages the complementary strengths of individual classifiers. The proposed two-stage framework significantly improved classification performance for PD detection using speech signals.

Identifying the most affected brain regions and corresponding EEG channels is crucial for achieving accurate diagnosis and meaningful neuroscientific interpretation in AD. AD causes progressive neurodegeneration that disrupts neuronal connectivity and alters the brain's rhythmic activity patterns. These abnormalities are not uniformly distributed but are concentrated in specific cortical areas. Therefore, it is essential to analyze EEG signals across multiple lobes: frontal, temporal, parietal, and occipital lobes to identify the dominant brain regions and EEG channels most influenced by

the disease. Identifying these regions enhances the interpretability of ML models, strengthens the physiological validity of classification outcomes, and supports targeted clinical assessments for early and precise AD diagnosis. For this purposes, a Fourier decomposition and Hilbert transform-based EEG signal analysis (FHESA) method is developed. The FHESA method integrates the Fourier Decomposition Method (FDM) and Hilbert Transform (HT) to extract meaningful features from the EEG signal for efficient classification and brain region analysis. The FHESA method aims to efficiently analyze the EEG data to identify the important brain regions vulnerable to AD, and to assess the impact of various EEG channels for the timely and early detection of AD.

The accurate detection and classification of neurological disorders is one of the most challenging tasks due to the overlapping clinical symptoms and shared pathological characteristics of diseases such as AD and Frontotemporal dementia (FTD). Both disorders lead to progressive cognitive decline and behavioral impairments, often resulting in misdiagnosis and delayed treatment. Traditional diagnostic methods heavily rely on neuroimaging and clinical assessments, which are both time-consuming and costly. Moreover, biomedical signals such as EEG exhibit non-linear and non-stationary behavior, making it difficult for conventional machine learning methods to capture underlying temporal–spectral dependencies. Therefore, there is a need for an algorithm that can extract robust, noise-invariant, and discriminative features capable of representing complex brain activities associated with different neurological conditions. To address this, wavelet scattering transform-based dementia identification and classification (WavDemNet) is proposed. The model leverages the wavelet scattering transform (WST) to extract robust, noise-invariant features that capture essential time-frequency characteristics and a 1-D convolutional neural network (CNN) to learn discriminative patterns for accurate identification and classification of brain diseases.

Manual analysis of biomedical signals is time-consuming. To assist clinicians in real-time decision-making, there is a requirement to develop automated and efficient algorithms that can process signals, extract optimal features, and accurately classify neurological disorders with minimal human intervention. For this purpose, an

automated algorithmic framework is developed for the early diagnosis of PD. The high-resolution superlet transform (SLT) technique is utilized to obtain the time-frequency representation (TFRs) of the signal. SLT employs multiple wavelets to achieve higher TF resolution while being less leaky than a single wavelet, which makes it more sustainable to apply to non-stationary signals. In order to identify PD and assess the PD severity rate, the TFRs are fed into deep neural network (DNN) models as input. This approach eliminates the need of additional handcrafted feature extraction methods, as the DNNs are capable of automatically learning hierarchical and discriminative patterns from the TFRs. This model captures signal variations associated with PD progression and results in accurate detection and severity assessment.

List of Publications

SCI/SCIE Indexed Journal Papers Accepted/Published

1. **K. Bhatt**, N. Jayanthi, and M. Kumar, "High-resolution superlet transform based techniques for parkinson's disease detection using speech signal," *Applied Acoustics*, vol. 214, pp. 109657, 2023. https://doi.org/10.1016/j.apacoust.2023.109657
2. **K. Bhatt**, N. Jayanthi, and M. Kumar, "A two-stage ensemble approach for the analysis of parkinson's disease using speech signals," *Multimedia Tools and Applications*, pp. 1–21, 2025. https://doi.org/10.1007/s11042-025-20599-3
3. **K. Bhatt**, N. Jayanthi, and M. Kumar, "FHESA: Fourier decomposition and hilbert transform based EEG signal analysis for alzheimer's disease detection," *Physical and Engineering Sciences in Medicine*, pp. 1–16, 2025. https://doi.org/10.1007/s13246-025-01644-9

Papers Submitted in SCI/SCIE Indexed Journals

1. **K. Bhatt**, N. Jayanthi, and M. Kumar, "A robust super resolution time-frequency framework for parkinson's disease severity assessment using gait signal,"*Computer Methods and Programs in Biomedicine.*
2. **K. Bhatt**, N. Jayanthi, and M. Kumar, "WavDemNet: Wavelet scattering transform-based dementia identification and classification network," *IEEE Sensors Journal*.
3. **K. Bhatt**, N. Jayanthi, and M. Kumar, "A structured analysis of artificial intelligence based computational techniques for parkinson's disease prediction and diagnosis: architecture, methodology, challenges and opportunities," *Neurocomputing.*

Scopus Indexed International Conference Papers

1. **K. Bhatt**, N. Jayanthi, and M. Kumar, "Machine learning based optimal feature selection technique for early stage prediction of alzheimer's disease," in *2023 Third International Conference on Secure Cyber Computing and Communication (ICSCCC)*, pp. 715–719, IEEE, 2023. https://doi.org/10.1109/ICSCCC58608.2023.10176873
2. **K. Bhatt**, N. Jayanthi, and M. Kumar, "Automatic detection of parkinson's disease using eeg signals: A machine learning approach," in *2024 IEEE International Conference on Interdisciplinary Approaches in Technology and Management for Social Innovation (IATMSI),* vol. 2, pp. 1–6, IEEE, 2024. https://doi.org/10.1109/IATMSI60426.2024.10503404

Contents

List of Figures

List of Tables

List of Abbreviations

AD	Alzheimer's Disease
PD	Parkinson's Disease
ML	Machine Learning
DL	Deep Learning
AI	Artificial Intelligence
EEG	Electroencephalography
ETC	Extra Tree Classifier
SMOTE	Synthetic Minority Oversampling Technique
FDM	Fourier Decomposition Method
HT	Hilbert transform
FTD	Frontotemporal Dementia and Classification Network
WST	Wavelet Scattering Transform
CNN	Convolutional Neural Network
SLT	Superlet Transform
TFR	Time-Frequency Representaion
DNN	Deep Neural Network
MCI	Mild Cognitive Impairment
DBS	Deep Brain Stimulation
MRI	Magnetic Resonance Imaging
CT	Computed Tomography
fMRI	Functional MRI
PET	Positron Emission Tomograph

DaTscan	Dopamine Transporter Scan
CSF	Cerebrospinal Fluid
ADNI	Alzheimer's Disease Neuroimaging Initiative
HC	Healthy Control
OASIS	Open Access Series of Imaging Studies
AIBL	Australian Imaging, Biomarkers, and Lifestyle Study of Ageing
PPMI	Parkinson's Progression Markers Initiative
UPDRS	Unified Parkinson's Disease Rating Scale
H&Y	Hoehn and Yahr Scale
PaHaw	PD Handwriting Dataset
TP	True Positive
FN	True Negative
FP	False Positive
TN	False Negative
AUC	Aree Under the Curve
ROC	Receiver Operating Characteristic
MCC	Matthew's Correlation Coefficient
MSE	Mean Squared Error
RMSE	Root Mean Squared Error
G-mean	Geometric-mean
LOSO	Leave-One-Subject-Out
FTD	Frontotemporal Dementia
DCT	Discrete Cosine Transform
MFCC	Mel-frequency Cepstral Coefficients
LPC	Linear Prediction Coefficients

HHT	Hilbert Hung Transform
TQWT	Tunable Q-factor Wavelet Transform
STFT	Short Time Fourier Transform;
CWT	Continuous Wavelet Transform
EMD	Empirical Mode Decomposition
VMD	Variational Mode Decomposition
ROI	Region of Interest
HOG	Histogram of Oriented Gradients
ICA	Independent Component Analysis
mRMR	Minimum Redundancy Maximum Relevance
PCA	Principal Component Analysis
PCC	Pearson Correlation Coefficients
KWST	Kruskal-Wallis statistical test
LDA	Linear Discriminant Analysis
RFE	Recursive Feature Elimination
GA	Genetic Algorithm
ARD	Automatic Relevance Determination
SVM	Support Vector Machine
TSVM	Twin-Support Vector Machine
RF	Random Forest
MIRFE	Mutual Information Gain and RFE
KNN	K-Nearest Neighbor
NB	Naive Bayes
LR	Logistic Regression
DT	Decision Tree

XG-Boost	Extreme Gradient Boosting
GMM	Gaussian Mixture Model
ANN	Artificial Neural Network
CNN	Convolutional Neural Network
RNN	Recurrent Neural Network
MLP	Multi-Layer Perceptron
LSTM	Long Short-Term Memory
ELM	Extreme Learning Machine
GNN	Graph Neural Network
ViT	Vision Transformer
MMSE	Minimental State Examination
LSSVM	Least-Square Support Vector Machine
GCN	Graph Convolutional Neural Network
MASS	Multi-Agent Salp Swarm Algorithm
LDFSF	Local Dynamic Feature Selection Fusion Method
FIBFs	Fourier Intrinsic Band Functions
LINOEP	Linearly Independent Non-Orthogonal yet Energy Preserving
ANOVA	Analysis of Variance
DICE-net	Dual-Input Convolution Encoder Network
DEL	Deep Ensemble Learning
IEDCC	Instantaneous Energy Deviation Cepstral Coefficient
IMU	Inertial Measurement Unit
FOG	Freezing of Gait
VGRF	Vertical Ground Reaction Force
SPWVD	Smoothed Pseudo-Wigner–Ville Distribution
WSST	Wavelet Synchrosqueezed Transform

Chapter 1

Introduction

The human brain is termed as an extraordinarily complex network. From controlling the voluntary and involuntary actions to being the commanding center of the nervous system, the brain does all the work. The primary functional unit of the brain is called a neuron, which helps the brain to transmit signals from all the sensory organs, to and fro. The human brain consists of 100 billion neurons connected to over 100 trillion synapses. The functionality of the human brain can be affected by multiple brain diseases. Brain diseases encompass a wide spectrum, including vascular disorders such as stroke, cerebrovascular disorders, traumatic injuries, psychiatric conditions, and neurodegenerative disorders. Collectively, these diseases contribute significantly to global morbidity and mortality, posing major challenges for healthcare systems worldwide. Neurodegenerative disorders are especially concerning among the various types of brain diseases due to their progressive nature and lack of curative treatment. These disorders are characterized by the gradual loss of structure and function of neurons, ultimately leading to functional decline. Alzheimer's disease (AD) and Parkinson's disease (PD) are the two most prevalent neurodegenerative disorders, together affecting millions of people globally.

1.1 Alzheimer's Disease

Alzheimer's Disease (AD) is the most common progressive neurodegenerative disorder that impairs the cognitive abilities of older people, consequently impairing their quality of life. Since the incidence of AD is closely correlated with aging, it is anticipated to rise by 5 million cases per year. As the global population ages, the prevalence will double every 20 years [1]. The word "dementia" refers to a broad category of brain diseases that impair memory, emotional regulation, logical thinking,

and even decision-making. There are various kinds of dementia, including Parkinson's disease dementia, mixed dementia, vascular dementia, Lewy body dementia, and frontotemporal dementia [2]. Dementia is the fifth most common cause of mortality worldwide [3]. In 2020, over 50 million cases of dementia were reported. AD is the most common cause of dementia, accounting for 60 to 70% of all cases [4]. The number of Alzheimer's patients is expected to increase to 75 million by 2030 and 131 million by 2050 [5].

AD is primarily caused by platelet aggregation, excitotoxicity, oxidative stress, neurofibrillary tangle formation, amyloid plaque deposition, and neuroinflammation [6]. The most affected brain regions by AD include the hippocampus, neocortex, and amygdala [7]. It is considered that the symptoms of AD develop 20 years after the disorder first emerges. Memory loss and language difficulties are indications of nerve cell injury that affects thinking, memory, and learning, making the patient unable to carry out his regular tasks. Gradually, the person becomes bedridden and eventually leads to death [8]. As AD is a progressive condition, its symptoms can range from mild ones that have no impact on a patient's day-to-day activities to severe ones that cause total cognitive decline, reliance, and ultimately death. Mild Cognitive Impairment (MCI) is the term used to describe people in the early stages of AD, although not all MCI patients will go on to acquire AD. A person with MCI who can still carry out daily tasks has noticeable changes in their cognitive abilities that are visible to them and their family. Patients with MCI can be classified as MCI converters or MCI non-converters depending on whether they converted to AD within 18 months [9].

1.1.1 Risk Factor of AD

AD is influenced by both non-modifiable and modifiable risk factors. Non-modifiable risk factors include older age (the strongest predictor), the presence of the APOE4 allele, and a first-degree family history of the disease [10]. Modifiable risks include cardiovascular and metabolic conditions such as hypertension, diabetes, obesity, and high cholesterol, as well as lifestyle variables such as smoking, physical

inactivity, poor food, a lack of education, social isolation, depression, and sleep disorders [11]. Environmental exposures, such as air pollution and head injuries, also increase risk.

1.1.2 Treatment of AD

Currently, there is no cure for AD, and treatment mainly focuses on managing symptoms, slowing disease progression, and improving quality of life. There are currently only two classes of drugs approved to treat Alzheimer's disease (AD): cholinesterase inhibitors (including naturally derived, synthetic, and hybrid analogues) and NMDA (N-methyl-D-aspartate) receptor antagonists [12]. Cholinesterase inhibitors help improve memory and thinking by increasing acetylcholine levels in the brain, while NMDA antagonists, such as memantine, regulate glutamate activity to protect brain cells in moderate-to-severe stages of AD.

1.2 Parkinson's Disease

In 1817, James Parkinson gave the earliest description of PD in his research paper "An essay on the shaking palsy" [13]. The root cause of PD is the degradation of dopamine-producing nerve cells [14]. Dopamine is a crucial chemical messenger that carries signals between cells and controls behavior such as learning, movement, and emotion. Dopamine also controls motor movements. After Alzheimer's, PD is the most common neurological condition worldwide [15]. It is found that till the year 2015, around 6.9 million people are affected by PD and it is estimated that it will reach 14.2 million by the year 2040 [16]. PD is affecting around 1-2% of the worldwide population above the age of 65 years [17]. Compared to women, men are more susceptible to developing PD [18].

The symptoms of PD are categorized as motor and non-motor symptoms. Movement-related symptoms are known as motor symptoms. Bradykinesia, muscle rigidity, tremor, postural instability, movement disorders, and muscle shrinkage are examples of motor symptoms [19]. Whereas, PD symptoms that have nothing to do

with movement are known as non-motor symptoms. Sleep disturbance, autonomic dysfunction, hypokinetic dysarthria, and neurobehavioral changes are examples of non-motor symptoms [20]. Every individual experiences PD symptoms differently.

1.2.1 Risk Factor of PD

The biggest risk factor for PD seems to be age. With a man-to-woman risk ratio of 1.46, men are more at risk than women [21]. Among PD patients, women have a higher likelihood of suffering from anxiety. In men, tremors are more frequently linked to mild motor impairment and more profound striatal degeneration [22]. In the majority of cases, people who have no known familial history of PD are affected by the disease but some cases have an inheritance pattern involving some altered genes that could increase the risk of getting PD. The onset of PD may be influenced by environmental factors. Stress and head injuries are additional factors linked to an increased incidence of PD [21].

1.2.2 Treatment of PD

Since PD is an incurable, physiotherapies, medications, surgeries, and other interventions help to manage the symptoms of the disease and maintain a higher quality of life. Levodopa is a drug that is frequently prescribed to treat PD. It helps neuronal cells make more dopamine [23]. Dopamine agonists can potentially take the place of the dopamine that the brain normally produces. Levodopa can also be replaced with monoamine. Monoamine oxidase-B inhibitors include medications like selegiline and rasagiline. Deep brain stimulation (DBS)is frequently used by patients who are in severe stages and find that their drugs are not very effective [24]. DBS is a process in which the implantation of electrodes is performed surgically in the brain. The process helps send electrical pulses to keep the movement-controlling parts of the brain in stimulation.

1.3 Modalities used for Brain Disease Diagnosis

The accurate diagnosis of AD and PD is essential for timely intervention and effective disease management. Various diagnostic approaches have been developed to detect structural, functional, and behavioral changes associated with these neurodegenerative disorders. Figure 1.1 depicts the various approaches used for the diagnosis of AD and PD.

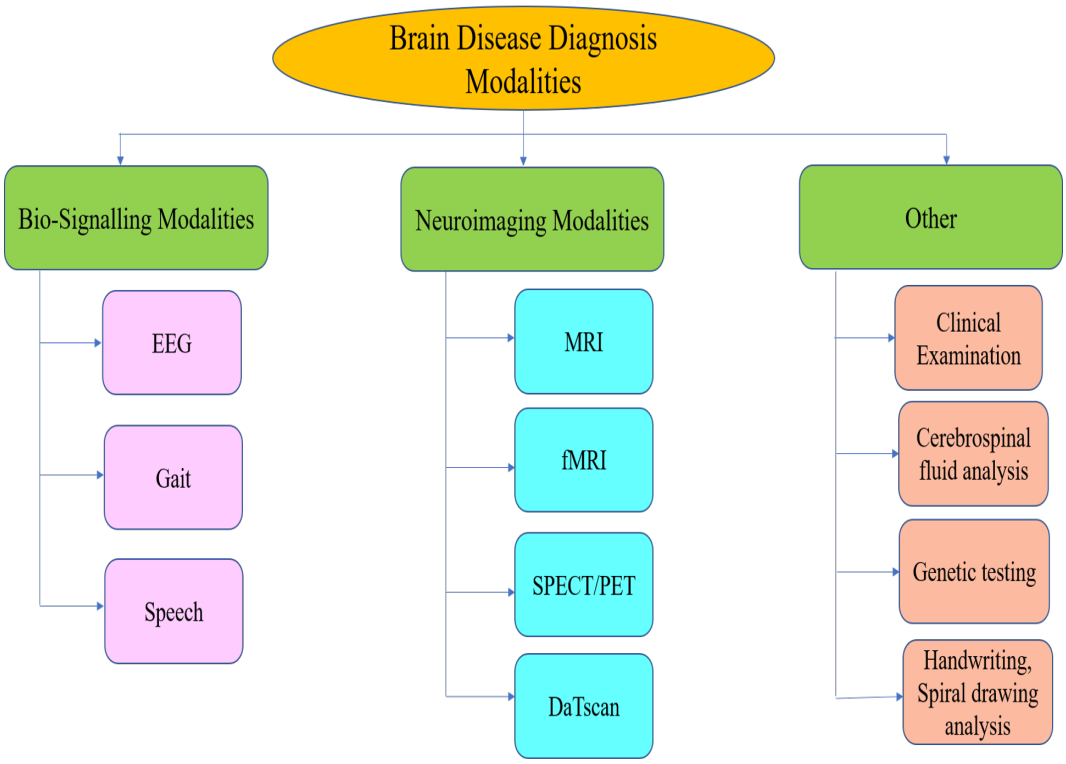

Figure 1.1: Modalities used for brain disease diagnosis

1.3.1 Bio-signaling Modalities

Several bio-signals have been used to diagnose AD and PD in the early stage. Among these modalities, EEG has been widely utilized to monitor the brain's electrical activity and detect functional changes associated with disease progression. EEG is used to record electrical activity. It is the most widely used technique to investigate the functional architecture of the brain and record brain activity. It is extensively utilized because it offers a higher temporal resolution, is safe, and is affordable. The EEG

signals have a non-linear and non-stationary nature. As a result, several nonlinear properties are extracted from EEG signals in order to detect mental disorders like PD, epilepsy, schizophrenia, and AD [25–27].

In addition to EEG, other bio-signals provide complementary diagnostic information. Gait patterns analyzed through wearable sensors or motion capture systems can reveal characteristic motor impairments, such as reduced stride length, increased variability, or asymmetry, which are early indicators of PD. Speech analysis has also shown promise, as changes in voice quality, articulation, and prosody can precede obvious motor symptoms in both AD and PD. It is found 90% of PD patients face vocal impairments [28]. These vocal impairments often appear in the early stages of the disease. Common symptoms include reduced loudness, vocal tremor, and breathiness while speaking.

1.3.2 Neuroimaging Modalities

Neuroimaging modalities are valuable tools for diagnosing and monitoring neurological disorders by revealing structural, functional, and molecular brain changes. The most commonly used neuroimaging modalities include magnetic resonance imaging (MRI), computed tomography (CT), positron emission tomography (PET), dopamine transporter scan (DaTscan), and functional MRI (fMRI) [29]. Brain MRI can be used for structural and functional imaging. It also reveals neurodegeneration-related patterns. Basal ganglia contours and shapes can be better seen with MRI's improved spatial resolution and higher contrast. The nigral structure of patients with PD exhibits neuroanatomical and pathophysiologic abnormalities that can be effectively described by a variety of MRI techniques [30]. It is a painless and safe diagnostic procedure that produces high-resolution 2D or 3D images of the brain stem using radio waves and a magnetic field.

fMRI measures brain activity by detecting changes in blood flow linked to neuronal activity. When a region is active, its blood supply increases, allowing fMRI to map functional areas with high spatial resolution [31]. PET is a functional imaging technique that visualizes brain activity using radioactive substances called radiotracers

[29]. A CT scan produces detailed X-ray images of the brain. MRI has largely replaced CT in the evaluation of many neurological conditions due to its superior soft-tissue contrast and detailed imaging capabilities. However, CT remains essential for the rapid assessment of acute conditions such as stroke, head trauma, and hemorrhage [29].

1.3.3 Other Modalities

Numerous biological markers are also employed in order to track the development of the condition and identify individuals who are at a high risk of developing AD and PD. Several studies have been conducted on the cerebrospinal fluid (CSF) biomarkers for PD to better understand this disease's pathophysiology and support the distinction between PD and healthy controls (HC) or other similar disorders [32]. In addition to these tests, handwriting evaluations are also conducted. Daily tasks like handwriting require a combination of cognitive, kinesthetic, and perceptual-motor skills. As a result, any alteration to certain brain regions has a direct impact on handwriting-related characteristics [33]. So, for early-stage prediction of AD and PD, numerous researchers have investigated the idea of leveraging handwriting changes as diagnostic measures. Table 1.1 depicts the evaluation of several brain disease diagnostic techniques.

Table 1.1: Evaluation of several brain disease diagnostic modalities

Modality	Advantages	Disadvantages	Image
EEG	Non-invasive, no radiation exposure, provides information about brain activity.	Affected by factors including background noise, movement, and eye blinking, poor signal-to-noise ratio, low sensitivity	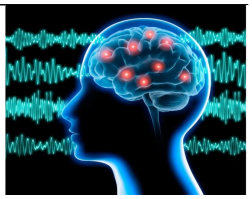
MRI	High-resolution brain image, non-invasive, no radiation exposure.	Noisy procedure, longer scan time, expensive, susceptible to movement artifacts, not for patients having metallic devices implanted.	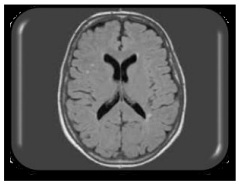

Modality	Advantages	Disadvantages	Image
fMRI	Provides detailed information about brain activity, identifies changes in the brain network and functional connectivity.	Expensive, time-consuming, less sensitive.	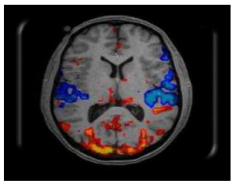
PET scan	Non-invasive, used in conjunction with other imaging modalities to provide a detailed view, provides detailed metabolic information.	Exposure to ionizing radiation, expensive, limited availability.	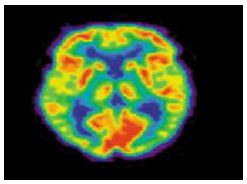
DaTscan	Non-invasive no radiation exposure, can provide a quantitative measure of dopamine transporter level in the brain.	Expensive, results can be affected by medication that alters dopamine levels.	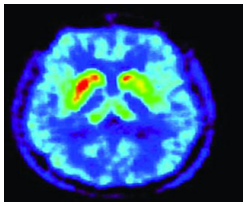
Speech	Non-invasive, low-cost diagnostic tool, easily recorded.	Lack of sensitivity, can be affected by noise.	
Handwritting/ Drawing	Simple, non-invasive, analyzed using various metrics such as speed, size, etc., can be used to monitor disease progression.	Can be affected by other factors such as fatigue, tremor, the side effect of medication, interpretation requires specialized training and expertise.	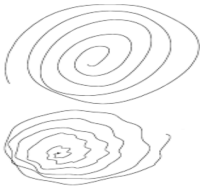

1.4 Benchmark Datasets for Brain Disease Identification and Classification

Brain disease identification and classification heavily rely on available datasets that provide diverse forms of data, such as neuroimaging, clinical assessments, genetic information, and physiological recordings. These datasets are essential for building

computational models that can assist in early diagnosis, monitor disease progression, and improve treatment planning. The following are some of the most widely used datasets.

1.4.1 Alzheimer's Disease Neuroimaging Initiative (ADNI)

ADNI is an association of universities and medical centers in the United States and Canada developed to provide open-source data sets to detect biomarkers and track the progression of AD [34]. It includes a variety of data types, including structural, functional, and molecular brain imaging, biofluid biomarkers, cognitive tests, genetic data, and demographic information. The ADNI study began in 2004 and is now in its fifth phase. The preceding phases were ADNI-1 (2004), ADNI-GO (2009), ADNI-2 (2011), ADNI-3 (2016), and ADNI-4 (2022 onwards). ADNI-1 comprises brain scans, genetic profiles, and biomarkers from blood and cerebrospinal fluid (CSF). The data set includes 200 HC, 400 people with MCI, and 200 AD patients. ADNI-GO investigates biomarkers for the early stages of AD and includes MRI images. It includes ADNI-1 participants and 200 new people with early mild cognitive impairment (eMCI). ADNI-2 is intended to identify biomarkers for predicting and analyzing cognitive deterioration. It comprises patients with both early MCI and late MCI and uses PET scans. The dataset includes the original ADNI-1 and ADNI-GO groups, as well as an additional 150 elderly HC, 100 early MCI participants, 150 late MCI participants, and 150 AD patients. ADNI-3 includes enhanced brain scans that reveal Tau protein tangles in the brain. The dataset contains participants from ADNI-1, ADNI-GO, and ADNI-2, as well as 133 elderly HC, 151 individuals with MCI, and 87 AD patients. ADNI 4 is the most recent phase of the program. It will include about 1500 patients aged 55 to 90 years. An estimated 500 to 750 new individuals will be registered along with ADNI-3 participants.

1.4.2 Open Access Series of Imaging Studies (OASIS)

OASIS is a collection of neuroimaging data sets that are freely accessible for research and analysis [35]. The initial OASIS set OASIS-1 is a cross-sectional

study of T1-weighted MRI scans of demented or non-demented individuals aged 18 to 96. The dataset includes a total of 416 people, out of which 20 were HC. OASIS-2 is a longitudinal study of 150 persons aged between 60 and 96 years. Each participant underwent three or four T1-weighted MRI images. The cohort contains 72 persons remaining non-demented, 64 initially demented, and 14 converting from non-demented to demented over the study period. OASIS-3 study includes MRI scans, PET scans, and clinical data from 1098 participants, out of which 605 were cognitively normal adults and 493 persons in various phases of cognitive impairment. The dataset contains a total of 2168 MRI scans and 1608 PET scans obtained during multiple visits. OASIS-4 is the latest release in this initiative. It contains 663 participants aged from 21 to 94 years. This clinical cohort was assessed for memory problems and dementia using clinical, CSF, neuropsychiatric, and neuroimaging methods.

1.4.3 DementiaBank

DementiaBank is a dedicated archive for speech and language data gathered from people with dementia, especially AD, as well as healthy control volunteers [36]. It is part of the larger TalkBank initiative, which aims to share structured language datasets for research and clinical application. DementiaBank is specifically designed to investigate linguistic changes associated with dementia, providing valuable resources for both scientific research and therapeutic treatment.

1.4.4 Australian Imaging, Biomarkers, and Lifestyle Study of Ageing (AIBL)

AIBL is a longitudinal study aimed at better understanding Alzheimer's disease and cognitive decline. It takes data from a diverse group of older persons, including those with healthy controls, MCI, and AD patients [37].

1.4.5 OpenNeuro

OpenNeuro is a free online platform for sharing and analysis of neuroimaging data. It contains a range of neuroimaging data, including PET scans, EEG, magnetoencephalography (MEG), and structural and functional MRI, focused on conditions like AD, cognitive disorders, and other neurological conditions. To enable maximum use, the uploaded datasets are made available to the public with minimal restrictions. OpenNeuro accepts datasets formatted according to the brain imaging data dtructure standard, which is a community-developed standard that attempts to encompass a wide range of neuroimaging data types while unifying metadata. The archive currently shares over 600 datasets, including data from over 20,000 people, spanning different species and measurement modalities, as well as a wide spectrum of characteristics. OpenNeuro aims to simplify the process of sharing raw imaging data, thereby enhancing opportunities for reuse and re-analysis [38].

1.4.6 UCI ML Reposatory

It is a set of databases, domain theories, and data generators used by the machine learning community to conduct empirical analyses of machine learning algorithms. There are around 600 datasets in the collection from a variety of fields, including business, social science, life science, etc. The most popular brain disease datasets from the UCI repository are:

- Parkinsons Data Set
- PD multiple Sound Recording Dataset
- Parkinsons Telemonitoring Data Set
- PD Spiral Drawings Using Digitized Graphics Tablet Dataset
- DARWIN

1.4.7 Kaggle Repository

Kaggle repository contains different types of data sets, which are publicly available. For AD and PD, different data sets, such as drawing and sketching, gate in PD, etc.,

are available.

1.4.8 Parkinson's Progression Markers Initiative (PPMI)

The Michael J. Fox Foundation founded PPMI in 2010 to help researchers find biomarkers associated with PD [39]. The study is a public-private partnership of academic researchers. PPMI has developed standardized processes for acquiring, transferring, and analyzing clinical, imaging, genetic, and biospecimen data that can track the progression of PD. The overall goal of PPMI is to investigate novel methods to establish longitudinal PD cohorts to examine PD progression markers that, individually or in combination, will rapidly demonstrate interval change in PD patients in comparison to HC or in sub-sets of PD patients.

1.4.9 Physionet

PhysioNet provides open-source software and free web access to substantial databases of recorded physiological signals. The National Institute of General Medical Sciences and the National institute of biomedical imaging and bioengineering both provide funding for PhysioNet [40]. The Gait data in PD includes 279 gait recordings from 93 PD patients and 73 HC. Eight sensors are inserted beneath each foot of each individual to measure force as a function of time. At 100 frames per second, the output of the 16 sensors is captured.

1.4.10 PC-GITA

The PC-GITA database includes voice recordings of HC and PD patients. The recordings were captured in a noise-free environment at a sampling rate of 44.1 kHz with a resolution of 16 bits [41]. This dataset includes 100 native Spanish speakers, out of which 50 were HC and the remaining 50 were PD patients. Each group had 25 men and 25 women. The recording process aims to analyze several tasks of the voice and speech of individuals with PD. These tasks were categorized into three categories: phonation, articulation, and prosody. All patients were diagnosed by

expert neurologists and classified according to the Unified Parkinson's Disease Rating Scale (UPDRS) and Hoehn and Yahr Scale (H&Y) scales. None of the HC showed any signs of PD or any other neurological disorder.

1.4.11 HandPD dataset

Pereira et al. [42] created this dataset. This dataset includes images taken from handwriting examinations of 92 people, 74 of them have PD, while the remaining 18 are healthy individuals. The dataset comprises 736 images, of which 368 are spiral images and 368 are meandering image drawings. Each drawing consists of 296 images drawn by the patient group and 72 images by the healthy group.

1.4.12 The NTUA Parkinson Dataset

This data was developed by the Intelligent Systems research group and the National Technical University of Athens, with the Department of Neurology, Georgios Gennimatas General Hospital, Athens, Greece [43]. The database consists of MRI scans, DaTscans, and clinical data of PD patients and healthy groups.

1.4.13 PD Handwriting Dataset (PaHaw)

This data collection includes the handwriting of 75 persons, of which 38 are healthy individuals and 37 have PD. Each subject completes eight distinct handwriting tasks, including drawing, writing cursive letters and sentences, and more. All of the participants in the sample are native Czech speakers, right-handed, and have at least 10 years of education. Wacom's Intuos digitizing tablet is used to capture the handwritten signals [44]. Table 1.2 describes the datasets for the identification and classification of brain diseases.

Table 1.2: Datasets for brain disease identification and classification

Disease	Dataset	Data Type	Availability
AD	ADNI [34]	Neuroimaging, blood biomarker, cognitive assessmen	Open access http://adni.loni.usc.edu/about/
	OASIS [35]	Neuroimaging, clinical assessment	Open access https://www.oasis-brains.org/
	Dementia Bank [36]	Audio recordings	https://dementia.talkbank.org/
	AIBL [37]	Neuroimaging, blood biomarker, cognitive assessment	Open access https://aibl.csiro.au/adni/index.html
	OpenNeuro [38]	EEG signals	Open access https://openneuro.org/
	UCI ML reposatory	Tabular data with features	Open access https://archive.ics.uci.edu/datasets
	Kaggle	Images, text, audio, and time-series data	Open access https://www.kaggle.com/datasets
PD	PPMI [39]	Imaging, biological, and clinical data	Open access https://www.ppmi-info.org/access-data-specimens/data
	PhysioNet [40]	Gait	Open access https://physionet.org/about/database/
	PC- GITA [41]	Speech signals	On request
	HandPD [42]	Drawing	Open access http://wwwp.fc.unesp.br/%7Epapa/pub/datasets/Handpd/
	NTUA [43]	MRI, DaTscans, and clinical data	Open access https://github.com/ails-lab/ntua-parkinson-dataset
	PaHaw [44]	Handwriting and drawing	https://bdalab.utko.fekt.vut.cz/

1.5 Performance Metrics

The performance metrics are used to evaluate the effectiveness and reliability of brain disease identification and classification models by quantitatively characterizing how well predicted outputs align with ground-truth clinical labels. These metrics provide an objective basis for measuring the predictive capability of a model, highlighting its strengths and weaknesses under different diagnostic conditions. Since a single metric cannot fully capture the complexity of classification performance, particularly in medical applications where class imbalance and clinical risks must be considered. Multiple measures are typically employed in combination. The most commonly used metrics in this domain, defined below. Each metric captures a distinct aspect of model behavior and contributes to a more comprehensive evaluation of diagnostic performance.

(i) *Confusion matrix:* The model's output for a classification purpose is often evaluated using a confusion matrix. The count values sum up how many of the real class's assumptions are true and how many are incorrect. Table 1.3 illustrates the confusion matrix.

Table 1.3: Confusion matrix of predicted and actual values for brain disease detection and classification model

Actual	**Predicted**	
	Positive	**Negative**
Positive	TP	FN
Negative	FP	TN

True Positive (TP) refers to patients who are correctly identified as having the brain disease, while True Negative (TN) refers to healthy individuals accurately recognized as not having brain disease. False Positive (FP) describes healthy individuals who are mistakenly classified as having brain disease, and False Negative (FN) refers to patients who are incorrectly classified as healthy.

(ii) *Accuracy (A_c):* It is the simplest performance indicator that indicates the proportion of accurate predictions provided by the classification model. It indicates the frequency of correct classifications made by the classifier.

$$A_c = \frac{TP+TN}{TP+FP+TN+FN} \tag{1.1}$$

(iii) *Sensitivity (S_n):* It is the ratio of classified true positive patients to all patients by the classification model. It is also known as the true positive rate or recall.

$$S_n = \frac{TP}{TP+FN} \tag{1.2}$$

(iv) *Specificity (S_p):* It showcases a report on those who are healthy and were predicted the same by the model. It is also known as the false positive rate.

$$S_p = \frac{TN}{TN+FP} \tag{1.3}$$

(v) *Precision (P_r):* It is also known as a predictive positive value defined as the quality of a successful prediction generated by the model. It can be calculated by dividing the total number of positive predictions by the percentage of positively predicted classes.

$$P_r = \frac{TP}{TP+FP} \tag{1.4}$$

(vi) *F1-score (F_1^{sr}):* It is defined as a combined measure of precision and sensitivity and is commonly used when a balance between the two measures is required.

$$F_1^{sr} = \frac{2\times\ P_r \times S_n}{P_r + S_n} \tag{1.5}$$

(vii) *Area under the curve (AUC):* The plot of the true positive rate against the false positive rate is called the Receiver Operating Characteristic (ROC) curve. The Area Under the ROC Curve (AUC-ROC) measures a model's capability to correctly classify instances into one of two categories. A higher AUC value indicates better predictive performance of the classifier.

(viii) *Matthew's Correlation Coefficient (MCC):* It describes the balanced measurement between observed and predicted cases.

$$MCC = \frac{TP\times TN - FP\times FN}{\sqrt{(TP+FP)(TP+FN)(TN+FP)(TN+FN)}} \tag{1.6}$$

(ix) *Mean Squared Error (MSE):* MSE is defined as the average of squared differences between the predicted output $(\hat{y}_i)$ and the actual output (y_i). It is always a non-negative number. The MSE value near zero represents a good prediction made by the model.

$$MSE = \frac{1}{N}\sum_{i=1}^{N}(y_i - \hat{y_i})^2 \tag{1.7}$$

where, N is the number of data points.

(x) *Root Mean Squared Error (RMSE):* RMSE is the standard deviation of the residuals (prediction errors). It is defined as the second moment of difference between the actual value and the predicted value.

$$RMSE = \sqrt{\frac{1}{N}\sum_{i=1}^{N}(y_i - \hat{y}_i)^2} \tag{1.8}$$

(xi) *Geometric-mean (G-mean):* G-mean is used to assess a classifier's performance, especially on class-imbalanced datasets. For binary classification, it is assessed using the square root of sensitivity and specificity. For multiclass problems, the G-mean is calculated by taking the geometric mean of the sensitivity for each class after taking into account each class's performance independently.

(xii) *Cohen's Kappa score:* The Kappa score is used to compare observed accuracy(P_o) to expected accuracy(P_e).

$$Kappa = \frac{P_o - P_e}{1 - P_e} \tag{1.9}$$

P_o is the number of instances correctly classified throughout the whole confusion matrix. P_e is the accuracy that any random classifier should be able to achieve. It is closely related to both the total number of examples in each class and the total number of instances where the machine learning classifier correctly identified the class based on the label provided by the ground truth. The Kappa score ranges from -1 (worst possible performance) to 1 (highest possible performance). A Kappa Score of 0 implies that the model is no better than random guessing, while a score of 1 suggests that the model is excellent.

1.6 Validation Methods

Validation methods are used to assess how well a model can generalize to unseen data. To evaluate the performance, different validation methods are used.

1.6.1 Hold out

In this method, the original data is divided into training data, validation data, and test data. This approach is simple and computationally efficient, but it can produce biased results depending on how the data is split.

1.6.2 Cross-validation

In this method, the data is divided into k parts, then iteratively the training is performed on the $k-1$ parts, and testing is done on the remaining part. This procedure is performed k times. The performance of the classifier is calculated by taking the average performance over k iterations. 5-fold and 10-fold cross-validation methods are mostly used.

1.6.3 Leave-one-subject-out (LOSO)

In this method, for each iteration of the validation, one subject is selected for testing while all remaining subjects for training. This process is repeated N times. Although this method provides a very thorough evaluation, it is computationally expensive for large datasets.

1.7 Research Motivation

AD and PD are the most prevalent neurodegenerative disorders, affecting millions of individuals worldwide. Both disorders are progressive in nature, leading to severe cognitive and motor impairments that drastically reduce quality of life for patients and place a substantial emotional and financial burden on families and healthcare systems. Despite decades of research, there is currently no cure for either disease, and treatment

options are primarily limited to managing symptoms rather than halting or reversing disease progression. This makes early and accurate identification of AD and PD a critical step toward improving clinical outcomes and enabling timely interventions. The diagnosis of AD and PD remains a significant challenge. AD generally begins with modest memory loss or cognitive impairment, which might be mistaken for normal ageing. Similarly, early indications of PD, such as modest tremors, rigidity, or abnormalities in movement, may not be detected until the disease has progressed. Current diagnostic approaches rely mainly on clinical examinations and medical imaging, which are time-consuming, necessitate professional interpretation, and may not always yield conclusive results. Furthermore, overlapping symptoms among neurological disorders can result in misdiagnosis or delayed treatment.

Amidst the rapid aging of populations worldwide, neurodegenerative diseases are emerging as one of the greatest public health challenges of our time. Addressing this crisis requires diagnostic solutions that are not only accurate but also scalable, affordable, and globally accessible. AI-powered classification models hold immense promise to reduce pressure on healthcare systems. The motivation of this thesis is to design and develop techniques to improve detection by merging state-of-the-art computational tools with medical insight. This thesis aims to enable earlier intervention, enhance diagnostic accuracy, and facilitate personalized treatment, helping to reduce the global burden of neurodegenerative conditions.

1.8 Problem Formulation

Manual examination of brain diseases is time-consuming, prone to variability, and can miss subtle indicators of disease progression. The primary objective is to develop an automated system capable of accurately identifying and classifying brain diseases based on bio-signaling modalities. The formulation of the problem is therefore to design and evaluate a computational model that can reliably detect and classify brain diseases, with the aim of supporting early diagnosis and assisting clinicians in treatment planning. Figure 1.2 illustrates the representative diagram of this problem formulation.

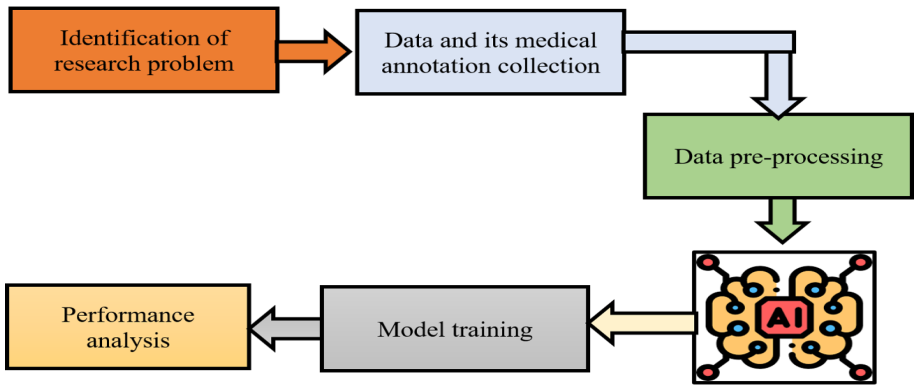

Figure 1.2: Problem formulation framework for brain disease identification and classification

As shown, the process begins with the acquisition of medical data (e.g., EEG, Gait, speech signals), followed by pre-processing steps to reduce noise and standardize inputs. Subsequently, relevant features are extracted either manually or through deep learning architectures. These features are then used by a classification model to distinguish between healthy and unhealthy, or to classify the unhealthy cases into specific disease categories. The final output of the model provides the predicted diagnosis, which can assist clinicians in early detection and decision-making.

1.9 Thesis Outline

The thesis is organized into six chapters, beginning with the first chapter dedicated to the introduction. In the second chapter, an overview of different brain disease identification and classification methods is provided. Chapters three to five are dedicated to the three objectives identified based on the research gaps. Finally, in chapter six, the key findings are summarized, and the future scope of the work is presented.

- ✓ **Chapter 1-Introduction:** This chapter provides a brief background on brain diseases and outlines the motivation for this thesis. It also presents the different modalities used for brain disease diagnosis, as well as the key performance metrics employed for disease identification and classification.
- ✓ **Chapter 2-Literature Review:** In this chapter, a detailed literature review

on brain diseases, with a focus on AD and PD, is presented, including the datasets commonly used for research and existing methodologies for automatic disease detection. Existing studies utilized for brain disease identification and classification tasks are also discussed. This review is followed by an analysis of the current limitations in existing research and the formulation of the objectives for the present research work.

- ✓ **Chapter 3-Feature Selection-Driven Optimization of Brain Disease Detection Models:** This chapter focuses on feature selection-driven methods for brain disease identification. It aims to enhance the accuracy and efficiency by employing robust feature selection techniques. This chapter highlights how irrelevant or redundant data can be eliminated, thereby improving classifier performance, reducing computational costs, and mitigating overfitting.
- ✓ **Chapter 4-Design and Analysis of an Algorithm for the Classification of Neurological Disorders:** This chapter focuses on the development of an algorithm for the identification and classification of different brain diseases. In this study, two neurological disorders, Alzheimer's Disease (AD) and Frontotemporal dementia (FTD), are considered. This approach first involves the identification of brain disorders, followed by their classification into the respective categories.
- ✓ **Chapter 5-Development of an Automated Algorithm for Early Diagnosis of Brain Diseases:** This chapter contributes to the development of an automated algorithm for brain disease diagnosis. In this, the speech and gait signal are considered as a diagnostic modality for early diagnosis of Parkinson's Disease (PD).
- ✓ **Chapter 6- Conclusions, Future Directions and Social Impact:** This chapter will contain a brief summary of all the methods, observations, and contributions of the results obtained in each objective. Also, it will include the future directions and social impact.

Chapter 2

Literature Review

This chapter presents a comprehensive review of the existing literature on the diagnosis of neurodegenerative brain diseases, with a particular emphasis on Alzheimer's Disease (AD) and Parkinson's Disease (PD). In addition, this chapter highlights the research gaps identified in the reviewed studies. Later, the research objectives have been formulated based on these research gaps.

2.1 Introduction

Neurodegenerative disorders affect millions of people worldwide and are one of the primary causes of impairment in the elderly. Early and precise diagnosis is critical for managing the disease and reducing its course. With recent improvements in computational approaches, artificial intelligence (AI), specifically machine learning (ML) and deep learning (DL), has emerged as a viable tool for boosting diagnostic precision. Researchers have proposed several methods for identifying brain disease using ML and DL techniques. This review focuses on the cutting-edge ML and DL techniques utilized in the identification and classification of neurodegenerative disorders, comparing methodologies, data sources, and performance.

2.1.1 Machine Learning-based Approach

Machine learning (ML) is a subset of AI that makes a machine able to learn automatically and improve from past experiences without programming it further. It uses data as input to anticipate new outcomes. The prime motive of ML is to create an

environment where the machine learns from experiences (i.e., data) to make decisions. ML techniques for brain disease detection typically use a structured pipeline that includes data preparation, feature extraction, feature selection, and classification. Figure 2.1 depicts the basic block diagram of the ML model.

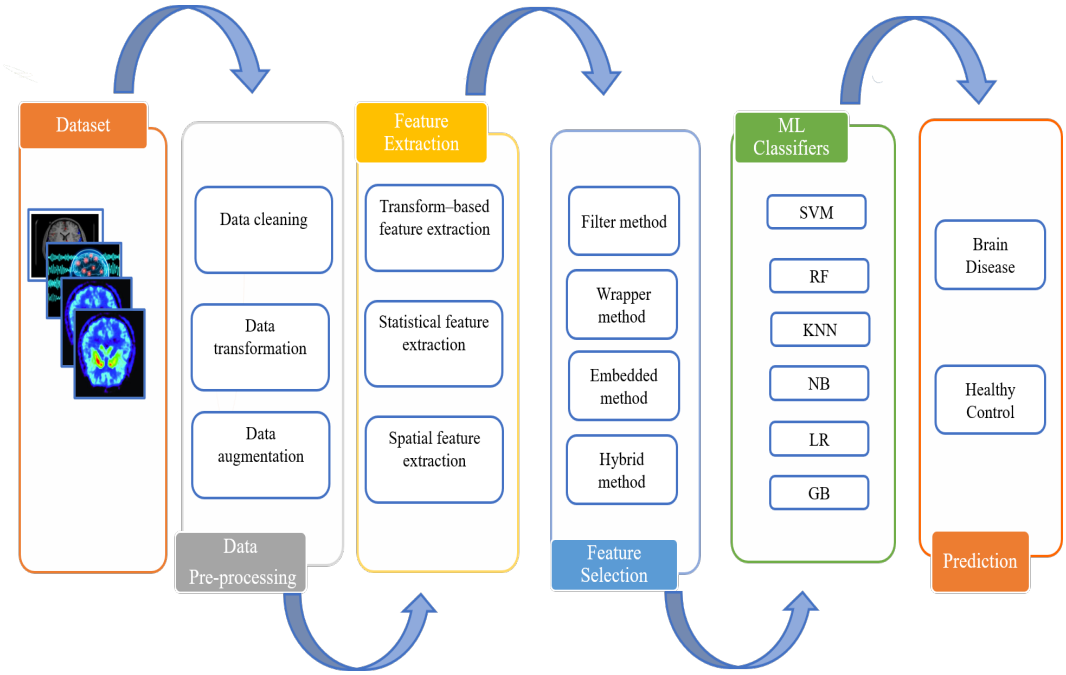

Figure 2.1: Basic block diagram of the machine learning model for brain disease identification and classification

1. *Data pre-processing:* Data pre-processing is the most fundamental and significant part of developing any ML model. It involves cleaning up and preparing the raw data [45]. Data pre-processing directly affects how well a model performs. For brain disease detection, the data is available in a variety of forms, including audio data, pictures, structured tables, etc. The data collected in these forms contains noise and inconsistency. Therefore, it becomes important to rectify these issues before any further processing. Some of the data pre-processing frequently includes null value elimination, data augmentation, noise removal, and standardization and normalization.

2. *Feature extraction:* The process of finding and extracting the right features for the desired system performance is complex and crucial. The basic feature

extraction process reduces large amounts of data into a smaller number of feature vectors to obtain relevant information from the raw signals [29]. A feature extraction technique boosts model explainability, decreases the chance of overfitting, speeds up training, and helps to improve model accuracy. The objective of feature extraction is typically to use domain expertise to extract unique data that precisely describes the occurrence of interest from raw data [46]. Researchers employed a variety of feature extraction methods depending on the data or image modalities to extract the necessary information so that the proposed ML model might perform better.

Table 2.1: Feature extraction methods used for brain disease identification and classification

Method	Type	Characteristics
Transform-based feature extraction	Wavelet Transform	Multi resolution analysis, good time-frequency localization, suitable for non-stationary signals, complex computation.
	Fourier Transform	Easy to compute, good for analyzing stationary signals, limited time-frequency resolution.
	DCT	Easy to compute, low computational complexity, robust to noise, and lack of localization.
	MFCC	Easy to compute, robust to noise, captures important spectral and temporal features.
	LPC	Computationally efficient, robust to noise, higher spectral resolution, low dimensionality, sensitive to window length.
	HHT	Can capture non-linear behavior of signal, higher resolution, computationally intensive, sensitive to noise.
	TQWT	Good time-frequency localization, robust to noise, higher computational complexity.
	STFT	Provides a localized frequency representation with fixed resolution, which is used to compute spectral, temporal, and statistical features.
	CWT	Provides a multi-resolution time–frequency representation with adaptive resolution used to compute multi-scale, temporal, and statistical features.
	EMD	Can analyze signals with complex and non-linear dynamics, good time-frequency localization, and sensitive to noise.
	VMD	Non-parametric robbers to noise, higher computational complexity.

Method	Type	Characteristics
Spatial Feature extraction	ROI based features	Less computational time, focuses on a specific region of the image rather than the whole image, overfitting, focuses on extracting features from a specific region of the image or video frame, which provides better results.
	Morphological features	Use to extract a variety of features including shape, size, texture, and connectivity, computationally intensive.
	HOG	Can capture information about the texture and shape of an object in an image, fast and efficient, sensitive to noise, not suitable for objects with complex or irregular shapes.
	Voxel-based features	Enables the analysis of 3D volumetric data, easy to extract.
	Acoustic features	Mostly used in speech and audio processing, provides valuable information about spectral and temporal characteristics, robust to noise.
	Intesnity features	Easy to implement, extracted from a small local region of an image, sensitive to noise, computationally efficient, may not capture the relevant information from a large or complex image.
	Kinematic features	Provides motion information, computationally intensive, most popular features are velocity, jerk, speed, and acceleration.
	Texture features	Captures the patterns, structures, and variations in pixel intensities within a local region of the image.
Statistical Feature extraction	Time-domain	Describe statistical properties of the raw signal.
	Frequency-domain	Describe spectral characteristics of the signal.
	Wavelet-domain	Describe multi-scale signal characteristics combining time and frequency information.
	Visual features	Computationally easy and effective, captures the overall quality of the image such as color, texture, etc.
	ICA	Computationally efficient, non-parametric, higher performance for a larger amount of data, higher complexity.

DCT, Discrete cosine transform;*MFCC*, mel-frequency cepstral coefficients; *LPC*, linear prediction coefficients; *HHT*, Hilbert hung transform; *TQWT*, tunable Q-factor wavelet transform; *STFT*, short time fourier transform; *CWT*, continuous wavelet transform; *EMD*, empirical mode decomposition; *VMD*, variational mode decomposition ; *ROI*, region of interest; *HOG*, histogram of oriented gradients; *ICA*, independent component analysis

In order to identify and categorize brain diseases, researchers have employed different feature extraction methods [26, 28, 47–122]. Table 2.1 depicts the feature extraction methods used for brain disease detection. These methods can

often be divided into three categories: transform-based feature extraction, spatial feature extraction, and statistical feature extraction. The primary objective of transform-based features is to find a lower-dimensional representation that is more condensed, with the majority of the data energy concentrated in the fewest possible uncorrelated coefficients. These techniques enable the extraction of useful features while maintaining generalization performance and reducing computational cost in the classification step by removing unnecessary information. Spatial features are objective-specific, which means that each parameter setting can recognize only one specific type of object. This method extracts relevant features or patterns from an image based on its spatial arrangement of pixels. It involves analyzing the image at different scales and levels of detail to identify patterns or structures. Statistical features involve computing statistical measures such as mean, standard deviation, variance, skewness, kurtosis, correlation, and covariance for each feature in the dataset.

3. *Feature selection:* The set of features is a crucial component in establishing the prediction models' hypotheses [123]. The relevancy of the feature is assessed in accordance with the data rather than the value of the data. It becomes necessary to identify the most significant features, as datasets with insignificant features reduce model accuracy. Feature Selection is the process of selecting the required attributes from the complete dataset. These methods are, thus, used to showcase the most relevant features.

   It consists of selecting a subset of features, followed by feature transformation. The process of selecting a subset of features includes both feature ranking and feature frequency calculation. The two primary goals of feature selection are to improve classification accuracy and feature reduction [124]. The process of feature selection is depicted in Figure 2.2.

   Based on evaluation criteria and interaction with the learning algorithm, feature selection methods are classified into four types: filter, wrapper, embedded, and hybrid feature selection methods. The filter method selects the feature subset using statistical measurements [125]. This technique uses several metrics and ranking to remove irrelevant features. The wrapper method relies on the

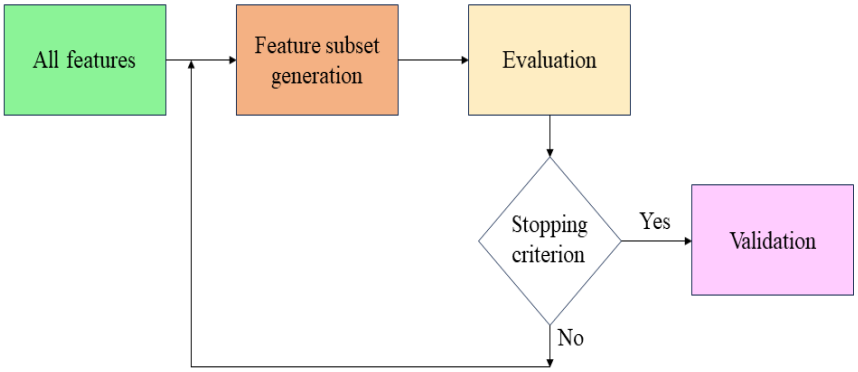

Figure 2.2: Feature selection process

classifier's performance in order to obtain a feature subset. Using the induction algorithm as a black box, this technique chooses the feature subset [123]. The embedded technique regards feature selection as a crucial component of learning algorithms. It reduces the computational time for selecting the feature subset. The hybrid feature selection method combines several feature selection strategies to provide a final set of features [126]. It takes advantage of different feature selection techniques and overcomes their individual limitations. Table 2.2 summarizes the techniques used by researchers with their salient features.

Table 2.2: Feature selection methods used for brain disease identification and classification

Method	Type	Advantage	Disadvantage	References
Filter method	Relief, mRMR, Mutual information gain, PCA, Chi-square test, Coorelation, PCC, KWST, LDA, t-test, ANOVA	Fast and computationally efficient, less computational complexity, works well with high-dimensional data, computationally less expensive, scalable approach to large datasets.	Ignores feature dependency, ignores interaction with the classifier, and fails to recognize the patterns properly during the learning phase.	[26, 47, 65–67, 69, 70, 77, 81, 83, 84, 92, 94, 97, 99, 107,111,115,127–132]

Method	Type	Advantage	Disadvantage	References
Wrapper method	RFE, GA, SVM-RFE, forward feature selection, stepwise selection	Better classifier interaction, finds the most useful features, optimizes the classifier performance.	Higher computational complexity, long execution time, susceptible to over-fitting on smaller training datasets, more expensive than filter approaches, less scalable for larger datasets.	[28, 48, 64, 75, 87, 88, 91, 112, 133, 134]
Embedded method	ARD, RF	Better classifier interaction, less prone to over-fitting, improved use of available data, faster solutions, effective capturing of feature dependencies.	Computationally costlier, not suitable for high dimensional data, specific to the learning machine.	[76, 98]

mRMR, minimum redundancy maximum relevance; *PCA*, principal component analysis; *PCC*, Pearson correlation coefficients; *KWST*, Kruskal-Wallis statistical tests; *LDA*, linear discriminant analysis; *RFE*, recursive feature elimination; *GA*, genetic algorithm; *SVM-RFE*, RFE combined with SVM; *ARD*, automatic relevance determination; *RF*, random forest; *MIRFE*, mutual information gain and RFE

4. *ML classifiers:* In the majority of cases, the challenge is determining if disease is present or not, or determining the stages of the disease. As a result, several researchers use various ML classifiers for these tasks. There are two types of ML classifiers: supervised and unsupervised. The majority of suggested techniques made use of supervised learning techniques, in which classifiers are given access to labeled training data in order to build effective models. These methods include support vector machine (SVM), K-nearest neighbor (KNN), random forest (RF), Naive Bayes (NB), logistic regression (LR), decision tree (DT), etc. For brain disease identification and classification, a wide range of supervised classifiers have been utilized. SVM, with its various implementations, is the most widely used method for all classification tasks by researchers [26, 28, 47–49,63,65,66,68,69,71,72,74,78–85,88,97–108,110–112,114–116,135–141]. In SVM, the features are mapped onto a high-dimensional space, and classification is employed to determine the most appropriate hyperplane [142]. The dataset's extreme points (support vectors) are used to construct the hyperplane. The hyperplane is generated to obtain the largest margin between the support vectors

of the opposing classes.

Researchers have also employed ensemble learning methods for identification [48–50, 69, 71, 73, 77, 83–86, 88, 99, 103, 111, 114]. The ensemble learning method uses multiple ML algorithms to produce weak predictive results based on features extracted through a variety of projections on data and then combines results from different voting mechanisms to improve performance over that of any individual component algorithm [143]. RF is an ensemble learning approach that employs bagging along with random feature selection. It constructs several DTs using different subsets of the data, and the final prediction is made based on majority voting among the trees. Extreme gradient boosting (XGBoost) is another ensemble method used for both classification and regression tasks. It operates under the principle of boosting, which entails combining the outcomes of weaker learners to produce stronger learners. By incorporating new features and addressing defects in older versions, new models are introduced to XGBoost until no more advancements are possible [50].

Other classification algorithms that are used in disease prediction are LR, NB, Gaussian mixture model (GMM), KNN, DT, and RF [26, 48, 62, 64, 65, 70–72, 74, 76, 78, 79, 82–85, 87, 91, 92, 94, 99, 102–104, 109–115, 127, 144–146]. LR is used to estimate the probability of an event occurring by fitting the data to a logistic function, or to calculate the odds ratio when multiple explanatory variables are present [147]. It maps the expected values with the sigmoid function. It extracts a set of weighted features from the input, applies the logarithm, and then integrates them linearly, where each feature is multiplied by its corresponding weight and then added. NB is a Bayes theorem-based probabilistic ML classifier [148]. NB is recognized as the simplest and efficient technique for building rapid ML models that can predict outcomes quickly. A GMM is a probabilistic model that represents a combination of a limited number of Gaussian distributions whose weights, means, and covariances are unknown. The parameters of the GMM are calculated using the expectation-maximization technique [91]. KNN is a non-parametric method used for both classification and regression. It makes predictions based on the K nearest training samples

in the feature space [65]. DT is also a non-parametric method used for both classification and regression. It is built using a top-down approach, where at each step the variable that best splits the dataset is selected. The resulting model has a tree-like structure, with decisions made from the root node down to the leaf nodes [149].

2.1.2 Deep Learning-based Approach

Deep learning is a field of AI concerned with algorithms inspired by the structure and function of the human brain. The key benefit of DL is its ability to extract data from a raw, unstructured, and unlabeled dataset without the need for human interaction. As a result, DL may become a crucial technique to examine enormous amounts of data. In the last few years, a number of DL-based methods have been used for brain disease identification and classification. This subsection includes an overview of different DL methods for disease diagnosis and prediction. Four basic categories can be used to generally categorize the DL approaches that researchers mostly use for brain disease detection: supervised or discriminative learning, unsupervised or generative learning, self-supervised learning, and hybrid learning. Figure 2.3 shows the most widely used DL methods of brain disease prediction.

Discriminative deep structures improve pattern categorization by modeling class distributions based on visible data. The Discriminative architectures primarily include convolutional neural networks (CNN), recurrent neural networks (RNN), and multi-layer perceptrons (MLP). CNNs are a popular DL model that is often utilized for brain disease detection. Unlike standard ML methods, this network can automatically recover features. CNN architectures are widely utilized in the diagnosis of brain diseases [131, 150–196]. Goyal et al. [151] introduced a hybrid feature extraction technique that combines time-frequency algorithms and resonance-based sparse signal decomposition (RSSD). CNN is utilized for classification purposes. The hybrid approach produces effective outcomes with 99.37% accuracy. Gazda et al. [153] employed a CNN to extensively analyze handwriting images to diagnose PD. A CNN ensemble is produced by combining the weights built by training multiple fine-tuning

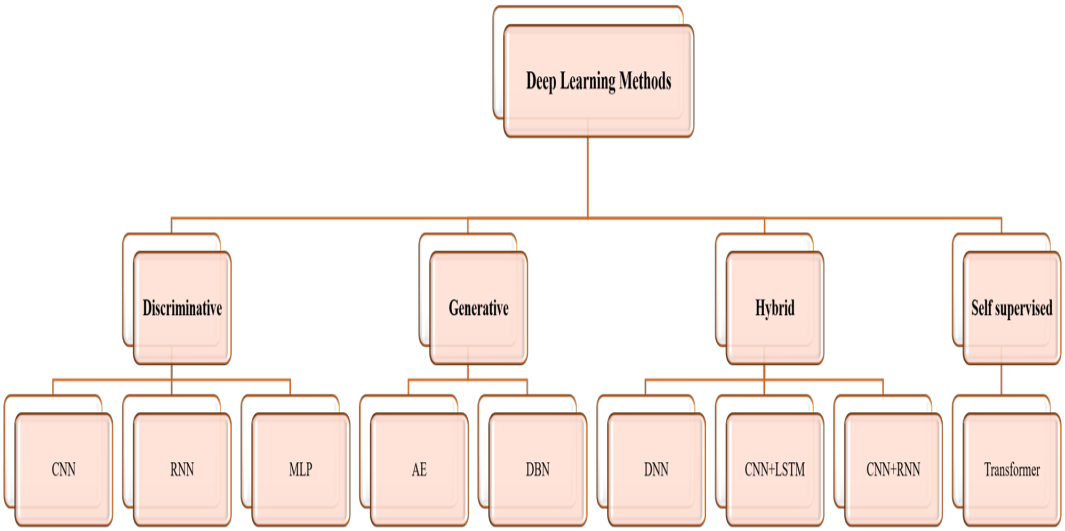

Figure 2.3: Deep learning architectures used for brain disease detection

methods. This architecture can identify PD from offline handwriting with 94.7% accuracy by combining several fine-tuned CNNs. A CNN model on drawing motions to identify PD is used in [154]. The coefficients of the fast Fourier transform (FFT) in the frequency range of 0 Hz to 25 Hz are used as input to the CNN. The impact of augmentation methods, various data formats, and various image resolutions on the efficacy of the trained CNN model was investigated for PD detection in [155]. Xia et al. [184] employed a deep pyramid CNN to diagnose AD. Sliding window augmentation of the 1-D EEG data was used to overcome the problem of restricted data size.

Canturk [157] adopted a CNN-based strategy with pre-trained AlexNet and GoogleNet models for feature extraction. He utilized a fuzzy recurrence plot in this instance to turn time-series signals into images with a greyscale texture, then used KNN and SVM as final classifiers. Alharthi et al. [159] employed a deep CNN for the interpretation of ground response force data from PD patients. Oh et al. [164] developed a thirteen-layer CNN architecture. The developed model offered an efficient classification accuracy of 88.25% on the EEG dataset. Kachare et al. [187] developed a lightweight CNN model to distinguish the EEG signal of AD and HC and

obtain 98.50% classification accuracy. The transform-based detection method used by several researchers [161, 162, 178, 197], the raw data is transformed and applied to CNN for PD detection. CNN is useful for detection and classification purposes. To create voiceprint samples for diagnosing PD, Xu et al. [197] employed a spectrogram deep convolutional generative adversarial network (S-DCGAN). The model is capable of creating a variety of high-resolution images. The accuracy and performance of CNN are enhanced by using the generated images during training. Loh et al. [160] employed EEG waves to identify PD. After splitting the EEG data in half, a Gabor transform is used to produce the spectrograms. Two spectrograms were consequently gathered from each EEG wave. The classification of the spectrogram signals of HCs, PD patients taking medication, and PD patients not taking medication is proposed using a 2D-CNN-based architecture. Kamran et al. [170] used a variety of transfer learning techniques on the HandPD, NewHandPD, and Parkinson's Drawing datasets. Additionally, they used multiple methods for augmentation. Using the AlexNet framework, they report a maximum accuracy of up to 99.22%. Naseer et al. [171] developed a deep 25-layer CNN classifier that combined transfer learning and data augmentation to achieve an exceptional accuracy of 98.28%. They applied the ImageNet and MNIST fine-tuning-based approach to the PaHaW dataset and found that it performed almost 3% better than the MNIST pre-trained version. Kurmi et al. [174] utilized DaTscan images to predict PD using a collection of DL models. The DL models VGG16, ResNet50, Inception-V3,and Xception are used for this purpose. A fuzzy fusion logic-based ensemble technique is used to increase the model's accuracy. The proposed model achieved recognition accuracy, sensitivity, and specificity of 98.45%, 98.84%, and 97.67%, respectively.

RNNs are another common neural network that uses sequential or time-series data to feed the result of previous steps into the current stage. Long short-term memory (LSTM) is a widely utilized RNN for PD detection [198–201]. MLPs are feedforward neural networks that serve as the foundation for deep networks. Er et al. [198] suggested an approach based on deep networks and LSTM for PD detection from voice data. The features extracted from the mel-spectrogram images of VMD

were applied to voice signals. They achieved a promising result of 98.61% accuracy. Lee et al. [201] employed the convolutional-recurrent neural network (CRNN), which offers great potential for aiding in diagnosing PD.

MLPs are feedforward artificial neural networks (ANNs). This architecture is sometimes referred to as a basis for deep learning. MLPs have been used in a number of studies to diagnose PD [99, 104, 128–130, 199, 202–206]. Peker et al. [130] proposed a complex-valued artificial neural network to diagnose PD. The proposed technique yielded a classification accuracy of 98.12%. Chen et al. [129] developed an efficient method using minimum redundancy maximum relevance (mRMR) feature selection and extreme learning machine (ELM) for PD detection. By lowering the feature space, they have seen an improvement in performance. The studies are run on various feature subsets. ELM is primarily dependent on the hidden neurons and the activation function. they have obtained a maximum accuracy of 96.47% on the voice dataset. The performances of three cascaded DL models, RNN, LSTM, and MLP, were compared for effective PD diagnosis in [199]. Ali et al. [203] developed a hybrid intelligence system that can automatically do acoustic analysis on spoken signals. To minimize dimensionality and optimize the hyperparameters of neural networks (NN), this intelligent system employs LDA and GA. Priya et al. [204] used a symmetrically weighted local neighbor gradient pattern method for extracting the features from the gait signal. The ANN classifier is utilized to categorize PD patients and HC, and provides an effective classification accuracy of 96.28%. Yurdaku et al. [205] developed a neighborhood representation local binary pattern approach for detecting PD. The statistical features are retrieved from the transformed data, and different feature sets are created using the t-test. ANN is utilized for classification and provides a classification accuracy of 98.3%.

Researchers also used hybrid deep-learning models for PD detection [207–217]. The hybrid deep learning models are generally made up of two or more deep basic learning models, with the discriminative or generative deep learning model serving as the base model. Narendra et al. [207] presented a DL model that combines CNN and MLP for automatic PD and HC classification that has a 68.56% accuracy rate.

Xia et al. [209] suggested a DL-based method for PD diagnosis using gait data. To extract local deep features from gait data, they merged the CNN and LSTM architectures. They compared several feature extraction techniques and ML models. Their method performed better than earlier research and other models in terms of precision, sensitivity, and specificity. Chowdhary and Srivatsan [211] developed a non-invasive early PD detection architecture based on CNN and feature extraction from HoG. This architecture provides an efficient classification accuracy of 94%. Abdullah et al. [212] developed a system that effectively distinguishes between PD patients and HCs by using information from handwritten data and applying deep transfer learning models, GA, and KNN techniques. The transfer learning approach is used for feature extraction, the GA is used for feature optimization, and KNN is used for classification purposes. Zeng et al. [213] suggested a radial basis function (RBF) neural network to analyze gait in order to detect PD. A five-fold cross-validation procedure is used to classify 93 PD patients and 73 HCs.

Due to the increasing success and popularity of transformer networks in image recognition and natural language processing in recent years, attention mechanism-based transform models have also been used to detect AD and PD [185, 218–223]. Miltiadous [185] deployed a dual-input convolution encoder network (DICE-net) for AD detection. The band power and coherence features derived from the EEG signal were taken out and fed into the DICE-net. The DICE-Net contains a feed-forward layer, a transformer encoder, and convolution layers. Naimi et al. [219] developed a hybrid ConvNet-Transformer model for PD identification. The ConvNet detects local patterns, while the transformer recognizes long-term linkages and temporal relationships between signals. Using these two elements, the model was able to identify complex signal correlations that indicate PD. Graph neural networks (GNNs) have become a popular graph analysis tool in recent years. By turning the data into graphs, the GNN network can find patterns with much less input. Additionally, by employing filtering algorithms, GNN determines which nodes and edges are crucial for completing a task. GNNs are capable of processing graph data in non-euclidean spaces. GNNs' messaging mechanism refreshes the central node description by

combining neighbor node properties and passing on surrounding information [224].

2.2 Research Gaps

Based on the comprehensive review of prior state-of-the-art studies on brain disease identification and classification tasks, the following research gaps have been identified and these are as follows:

1. Current feature selection methods are inadequate for handling the high dimensionality, noise, and complexity of data. Most studies lack robust feature selection tailored to physiological and behavioral signals and fail to ensure interpretability, limiting their applicability for early diagnosis of brain diseases.
2. EEG-based brain disease classification often relies on all channels due to the absence of robust and validated channel selection frameworks. Resulting in redundant data processing, increased computational complexity, and reduced interpretability of neural activity patterns.
3. There is a lack of hierarchical EEG-based diagnostic frameworks that first detect the presence of brain disease and then classify its specific type. Most existing studies address disease detection (healthy vs. diseased) and disease classification (differentiating between multiple disorders) as separate tasks, using independent models and feature sets. This approach fails to leverage the shared representations between detection and classification, leading to inefficiencies and reduced diagnostic accuracy.
4. Existing disease classification studies rely heavily on manual feature engineering, fragmented pipelines, and expert intervention, which limit reproducibility, scalability, and clinical adoption. There is a need for an automated, end-to-end framework that standardizes preprocessing, feature selection, and classification to enable robust, scalable, and viable disease diagnosis.

2.3 Research Objectives

The challenges associated with the identification and classification of brain diseases highlight the need for the development of efficient models and frameworks to build a robust diagnostic system. To address these practical challenges effectively, three research objectives have been formulated as follows:

- **Objective 1:** Design and development of algorithms for optimal feature selection in brain disease diagnosis.
- **Objective 2:** Design and analysis of an algorithm for the classification of neurological disorders.
- **Objective 3:** Design and development of automated algorithms in the early diagnosis of brain diseases.

Chapter 3

Feature Selection-Driven Optimization of Brain Disease Detection Models

This chapter focuses on feature selection-driven optimization of machine learning models for brain disease detection. Three studies are presented. The first study focuses on EEG-based PD detection by extracting statistical and Hjorth features from the EEG signal and selecting optimal features. The second study addresses speech-based PD diagnosis using a two-stage stacked ensemble model, which combines feature selection, oversampling, and multiple base classifiers for robust detection. The third study targets EEG-based AD detection using a Fourier Decomposition and Hilbert Transform-based framework. These studies emphasize the role of feature selection and model optimization in developing reliable, non-invasive, and intelligent systems for early detection of neurodegenerative diseases.

3.1 Automatic Detection of Parkinson's Disease using EEG Signals: A Machine Learning Approach

3.1.1 Introduction

The diagnosis of PD is extremely challenging due to the lack of a recognizable pattern in the symptoms or progression of the disease. To diagnose PD, a variety of neuroimaging tests, including a dopamine active transporter scan, computerized tomography, and magnetic resonance imaging, are performed. Despite being approved by clinicians, these biomarkers may have several drawbacks, including high

costs, poor temporal resolution, accessibility issues, radiation exposure, or regional exclusivity. In recent years, EEG has been explored as a potential diagnostic tool for several neurodegenerative diseases. The neurodegenerative disorders decrease the connectivity of the brain network, which can be recorded by EEG signals [111]. The EEG holds the potential to overcome the shortcomings of diagnostic tools due to its low cost, accessibility, non-invasive nature, and mobility [223].

Several methods based on ML and DL have been utilized by researchers to detect PD using EEG signals. Wang et al. [225] employed a capsule network to detect PD. An interpolation method was used to map the frequency band energies of the EEG signal into a two-dimensional image and achieved an accuracy of 89.34% utilizing capsule networks. Khoshnevis and Sankar [110] employed a higher-order statistics technique to detect PD. The EEG recordings of 20 PD patients and 20 HC were used to extract thirty higher-order and six lower-order statistical characteristics. An ensemble RUSBoosted trees classifier was used for classification and obtained an accuracy of 87%. Murugappan et al. [226] incorporated tunable Q wavelet transform (TQWT) and probabilistic neural networks to classify HC and PD patients. The features were extracted from the sub-bands obtained by TQWT, and classification was performed by the neural network. Khare et al. [114] employed TQWT to decompose EEG signals into multiple subbands. Five features were extracted from each subband and classified using ML classifier. Kamalakanna et al. [227] employed an artificial neural network (ANN) with ReLU and sigmoidal activation function and attained 93.3% classification accuracy using the EEG dataset. Oh et al. [164] employed DL methods to distinguish healthy controls (HCs) and PD patients. A thirteen-layer convolutional neural network (CNN) was used for this purpose and provided an accuracy of 88.25%. The EEG signals were employed as one-dimensional time series data for the DL techniques. Time-frequency analysis methods were also used to convert the EEG signals into images and applied as input to the DL modules for PD detection [160, 162].

ML methods have been widely used for EEG signal analysis, but their performance largely depends on the quality of manually extracted features, which may not capture the nonlinear and nonstationary nature of EEG signals. In contrast, DL models can

automatically learn hierarchical feature representations and achieve higher accuracy; however, they require large amounts of training data, high computational power, and extended training time, which hinder their applicability in real-time or embedded systems. Therefore, there remains a need for an efficient approach that combines effective feature extraction and selection to achieve high accuracy while maintaining low computational complexity. The proposed work intends to develop a computationally effective framework to detect PD automatically. The major contribution of this work is as follows:

- Statistical features and Hjorth parameters are extracted from different EEG channels.
- Optimum attributes are obtained utilizing statistical tests and the extra tree classifier (ETC) based feature importance method.
- The optimum attributes are applied to the ML classifier for accurate detection of PD.
- A comparative analysis is performed between the proposed approach and existing PD detection approaches.

3.1.2 Proposed Methodology

The methodology is based on feature extraction and discovering the pertinent and essential features required to accurately detect PD. The aim is to develop a low-cost training model that is relatively easy to compute. Different feature extraction metrics and popular ML methods are employed individually to detect the disease. Figure 3.1 depicts the block diagram of the feature selection-driven PD detection method.

3.1.2.1 Dataset

The dataset employed in this work is obtained from OpenNeuro [38]. This data is initially generated at the University of California, San Diego. The data includes the EEG recordings of fifteen people with PD and sixteen HCs. During the EEG recording, participants were directed to focus on a cross-image displayed on the computer screen. The recording is done at a 512 Hz sampling frequency for approximately three minutes.

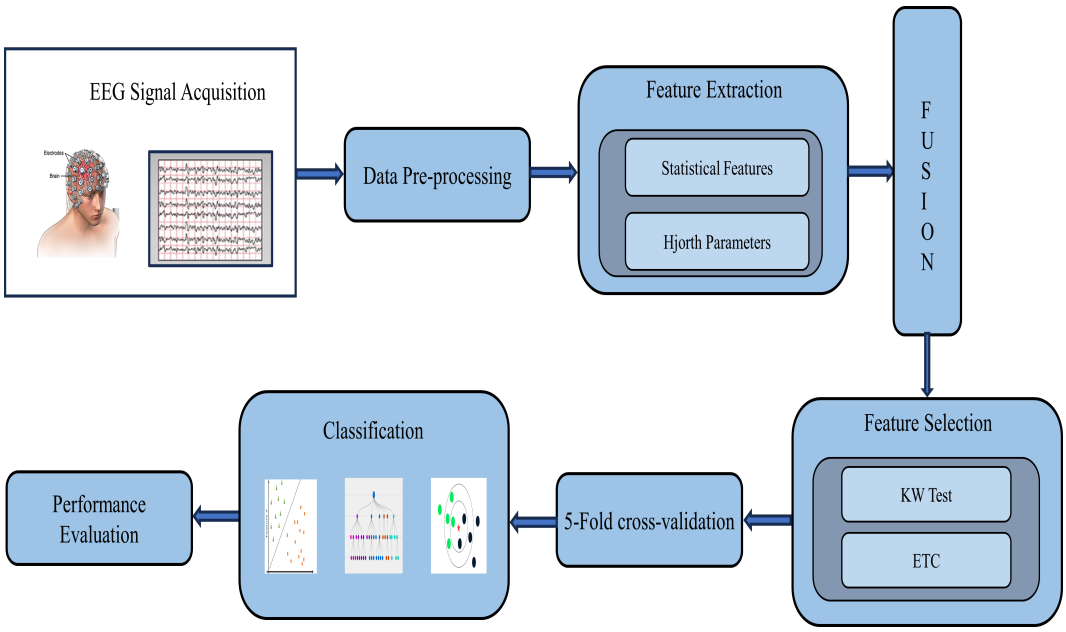

Figure 3.1: Block diagram of the feature selection-driven PD detection method

For each individual, 32 EEG channels were recorded. All PD patients have been categorized as Stage 2 or 3 on the Hoehn and Yahr scale. Figure 3.2 depicts the positions of the 32-channel EEG electrodes for data acquisition.

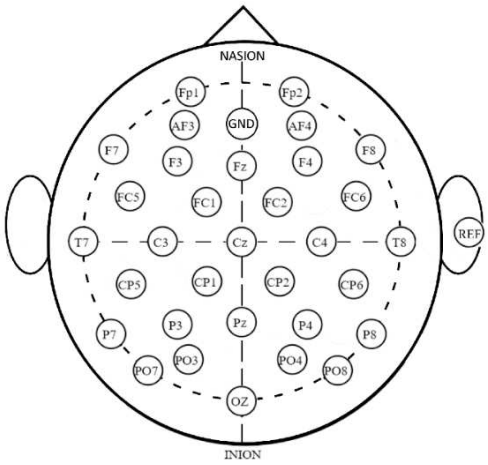

Figure 3.2: EEG electrode locations for OpenNeuro EEG data acquisition

In the pre-processing steps, each single-channel EEG data is stratified into 20-second non-overlapping epochs of 1024 samples. The complete demographic information for all participants is presented in Table 3.1.

Table 3.1: OpenNeuro EEG dataset description

Class	Healthy	PD patients
Male	7	7
Female	9	8
Age (years)	63.5±9.6	63.2±8.2
MMSE score	29.2±1.1	28.4±1

3.1.2.2 Feature Extraction

In this work, features are extracted from each segment of all 32 channels for every participant. All the features are essentially divided into two groups: statistical features and Hjorth parameters. Table 3.2 contains information about the extracted features.

Table 3.2: Features extracted from the EEG signal

Feature	Type
Statistical features	Mean (M)
	Standard deviation (S_d)
	Kurtosis (K_u)
	Skewness (S_k)
Hjorth Parameters	Hjorth activity (H_A)
	Hjorth mobility (H_M)
	Hjorth complexity (H_C)

1. *Statistical Features:* From the signals, several statistical features are extracted. These features are listed as follows:
   (a) *Mean (M):* Mean is defined as the average value of data. It is determined by dividing the complete data by the number of entries. It is calculated as follows:
   $$M = \frac{1}{N}\sum_{n=1}^{N} x_n \tag{3.1}$$
   Where x_n denotes the n^{th} sample's value of the EEG signal and N represents the total number of samples.
   (b) *Standard Deviation (S_d):* The standard deviation is a measure that indicates how much variation is present from the mean value, given as follows:
   $$S_d = \frac{1}{N}\sqrt{\sum_{n=1}^{N}(x_n - M)^2} \tag{3.2}$$

(c) *Skewness (S_k):* It is used to validate and calculate data symmetry, as well as for determining the probability of variable distribution. It can be stated as follows:

$$S_k = \frac{1}{N}\sqrt{\frac{\sum_{n=1}^{N}(x_n - M)^3}{{S_d}^3}} \tag{3.3}$$

(d) *Kurtosis (K_u):* Kurtosis is used to indicate the existence of large peaks in the temporal domain of a signal, determined as follows:

$$K_u = \frac{1}{N}\sqrt{\frac{\sum_{n=1}^{N}(x_n - M)^4}{{S_d}^4}} \tag{3.4}$$

2. *Hjorth Parameters:* The Hjorth Parameters are representations of time series statistical features and widely employed in signal processing [228]. Activity, mobility, and complexity are prominent parameters used to detect characteristics for the analysis of EEG data.

(a) *Hjorth Activity (H_A):* Hjorth activity is used to determine the mean signal strength, which is the variance of the signal, given as follows:

$$H_A = Var(x(t)) \tag{3.5}$$

(b) *Hjorth Mobility (H_M):* Hjorth mobility denotes the mean frequency of a signal and is computed by dividing the variance of the signal by the square root of the variance of the first derivative of the signal, as follows:

$$H_M = \sqrt{\frac{\mathrm{Var}\left(\frac{dx(t)}{dt}\right)}{\mathrm{Var}(x(t))}} \tag{3.6}$$

(c) *Hjorth Complexity (H_C):* Hjorth complexity determines the change in frequency. It is described as the mobility ratio of its first derivative to its mobility, expressed as follows:

$$H_C = \sqrt{\frac{H_M(\frac{dx(t)}{dt})}{H_M(x(t))}} \tag{3.7}$$

3.1.2.3 Feature Selection

To identify the optimal features, firstly, the Kruskal–Wallis (KW) test is used. The features having higher f-scores and p-values less than 0.05 are selected. Then, a

feature selection method based on ETC is employed. ETC is a tree-based supervised machine learning technique for extracting the most crucial features. The ETC is an ensemble algorithm that works on datasets by developing multiple tree models, which are constructed at random and sort out the most important features that are also voted the most [229]. It splits the nodes by fitting each decision tree and determining a split point. Nodes are divided based on the measure of random sub-nodes. These nodes are split on available variables and the obtained split gained in the results is selected in the constituent tree models, which helps to make the model less prone to overfitting by lowering the variance.

ETC calculates feature importance based on the average impurity reduction caused by a feature across all decision trees in the ensemble. The most relevant feature based on the Gini index (GI) is used by the corresponding decision tree to split the data. GI measures the probability of a specific feature being incorrectly classified when it is chosen randomly and is represented as follows:

$$GI = 1 - \sum_{i=1}^{n} p_i^2 \tag{3.8}$$

where n denotes the number of data points, and p_i denotes the probability that a feature will be assigned to a specific class.

3.1.2.4 Classification

To evaluate the proposed work performance, some widely recognized ML techniques, namely NB, SVM, KNN, and DT, are used. ML methods could not produce the intended outcome if the input range fluctuates more than normal because of their distinct cost functions. Thus, data standardization is conducted by standardizing EEG features.

3.1.3 Results

A 5-fold cross-validation method on the OpenNeuro dataset is used to assess the performance. Several performance parameters, such as accuracy, precision, sensitivity, and F-1 score, are used to assess the effectiveness of the proposed method. This

section presents the outcomes derived from the statistical characteristics, Hajorth parameters, fusion features, and top-ranked features.

3.1.3.1 Statistical Features Result

Four distinct ML classifiers, NB, SVM, KNN, and DT, have been used to evaluate the statistical features. Table 3.3 presents outcomes of the four statistical features, including skewness, kurtosis, mean, and standard deviation. For the statistical features, DT achieved a maximum classification accuracy of 96%.

Table 3.3: Performance analysis using statistical features for PD detection

Classifier	A_c	P_r	S_n	F_1^{sr}
NB	0.74±0.04	0.77±0.09	0.69±0.07	0.72±0.05
SVM	0.92±0.02	0.92±0.03	0.91±0.05	0.91±0.04
KNN	0.90±0.03	0.90±0.04	0.90±0.06	0.90±0.02
DT	**0.96±0.03**	**0.97±0.02**	**0.96±0.05**	**0.96±0.03**

3.1.3.2 Hjorth Parameter Results

Hjorth parameters were calculated to analyze model performance. Table 3.4 displays the classification outcomes based on the three Hjorth parameters. With 87% classification accuracy, KNN outperforms other classifiers in terms of performance.

Table 3.4: Performance analysis using Hjorth parameters for PD detection

Classifier	A_c	P_r	S_n	F_1^{sr}
NB	0.63±0.09	0.75±0.12	0.36±0.23	0.46±0.19
SVM	0.80±0.04	0.79±0.06	0.81±0.04	0.80±0.03
KNN	**0.87±0.02**	**0.83±0.06**	**0.92±0.03**	**0.87±0.03**
DT	0.69±0.03	0.68±0.05	0.68±0.05	0.68±0.04

3.1.3.3 Feature Fusion Results

The DT classifier's output beats that of SVM, NB, and KNN. Compared to statistical features and Hajorth parameters separately, the feature fusion set enhances the classification performance. The outcome of the feature fusion is displayed in Table 3.5.

Table 3.5: Performance analysis using feature fusion for PD detection

Classifier	A_c	P_r	S_n	F_1^{sr}
NB	0.69±0.09	0.83±0.13	0.45±0.21	0.56±0.16
SVM	**0.97±0.01**	0.95±0.02	**0.98±0.02**	**0.96±0.01**
KNN	0.94±0.02	0.92±0.02	0.96±0.01	0.94±0.01
DT	0.96±0.03	**0.97±0.02**	0.95±0.05	0.96±0.03

3.1.3.4 Effect of Top-Ranked Features on Classification Result

Classifier performance may be impacted by features with low separability. Significant features are chosen using the KW test, and the ETC-based feature selection technique from the fusion features set to acquire an accurate and rapid classification with a high diagnostic rate for PD. The KW test is conducted to evaluate the discriminating capacity of the features. Features having a p-value less than 0.05 are selected. Further, the optimum set of features is found by utilizing the ETC-based feature selection technique. The top 50 attributes are considered for classification based on data reduction and the best score produced by ETC. The highest-ranked attributes are indicated in Table 3.6. The top-ranking features have greater PD classification accuracy ratings. Table 3.7 shows the outcomes of feature selection for PD detection. The highest-ranking features improve the accuracy of each classifier model. The PD classification accuracy for NB, SVM, KNN, and DT is 78%, 96%, 98% and 98%, respectively. Figure 3.3 shows the performance comparison of different ML classifiers for PD detection.

The results demonstrate that DT outperformed the other classifiers. The confusion matrix of the DT classifier for PD detection is portrayed in Figure 3.4.

3.1.4 Discussion

The experimental findings show that PD can be automatically identified using ML models and hybrid feature extraction techniques. In addition to emphasizing individual features, the proposed methodology leverages feature fusion to provide an automated way to differentiate between PD and HC. Recently, various approaches for detecting PD have been utilized using EEG data. Compared to the proposed approach,

Table 3.6: The top-ranked features based on ETC

Channel	Feature
P4	Mean
F7	Mean, Standard deviation
AF3	Mean
FC1	Mean, Standard deviation
F3	Mean
O1	Mean, Hjorth complexity, Hjorth mobility
FZ	Mean, Standard deviation, Hjorth activity
PO4	Mean
O2	Mean, Hjorth mobility, Standard deviation
F8	Mean
FP2	Mean, Standard deviation
P8	Mean
F4	Mean
OZ	Mean, Hjorth complexity
FC5	Mean, Hjorth mobility
T7	Mean, Hjorth mobility, Hjorth complexity
PO3	Mean, Hjorth mobility, Standard deviation
CP6	Mean
CZ	Mean, Hjorth mobility, Hjorth complexity
FP1	Mean, Hjorth mobility, Hjorth complexity
C4	Standard deviation, Hjorth activity
PZ	Hjorth mobility
C3	Mean
CP1	Hjorth mobility, Standard deviation
P7	Hjorth complexity, Standard deviation
CP2	Standard deviation
FC6	Hjorth mobility, Standard deviation

Table 3.7: Performance analysis using top-ranked features for PD detection

Classifier	A_c	P_r	S_n	F_1^{sr}
NB	0.78±0.04	0.92±0.07	0.60±0.07	0.73±0.05
SVM	0.96±0.02	0.94±0.05	0.97±0.03	0.95±0.03
KNN	0.98±0.01	**0.98±0.02**	0.98±0.02	0.98±0.01
DT	**0.98±0.02**	0.97±0.03	**0.99±0.01**	**0.98±0.02**

they have employed distinct characteristics and classifiers.

Table 3.8 shows a comparison of classification performance to other existing approaches for PD detection. The average classification accuracy, precision, sensitivity, and F-1 score achieved using the 5-fold cross-validation technique are 98%, 97%,

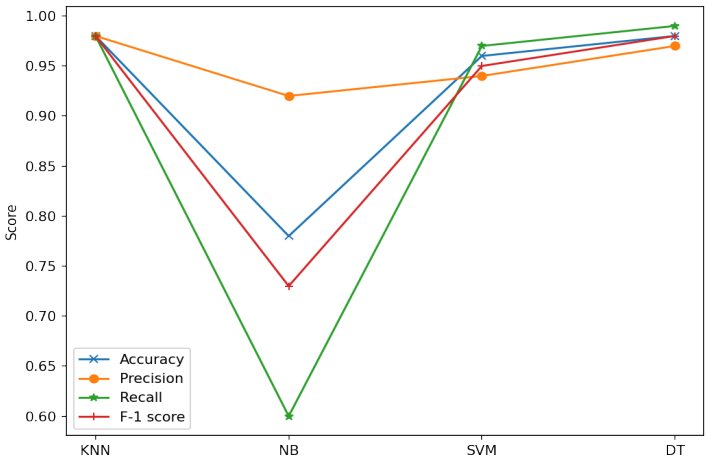

Figure 3.3: Performance comparison of different models for PD detection

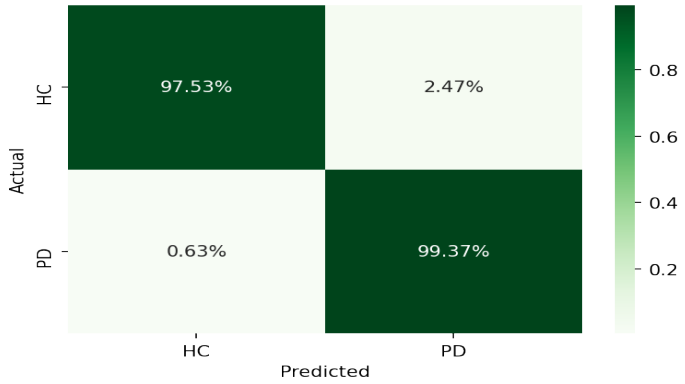

Figure 3.4: Confusion matrix of DT classifier for PD detection

Table 3.8: Performance evaluation of the feature selection driven PD detection method in contrast to existing methods

Authors	Dataset	Classifier	$A_c(\%)$
Chawla et al. 2023 [111]	EEG	KNN	95.85
Kamalakannan et al. 2021 [227]	EEG	ANN	88.17
Khare et al. 2021 [114]	EEG	LSSVM	96.13
Khoshnevis and Sankar 2021 [110]	EEG	Ensemble RUSBoosted trees	87
Proposed method	**EEG**	**DT**	**98**

99%, and 98%, respectively. The proposed method has the potential to detect PD effectively with less computational complexity.

3.2 A Two-Stage Ensemble Approach for the Analysis of Parkinson's Disease Using Speech Signals

3.2.1 Introduction

Speech disorders are experienced by approximately 90% of patients in the early stages of PD [230]. The speech impairment commonly observed in PD is known as hypokinetic dysarthria, which primarily affects articulation, respiration, and voice quality. Recently, many studies have been conducted utilizing speech datasets to detect PD in the initial stage. In earlier research, limited attention has been given to effective feature selection methods. Many existing studies have either not utilized feature selection or have employed only basic techniques, which may not fully capture the most informative attributes for model learning. Additionally, the majority of earlier research focused on single classifiers. But the problem with single classifiers is that, at times, they may lack accuracy and precision, which can be achieved using a stacking-based method. Sometimes, these classifiers adversely affect the errors and downgrade their performance with respect to overfitting, generalization, and bias of the model, hence resulting in poor prediction. Also, most of the research has not dealt with class imbalance problems, which could result in biased model performance favoring the majority class and decreasing diagnosis reliability. To address all these problems, this work proposes a two-stage PD detection approach. In the first stage, an ETC-based feature selection approach has been applied in order to reduce the non-required speech features, and in the second stage, a new model is built by stacking three ML algorithms. The proposed method provides better results by simply taking the speech features of PD patients.

3.2.2 Proposed Methodology

This method aims to boost the accuracy and speed of PD diagnosis in the context of an intelligent network by a stacked ensemble model. Figure 3.5 illustrates the block diagram of the stacked ensemble model for PD detection. The acquired PD speech data is used to train the classifier using the following steps. Firstly, the raw data is

pre-processed, and then the ETC-based feature selection technique is used to acquire the optimum set of features. Afterward, SMOTE is applied to overcome the class imbalance problem. Different base learners and meta-learners are used separately to evaluate their performance.

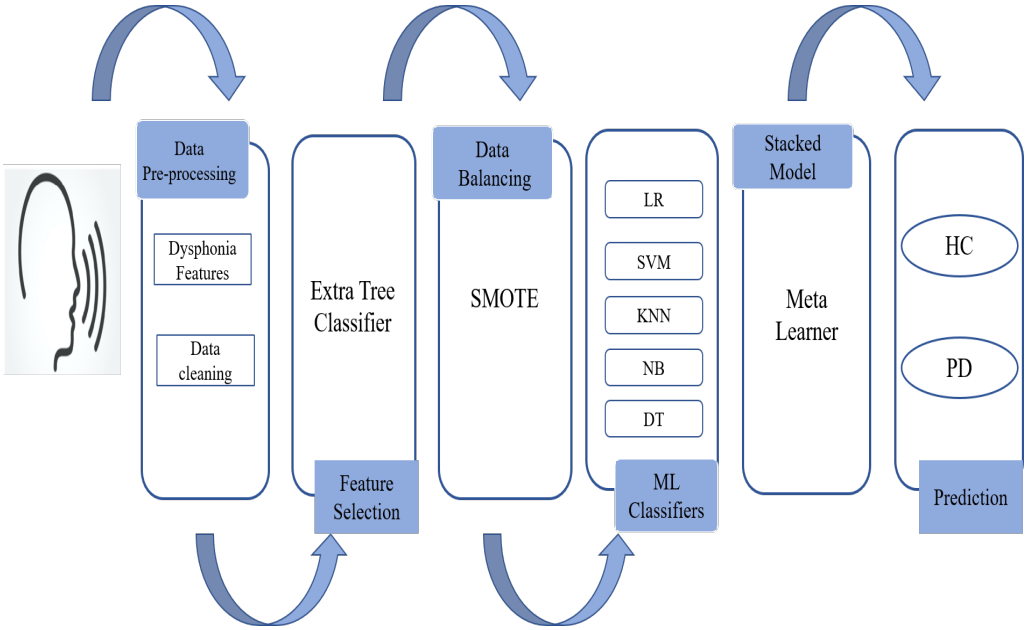

Figure 3.5: Block diagram of the stacked ensemble model for PD detection

3.2.2.1 Dataset Description

This work utilizes the dataset from the renowned UCI ML repository [231]. It is the speech dataset of 31 people whose age ranges from 46 to 85, of which 23 are diagnosed with PD, while the rest are HC. The speech signals are sampled at 44.1 kHz and 16 bits of resolution. Amplitude normalization is performed before calculating the features. The dataset comprises 195 sustained vowel phonations extracted from the speech signals of 31 individuals. Each person provides an average of six phonation recordings. Dysphonia measurements are utilized to distinguish between HC and PD patients. Table 3.9 portrays the features retrieved from speech signals. The dataset contains 22 features derived from speech signals using the Pratt software. The data does not contain any missing values. There are 147 PD phonetics and 48 healthy phonetics. The class is specified by the status column in the data, where 0 represents HC and 1 represents PD patients.

Table 3.9: List of dysphonia features extracted from speech signals for PD detection

Feature Name	Feature Description
Shimmer: APQ3	3- Point amplitude perturbation quotient.
Shimmer: APQ5	5- Point amplitude perturbation quotient.
Shimmer: DDA	Difference of amplitude differences.
Jitter: DDP	Variation in fundamental frequency.
MDVP: Jitter(%)	Jitter value in percentage.
MDVP: Jitter(Abs)	Absolute value.
MDVP: Fo (Hz)	Average vocal fundamental frequency.
MDVP: Fhi (HZ)	Maximum vocal fundamental frequency.
MDVP: Flo (HZ)	Minimum vocal fundamental frequency.
MDVP: PPQ	Five point period perturbation quotient.
MDVP: APQ	Variation in amplitude.
MDVP: RAP	Relative average perturbation.
MDVP: Shimmer	Amplitude variation.
MDVP: Shimmer (dB)	Amplitude variation in dB.
Spread 1	Nonlinear measure of fundamental frequency.
Spread 2	Nonlinear measure of fundamental frequency.
HNR	Harmonic to Noise ratio.
NHR	Noise to Harmonic ratio.
DFA	Detrended fluctuation analysis.
D2	Correlation dimension.
PPE	Pitch period entropy.
RPDE	Recurrence period density entropy.
Status	Health status of the person
	1: Person with PD.
	0: Healthy person.

3.2.2.2 Feature Selection

Feature selection aims to remove features that are insignificant or irrelevant. This is a technique for selecting a subset of crucial characteristics that accurately identify the

problem. It becomes a necessity to determine the most important features as datasets having insignificant features result in the reduction of the model accuracy. Feature selection proceeds through a process of selecting requisite features from the prime features [232]. In this work, an ETC-based feature selection approach is utilized for selecting the optimal set of features. For this dataset, the top ten features are selected by ETC. Figure 3.6 represents the ranking of the top ten features generated by ETC.

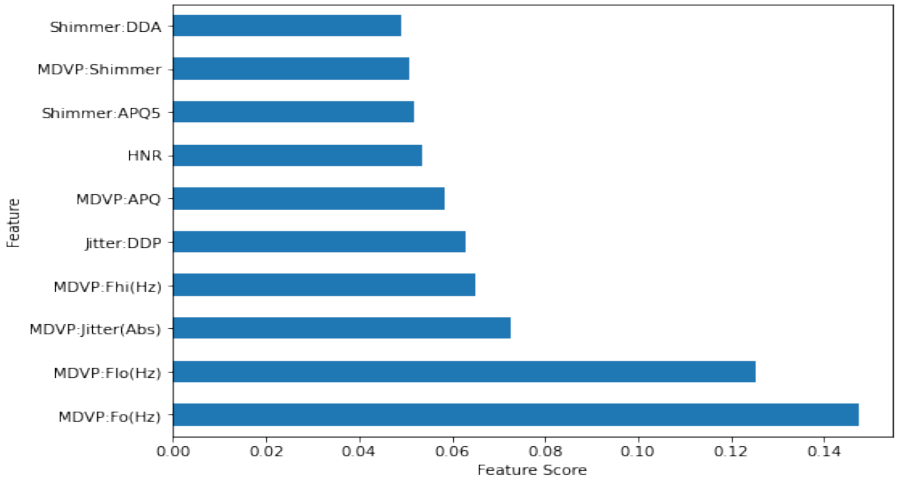

Figure 3.6: Optimal subset of features obtained using ETC-based feature selection

3.2.2.3 Data Balancing

One of the main issues with the healthcare dataset is the imbalance of class instances. This indicates the instance is not being appropriately distributed among the different classes. As a result, the classification results from the imbalanced class data are biased, favoring the dominating class. So, SMOTE is used to balance the dataset. SMOTE is an oversampling technique where the minority class generates the synthetic samples [233]. The problems like overfitting, posed by random oversampling, can be overcome by this algorithm. It primarily focuses on the feature space, which, using interpolation between the positive instances, goes side by side, resulting in bringing out new instances. SMOTE sorts out examples that have occurred in proximity to a feature space. It then picks up a new example at a certain point along with the segment, while also joining other adjacent examples. SMOTE then, at random, opts for an instance from the minority class and then computes its KNN. After that, a

random neighbor is chosen. Then, at a point selected at random between the two examples, a synthetic example is created. This process can help in generating as many synthetic examples as are needed for any particular minority class to create a balance.

3.2.2.4 Classifiers

In this work, various types of prominent supervised ML algorithms are used for PD detection. The labeled training dataset is initially utilized in supervised ML algorithms to evaluate the basic algorithm, and in the testing phase, these classifiers are used to identify whether a test instance is an HC or a PD patient.

3.2.2.5 Stacked-based Model

Stacking is one of the most renowned ensemble modeling techniques used in ML. To predict better predictions, a number of weak learners are ensembled in a parallel manner, such as to make a combination with meta learners. Algorithm 1 describes the stages involved in the stacked model.

Algorithm 1: Algorithm of stacked model for PD prediction

Input: Speech dataset, $D = \{d_1, d_2, \ldots, d_n\}$,

Base learners = DT, NB, KNN

Base learner's predictions, $BP = \{BP_1, BP_2, BP_3\}$.

Output: Classification of speech signals [PD or HC].

1: Data collection.

2: Data distribution into train and test data.

Training data=0.8

Testing data=0.2

for each learner $BP = \{BP_1, BP_2, BP_3\}$ **do**

3: Train base learners using training data (D),

4: Optimize the base learners until the minimum error is achieved.

end for

5: Integrate the predictions from base learners.

6: Training of Meta learner.

7: Apply test data on meta learner

8: Return Predicted Results.

This ensemble technique is used to achieve an improved model for output prediction by applying the input of meta-learners and combining multiple weak learners' predictions. While performing stacking, the outputs of sub-models are taken as input

and combined to anticipate the desired outcome. Stacking, at times, is also called a stacked generalization. Multiple base learners are trained on the same data and then use a meta learner to keep the predictions synthesized. Figure 3.7 portrays the flow chart of the stacked model.

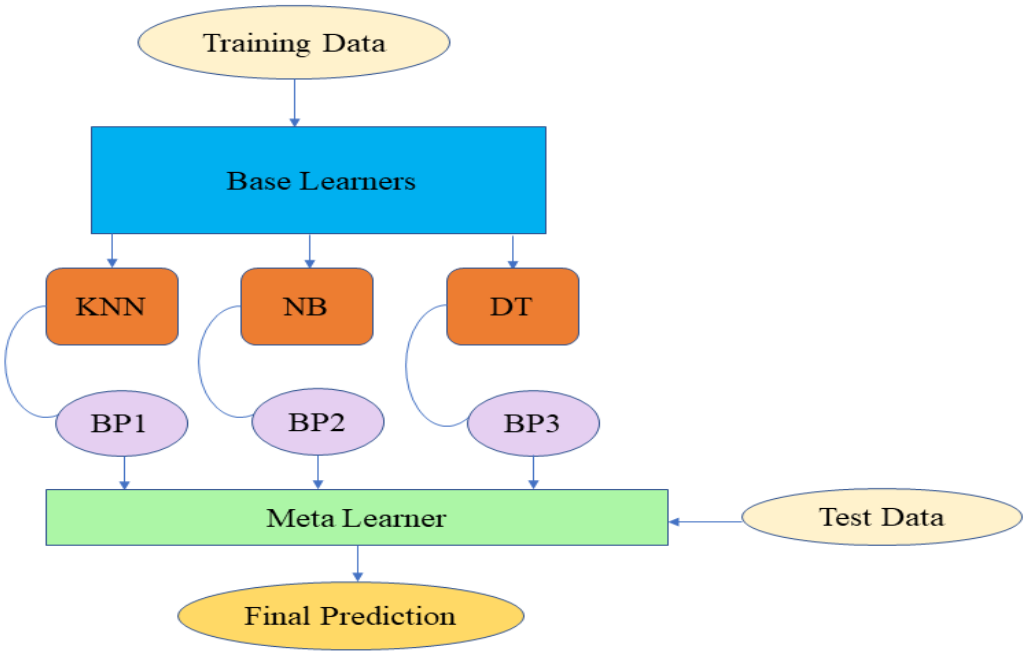

Figure 3.7: Flow chart of stacked-based ensemble model for PD detection

3.2.3 Experimental Results

The proposed work's performance is assessed using a variety of performance metrics, like accuracy, selectivity, sensitivity, and AUC.

3.2.3.1 Impact of Feature Selection

Prior to feature selection, the dataset had 22 features. To acquire the strongly linked features, the ETC-based feature selection approach is used. The top ten optimal features are selected based on their scores. As the dataset was imbalanced, SMOTE was used to balance the dataset. The dataset is divided into training and testing sections. 80% of the data is used for training, while 20% is used for testing purposes.

In order to analyze the performance, popular ML classifiers are utilized.

To increase the performance of classification models, feature selection plays a crucial role by removing extraneous attributes from the dataset. The dataset is condensed using feature selection into a subset that retains the same degree of classification or information as the data in its initial form. The ranking of the most important attributes is determined using the inferences drawn from the proposed method. The ETC-based feature selection procedure is carried out to determine the top ten attributes. These features are used as input to different ML classifiers, which distinguish them into speech samples from healthy or PD patients. Each classifier included in the model has undergone extensive training using several feature combinations. The results of the single classifiers without feature selection are presented in Table 3.10.

Table 3.10: Performance comparison of different ML algorithms without feature selection for PD detection.

Classifier	A_c (%)	S_n (%)	S_p (%)	AUC (%)	P_r (%)	F_1^{sr} (%)
LR	71.79	78.12	42.85	60.49	86.21	81.97
KNN	76.92	84.38	42.85	63.61	87.10	85.71
SVM	74.35	81.25	42.85	62.05	86.67	83.87
DT	79.49	90.62	28.57	59.60	85.29	87.88
NB	61.54	56.25	85.70	70.98	94.74	70.59

3.2.3.2 Impact of Stacked-based Ensemble Model

The stacked model combines the advantages of several distinct models to improve prediction accuracy and performance parameters. A stacked-based ensemble method that consists of DT, NB, and KNN is used after selecting the most relevant features. The selection of the classifier is done on the basis of their individual performance. The top ten features based on their feature score are taken into account for PD detection. Table 3.11 depicts the proposed model's detection results in the UCI PD speech dataset. The results of the stacked model for classification are compared to various classifiers, such as LR, NB, DT, KNN, and SVM.

As demonstrated in Table 3.11, the stacked model outperformed the distinct clas-

Table 3.11: Performance comparison of different ML algorithms and proposed stacked model with ETC-based feature selection method for PD detection

Classifier	A_c (%)	S_n (%)	S_p (%)	AUC (%)	P_r (%)	F_1^{sr} (%)
LR	79.67	82.76	76.67	79.71	77.42	80
KNN	89.83	79.31	100	89.65	100	88.46
SVM	79.67	75.86	83.34	79.59	81.48	78.57
DT	96.61	93.10	100	96.55	100	96.43
NB	83.05	68.97	96.67	82.81	95.24	80
Stacked Model	98.31	96.55	100	98.27	100	98.25

sifiers, with accuracy, sensitivity, specificity, and AUC values of 98.31%, 96.55%, 100%, and 98.27%, respectively. Furthermore, selecting features based on ETC not only improves the performance of the model but also considerably upgrades the overall performance of conventional ML methods. Figure 3.8 depicts the proposed method's performance metrics comparison with several classifiers.

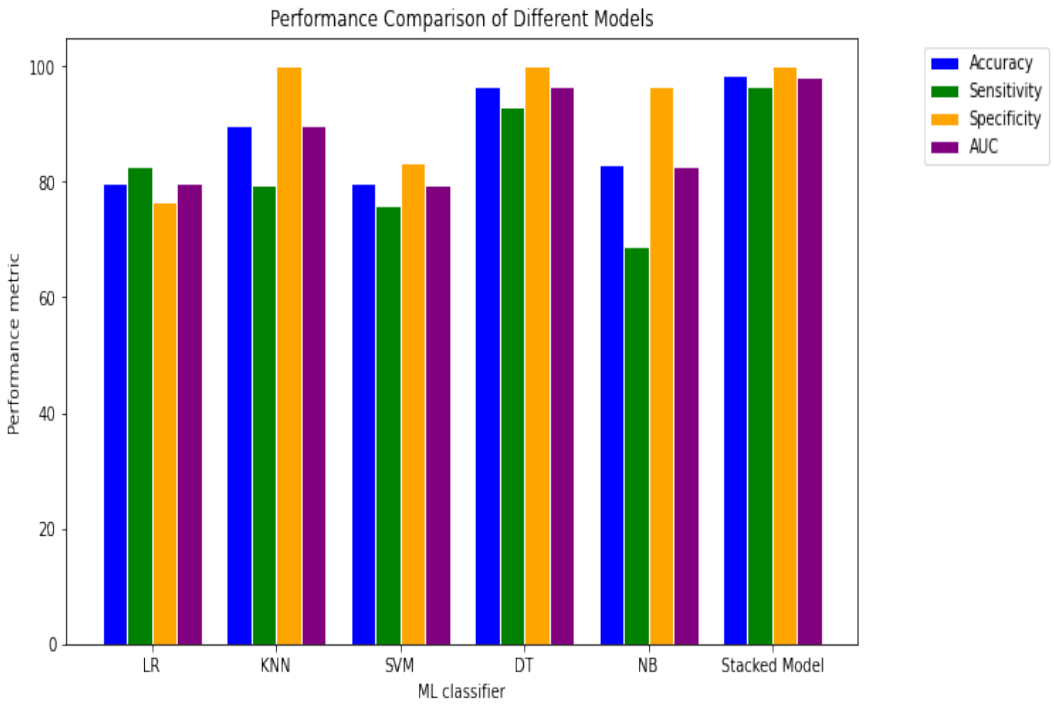

Figure 3.8: Performance measure comparison for PD detection

3.2.4 Discussion

Speech signals are widely used to analyze and detect PD. To detect PD using speech signals, a two-stage stacked-based ensemble technique has been presented in this work. The results of the suggested framework are compared with existing approaches on the same dataset. Table 3.12 shows the performance comparison of the two-stage stacked-based ensemble framework with other existing methods.

Table 3.12: Performance evaluation of the two-stage stacked-based ensemble method in comparison to other existing methods

Year	Authors	Feature selection	Number of features	Classifier	Results			
					A_c (%)	S_n (%)	S_p (%)	AUC (%)
2020	Thapa et al. [132]	Correlation	13	TSVM	93.90	88	99	93.9
2020	Senturk et al. [28]	RFE	13	SVM	93.84	-	-	-
2020	Despotovic et al. [76]	ARD	-	Gaussian Process	96.92	90	99.29	-
2021	Liu et al. [234]	wLDPP	-	ELM	89.17	90.69	95	-
2021	Ouhmida et al. [65]	mrMR and Relief	8	KNN	97.92	97.92	100	98.26
2022	Li et al. [77]	LDA	-	RF	97.50	98.33	95	-
2022	Haritha et al. [146]	FCM	10	RF	91.83	-	-	-
2023	Xue et al. [235]	LDFSF	5	Gaussian process	98.20	92	99.50	-
2023	Rahman et al. [180]	-	-	DNN	95.41	95	-	-
2023	Elshewey et al. [135]	-	-	Bo-SVM	92.3	92.3	-	-
2024	Shyamala and Navamani [134]	RFE	15	XGB	96.61	97.73	-	97.73
2024	Akila and Nayahi [152]	MASS	-	Neural netwwork	96.77	-	-	-
2024	Saha et al. [236]	-	-	GCN	97.4	97.4	-	-
2024	**Proposed method**	**ETC**	**10**	**Stacked model**	**98.31**	**96.55**	**100**	**98.27**

In this work, a feature selection-based decision support system is developed by extracting features from PD patients' and HCs' speech signals. Distinct feature selection approaches were applied by various researchers. Thapa et al. [132] utilized a correlation-based feature selection approach and attained an accuracy of 93.90% using

the TSVM classifier. Senturk et al. [28] incorporated RFE feature selection method in conjunction with the SVM classifier, and obtained 93.84% accuracy. Authors in [65, 76, 77, 134, 146, 152, 234] used different feature selection approaches such as ARD, wLDPP, mrMR, Relief, LDA, RFE, FCM, and multi-agent salp swarm algorithm (MASS) with different ML models, achieving an accuracy of 96.92%, 89.17%, 97.92%, 97.50, 96.61%,91.83%, and 96.77%, respectively. Rahman et al. [180] explored different ML methods and deep neural networks (DNN) to predict and categorize PD. A hyperparameter tuning technique based on Bayesian optimization (BO) was used to obtain better PD detection accuracy in [135]. Recently, Xue et al. [235]. utilized the Local dynamic feature selection fusion method (LDFSF) and obtained an accuracy of 98.20%. Saha et al. [236] developed a Euclidean distance-based-graph convolutional neural network (GCN) and achieved 97.4% classification accuracy.

Existing studies employed single classifiers along with various feature selection strategies. To enhance the overall performance of PD detection, this work introduces a two-stage stacked-based approach. The proposed technique differs from the literature in terms of the feature selection method and a stacked-based classifier. The suggested model effectively reduces computation time by taking less number of features and outperforms the current methods with a maximum accuracy of 98.31% for PD detection.

3.3 FHESA: Fourier Decomposition and Hilbert Transform Based EEG Signal Analysis for Alzheimer's Disease Detection

3.3.1 Introduction

AD is a progressive condition; its symptoms can range from mild ones that have no impact on a patient's day-to-day activities to severe ones that cause total cognitive decline, reliance, and ultimately death. Accurate and automatic detection of AD is important for preventing the progression of the disorder and providing appropriate

treatment so that individuals can carry out their daily activities effectively. EEG has been used as a viable diagnostic method for numerous neurodegenerative disorders due to its non-invasive nature and ease of availability. The proposed FHESA method aims to present a computationally efficient framework to accurately detect AD using EEG signals. The FDM decomposes the EEG signals into a limited number of orthogonal components known as Fourier intrinsic band functions (FIBFs). The HT method is employed to extract prominent features from each FIBF. These features are taken as inputs for several ML algorithms for detecting AD. The key contributions of the work are as follows:

- FDM is employed for the decomposition of EEG signals into a set of FIBFs , and valuable features are extracted using the HT method.
- Various ML algorithms (KNN, NB, DT, SVM, and LR) are used to evaluate model performance using a ten-fold cross-validation technique. The optimal classifier combination with the feature set is determined to obtain an accurate model for automatic AD detection.
- Analyzed the influence of various channels and performed brain area analysis at various lobes to identify significant regions affected by AD.
- The proposed FHESA approach for AD detection has been empirically validated using two distinct datasets (dataset-I and dataset-II), including EEG recordings from HCs and AD patients.
- The results of the experiments showed that the proposed FHESA method performs better than the existing state-of-the-art techniques used for AD detection.

3.3.2 Proposed Methodology

The proposed methodology consists of the following steps: (i) dataset acquisition and pre-processing; (ii) EEG signal decomposition using FDM; (iii) feature extraction; and lastly (iv) classification. The block diagram of the FHESA method is depicted in Figure 3.9.

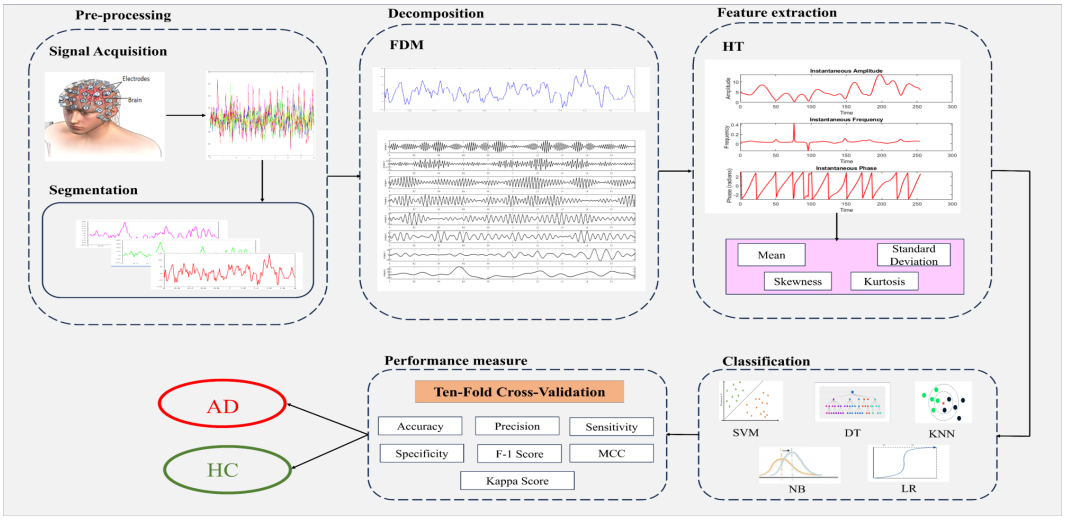

Figure 3.9: Block diagram of the FHESA method for AD detection

3.3.2.1 Dataset

Two distinct datasets (dataset-I and dataset-II) are used in this study to assess the capability of the proposed FHESA method. The datasets used are obtained from Florida State University researchers and are publicly available [237, 238].

- Dataset I:

  The dataset includes recordings obtained during two resting situations from four groups (A, B, C, and D). Groups A and C, who underwent visual fixation, kept their eyes open, while groups B and D kept their eyes closed during the recording. Groups A and B included 24 healthy older individuals aged 61 to 83 years. Groups C and D included 24 AD patients between the ages of 53 and 85 years, identified by the National Institute of Neurological and Communicative Disorders and Stroke and the Alzheimer's Disease and Associated Disorders Association. The International 10–20 system was used for signal recording from the brain's frontal (Fp1, Fp2, Fz, F3, F4, F7, F8), central (Cz, C3, C4), parietal (Pz, P3, P4), occipital (O1, O2), and temporal (T3, T4, T5, T6) regions using a Biologic Systems Brain Atlas III Plus workstation. The frequency range of the signals in the EEG recordings was restricted to the band of 1-30 Hz. The recordings were made for a duration of 8 seconds. Throughout the recording process, a technician was tasked with keeping an eye on the patient's level of

attentiveness. The EEG signals were recorded at a sampling frequency of 128 Hz (free of myogenic artifacts, eye movements, and blinking).

- Dataset II: Four separate groups are identified from the EEG signals in the dataset: Group A: Twelve old, healthy subjects who kept their eyes open and maintained visual fixation; Group B: Twelve old, healthy subjects who closed their eyes; Group C: Eighty AD patients who kept their eyes open; and Group D: Eighty AD patients who closed their eyes. The study did not categorize patients based on their level of cognitive impairment due to insufficient information on disease severity. The eight-second EEG segments were recorded with 19 scalp electrodes positioned in accordance with the International 10-20 technique and sampled at 128 Hz. The EEG signals were preprocessed by band-limiting them between 0.5-30 Hz and removing artifacts caused by subject movements by an expert EEG technician. To resolve the issue of data imbalance, out of each group, only 12 HC and 12 AD subjects are chosen for implementation. To analyze the EEG signals more precisely, they are separated into equal time segments. To obtain representative data, each participant's data is divided into two-second segments without overlapping.

3.3.2.2 Fourier Decomposition Method

The FDM is an adaptive signal-processing technique based on the Fourier theory and zero-phase filtering approach employed for analyzing the non-stationary and nonlinear characteristics of real-time signals [239]. It decomposes a given signal into a set of finite number of components (amplitude and frequency-modulated components) known as FIBFs. The FIBFs are intrinsic in the signal itself and are complete, local, adaptive, and an orthogonal set or a Linearly Independent Non-Orthogonal yet Energy Preserving (LINOEP) set such that the instantaneous amplitudes of these functions are always positive, and the instantaneous phases are nondecreasing functions that yield positive instantaneous frequencies. The EEG signals are decomposed using DCT. Figure 3.10 depicts the illustration of the FDM using a zero-phase filter bank based on DCT.

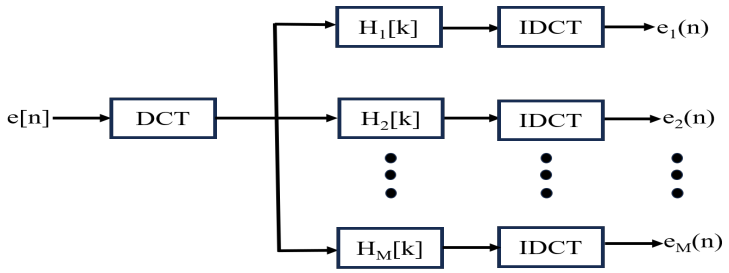

Figure 3.10: Decomposition of EEG signal $e[n]$ into a set of FIBFs of required frequency bands using DCT-based FDM

Eq. (3.9) represents the decomposition of a time series signal $e[n]$) of length M as follows:

$$e[n] = e_0 + \sum_{m=1}^{M} e_m[n] = e_0 + \sum_{m=1}^{M} l_m[n] \tag{3.9}$$

where, e_0 represents the mean value of the signal, $e_m[n]$ represents the m^{th} orthogonal FIBFs, and $l_m[n]$ denotes the m^{th} LINOEP. For the DCT-based FDM, the zero-phase filter response to decompose the signal $e[n]$ into various relevant frequency bands can be expressed as follows:

$$H_m[k] = \begin{cases} 1, & \mathrm{K}_{m-1} + 1 \leq k \leq K_m \\ 0, & \text{otherwise} \end{cases} \tag{3.10}$$

where, $m \in [1, M]$, K_0 = 0 and K_1, K_2,.., K_{m-1} are desired cutoff frequencies. The zero-phase filter frequency response $H_m[k]$ is 1 for required frequencies and 0 for other cases. In this work, the inverse DCT is employed to obtain the m^{th} FIBF $e_m[n]$ as,

$$e_m[n] = \sqrt{\frac{2}{N}} \sum_{k=0}^{N-1} \sigma_k H_m[k] E_{c2}[k] \cos\left(\frac{\pi k(2n+1)}{2N}\right) \tag{3.11}$$

The N length DCT of signal $e[n]$ is represented as $E_{c2}[k]$ and the normalization factor defined as,

$$\sigma_k = \begin{cases} 1, & \mathrm{k} \neq 0 \\ \frac{1}{\sqrt{2}}, & \mathrm{k} = 0 \end{cases} \tag{3.12}$$

After decomposing the original signal, the obtained FIBFs are zero-mean functions. The desired and valuable signal components can be more easily distinguished from the unwanted signal components with the help of the FIBFs. FDM can be implemented by FFT, making it computationally more efficient. The FDM presents a generalized Fourier expansion with variable amplitudes and variable frequencies of a time series by the Fourier method. Unlike EMD, which utilizes an empirical methodology and thus is not feasible to analyze analytically, the FDM approach has an extensive mathematical background. FDM can remove artifacts present in the signal and model mixing issues more effectively than EMD. Additionally, FDM can decompose the EEG into a set of FIBF with the required cutoff frequencies. The FIBFs generated by FDM for the EEG signals of HC and AD patients are depicted in Figure 3.11.

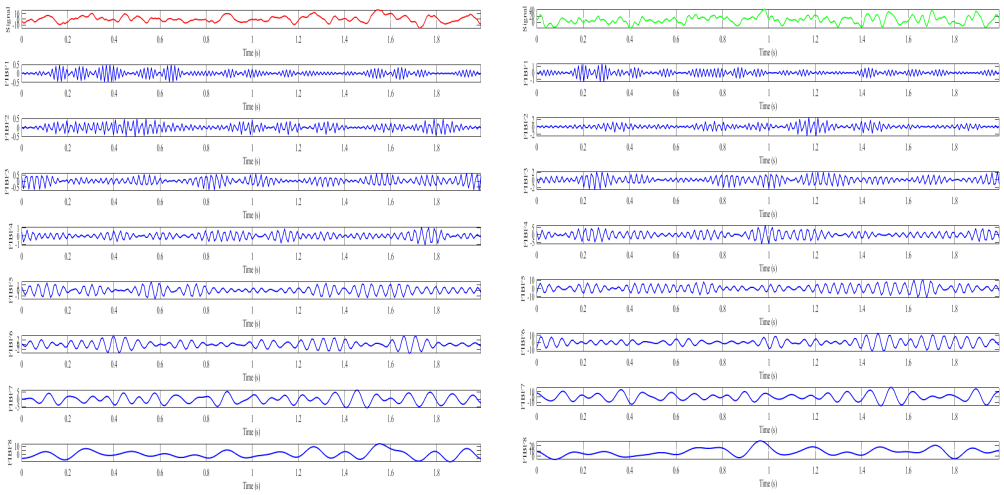

(a) AD (b) HC

Figure 3.11: Decomposition of AD and HC EEG recordings into identical frequency bands: FIBF1: 0–8 Hz, FIBF2: 8–16 Hz, FIBF3: 16-24 Hz, FIBF4: 24-32 Hz, FIBF5: 32-40 Hz, FIBF6: 40-48 Hz, FIBF7: 48-56 Hz, and FIBF8: 56-64 Hz

3.3.2.3 Feature Extraction

Extracting relevant information from the data is one of the crucial tasks. Identifying minor characteristics that aid in disease classification can be considered a feature. FDM expresses the signal as a set of FIBFs. HT is applied to all FIBFs to obtain instantaneous amplitude, frequency, and phase, which generate feature vectors for

categorization. In this work, HT is implemented to extract features from the FIBFs of both AD and HC classes.

3.3.2.4 Hilbert Transform

HT is a linear operator used to change a real signal's phase by Π/2. The HT of a time-domain signal x(t) can be defined as Eq. (3.13)

$$H(x(t)) = x(t) \circledast \frac{1}{\pi t} \tag{3.13}$$

The complex analytic signal of x(t) is presented by Eq (3.14)

$$X(t) = x(t) + jx_h(t) \tag{3.14}$$

where, $x_h(t))$ is the HT of signal $x(t)$. From the signal, the instantaneous amplitude, phase, and frequency can be determined as

$$|X(t)| = \sqrt{x^2(t) + x_h^2(t)} \tag{3.15}$$

$$\phi(t) = \arctan\left(\frac{x_h(t)}{x(t)}\right) \tag{3.16}$$

$$w(t) = \frac{d\phi(t)}{dt} \tag{3.17}$$

The instantaneous amplitude, phase, and frequency of the signal play a significant role in many scientific domains, including signal processing and medicinal applications [240, 241].

In this work, the FDM approach decomposes the EEG signal into eight FIBFs, which are then analyzed using the HT method for feature extraction. From each FIBF, the instantaneous amplitude, phase, and frequency are calculated, and four statistical features, including skewness, kurtosis, mean, and standard deviation, are derived from them. The extracted features from each segment of the EEG data produce a full set of feature vectors for different EEG channels. To make each attribute compatible with ML classifiers, they are all transformed into uniform scale values between 0 and 1.

3.3.2.5 Classification

In this work, we have employed several ML algorithms to create an AD detection model based on the feature vector computed with the proposed FHESA method.

Furthermore, the goal is to find the best classifier by contrasting the performance of the classifiers for AD detection. The acquired features are analyzed using ML methods such as KNN, SVM, DT, NB, and LR. The primary rationale for preferring these classifiers is that they are often utilized in the literature and have excellent classification performance in different medical applications. The algorithm of the proposed FHESA method is given in Algorithm 2.

Algorithm 2: AD detection using proposed FHESA method

Input: EEG signals

Output: Classification of EEG signals [AD or HC]

Step 1: Preprocessing

(i) Load the EEG signal

(ii) Read an EEG channel from EEG signals

(iii) Divide the EEG channel into non-overlapped segments

Let there is M number of segments e_1, e_2..., e_m.

Step 2: Decomposition

for each segment decompose it into FIBFs **do**

$$e_m[n] = \sqrt{\frac{2}{N}} \sum_{k=0}^{N-1} \sigma_k H_m[k] E_{c2}[k] \cos\left(\frac{\pi k(2n+1)}{2N}\right)$$

such that

$$e_1[n] = e_0 + \sum_{m=1}^{M} e_m[n] = e_0 + \sum_{m=1}^{M} l_m[n]$$

Let the FIBFs are FIBF-1, FIBF-2,...., FIBF-M.

Step 3: Feature extraction

for each FIBF **do**

(i) Apply HT to obtain the instantaneous amplitude, phase, and frequency corresponding to each FIBF

(ii) Concatenate all the features to get the corresponding feature vector

Step 4: Model Selection

for each classifier in KNN, NB, DT, SVM, and LR **do**

(i) Divide the feature vector into ten-folds

(ii) Train and test the ML classifier using one fold at a time.

(iii) Record the classifier's accuracy

(iv) Select the best-performing classifier

return Best combination of FIBF and classifier for AD detection

3.3.3 Results

To evaluate the effectiveness of the FHESA method, evaluation parameters such as accuracy (A_c), sensitivity (S_n), specificity (S_p), precision (P_r), F-1 score (F_1^{sr}), Cohen's Kappa score (K_{sr}), and Matthew's Correlation Coefficient (MCC) are used.

3.3.4 Performance Analysis

Dataset I

3.3.4.1 Analyzing the Eyes Open EEG Data

In this subsection, the classification findings for the AD vs HC classes utilizing all EEG channels are presented. The evaluation metrics of the classification process carried out by applying the ML approach for the features of the computed FIBFs for Dataset I are displayed in Table 3.13. For FIBF 1, the highest classification accuracy is achieved by the DT classifier with 97%, and the overall values of precision, sensitivity, specificity, F1-score, MCC, and Kappa score are 98%, 97%, 99%, 97%, 0.94, and 0.94, respectively. For FIBFs 2, 3, 4, and 5, the DT classifier also provides maximum classification accuracy. Experimental results indicate that FIBF 8 yields the best appropriate outcomes with NB classifier for AD and HC classification with an accuracy of 99%, and the overall value of precision, sensitivity, specificity, F1-score, MCC value, and Kappa score are 98%, 100%, 99%, 99%, 0.98, and 0.98 respectively, as presented in Table 3.13. Subsequently, the second-highest accuracy is obtained from FIBF 1. The least accurate performance of 63% is observed in the FIBF-2 for the KNN classifier using the eyes open EEG dataset.

3.3.4.2 Analyzing the Eyes Closed EEG Data

The EEG signals of subjects with closed eyes are taken independently for classification, and the assessment is obtained using the same criteria as those with open eyes. Table 3.14 demonstrates the classification results using closed-eye EEG recording on Dataset I. Table 3.14 illustrates that FIBF 8 produces the most accurate results for

Table 3.13: Performance analysis on Dataset I (eyes-open) using FHESA method for AD detection

FIBF	Classifier	Evaluation parameters						
		A_c	P_r	S_n	S_p	F_1^{sr}	MCC	K_{sr}
1	KNN	0.80±0.12	0.72±0.18	1.00±0.00	0.58±0.28	0.82±0.12	0.60±0.27	0.55±0.29
	NB	0.93±0.07	0.92±0.09	0.96±0.07	0.88±0.15	0.94±0.06	0.83±0.17	0.81±0.19
	DT	0.97±0.06	0.98±0.07	0.97±0.07	0.99±0.04	0.97±0.05	0.94±0.12	0.94±0.14
	SVM	0.97±0.04	0.96±0.07	1.00±0.00	0.92±0.15	0.98±0.04	0.94±0.12	0.92±0.13
	LR	0.97±0.04	0.95±0.08	1.00±0.00	0.92±0.15	0.97±0.05	0.93±0.11	0.92±0.13
2	KNN	0.63±0.08	0.68±0.19	0.74±0.19	0.63±0.20	0.67±0.08	0.33±0.18	0.28±0.15
	NB	0.78±0.09	0.83±0.15	0.78±0.10	0.79±0.20	0.79±0.07	0.53±0.20	0.50±0.20
	DT	0.83±0.08	0.88±0.12	0.81±0.13	0.85±0.15	0.83±0.08	0.65±0.15	0.62±0.17
	SVM	0.70±0.10	0.70±0.19	0.87±0.15	0.61±0.24	0.74±0.10	0.55±0.19	0.39±0.18
	LR	0.74±0.06	0.75±0.18	0.81±0.14	0.73±0.16	0.76±0.10	0.49±0.17	0.45±0.17
3	KNN	0.71±0.09	0.73±0.20	0.82±0.15	0.69±0.19	0.74±0.11	0.46±0.19	0.41±0.19
	NB	0.75±0.11	0.79±0.16	0.77±0.16	0.77±.19	0.76±0.11	0.50±0.23	0.47±0.24
	DT	0.87±0.14	0.86±0.20	0.84±0.16	0.89±0.16	0.84±0.17	0.74±0.28	0.73±0.28
	SVM	0.67±0.13	0.67±0.22	0.84±0.15	0.57±0.25	0.71±0.14	0.46±0.23	0$\dot{3}$3±0.18
	LR	0.75±0.13	0.76±0.20	0.84±0.17	0.74±0.23	0.77±0.14	0.53±0.23	0.49±0.23
4	KNN	0.68±0.13	0.65±0.22	0.84±0.22	0.50±0.28	0.71±0.18	0.34±0.30	0.28±0.29
	NB	0.72±0.06	0.73±0.13	0.72±0.09	0.67±0.26	0.72±0.10	0.35±0.22	0.34±0.21
	DT	0.81±0.11	0.80±0.16	0.82±0.15	0.84±0.12	0.80±0.13	0.60±0.21	0.58±0.21
	SVM	0.72±0.09	0.70±0.13	0.86±0.12	0.56±0.26	0.76±0.07	0.50±0.27	0.36±0.26
	LR	0.76±0.14	0.77±0.14	0.82±0.15	0.62±0.33	0.79±0.13	0.42±0.34	0.41±0.34
5	KNN	0.67±0.16	0.77±0.18	0.61±0.21	0.84±0.12	0.65±0.16	0.42±0.19	0.38±0.20
	NB	0.71±0.13	0.76±0.19	0.74±0.16	0.72±0.21	0.73±0.12	0.42±0.27	0.39±0.26
	DT	0.80±0.11	0.78±0.13	0.88±0.15	0.62±0.26	0.81±0.11	0.49±0.28	0.47±0.27
	SVM	0.65±0.12	0.67±0.23	0.79±0.16	0.59±0.24	0.69±0.14	0.42±0.26	0.29±0.19
	LR	0.69±0.07	0.71±0.20	0.74±0.21	0.70±0.24	0.69±0.13	0.40±0.15	0.34±0.13
6	KNN	0.80±0.12	0.76±0.19	0.90±0.14	0.62±0.27	0.81±0.15	0.53±0.31	0.50±0.30
	NB	0.72±0.11	0.71±0.16	0.81±0.21	0.64±0.20	0.73±0.15	0.42±0.18	0.38±0.18
	DT	0.81±0.14	0.82±0.16	0.78±0.18	0.84±0.16	0.79±0.15	0.59±0.28	0.58±0.28
	SVM	0.84±0.09	0.78±0.16	0.97±0.06	0.72±0.19	0.85±0.10	0.64±0.23	0.65±0.17
	LR	0.84±0.08	0.82±0.16	0.88±0.11	0.80±0.16	0.84±0.11	0.66±0.16	0.63±0.17
7	KNN	0.86±0.12	0.83±0.19	0.92±0.16	0.81±0.19	0.86±0.16	0.70±0.25	0.67±0.25
	NB	0.84±0.12	0.88±0.14	0.81±0.20	0.92±0.08	0.83±0.15	0.68±0.23	0.65±0.26
	DT	0.81±0.12	0.88±0.16	0.76±0.19	0.90±0.14	0.79±0.14	0.64±0.23	0.60±0.25
	SVM	0.90±0.10	0.86±0.17	0.93±0.15	0.89±0.12	0.89±0.14	0.71±0.24	0.76±0.23
	LR	0.90±0.11	0.89±0.18	0.90±0.17	0.93±0.11	0.88±0.15	0.78±0.23	0.77±0.24
8	KNN	0.97±0.04	0.95±0.08	1.00±0.00	0.95±0.08	0.97±0.05	0.95±0.08	0.94±0.09
	NB	**0.99±0.03**	**0.98±0.06**	**1.00±0.00**	**0.99±0.04**	**0.99±0.03**	**0.98±0.05**	**0.98±0.06**
	DT	0.90±0.06	0.93±0.11	0.88±0.11	0.96±0.06	0.90±0.07	0.78±0.15	0.75±0.17
	SVM	0.97±0.04	0.98±0.06	0.96±0.09	0.99±0.04	0.97±0.05	0.86±0.15	0.94±0.09
	LR	0.98±0.04	0.97±0.07	1.00±0.00	0.97±0.07	0.98±0.04	0.97±0.07	0.96±0.07

Table 3.14: Performance analysison Dataset I (eyes-closed) using FHESA method for AD detection

FIBF	Classifier	Evaluation parameters						
		A_c	P_r	S_n	S_p	F_1^{sr}	MCC	K_{sr}
1	KNN	0.77±0.13	0.68±0.18	1.00±0.00	0.53±0.16	0.79±0.13	0.60±0.14	0.53±0.17
	NB	0.93±0.07	0.92±0.11	0.95±0.10	0.90±0.15	0.93±0.07	0.85±0.13	0.83±0.15
	DT	0.97±0.05	0.95±0.10	0.99±0.04	0.97±0.06	0.96±0.06	0.94±0.10	0.93±0.11
	SVM	0.91±0.12	0.91±0.15	0.94±0.15	0.89±0.18	0.91±0.12	0.88±0.19	0.80±0.25
	LR	0.97±0.07	0.99±0.04	0.97±0.10	0.95±0.15	0.97±0.06	0.93±0.13	0.92±0.16
2	KNN	0.86±0.11	0.89±0.15	0.89±0.14	0.87±0.17	0.87±0.09	0.74±0.24	0.71±0.25
	NB	0.86±0.10	0.79±0.19	0.90±0.20	0.78±0.30	0.83±0.17	0.66±0.31	0.63±0.31
	DT	0.85±0.12	0.81±0.19	0.95±0.08	0.74±0.32	0.86±0.11	0.67±0.29	0.64±0.30
	SVM	0.89±0.09	0.85±0.16	0.94±0.11	0.81±0.30	0.88±0.11	0.70±0.29	0.70±0.29
	LR	0.87±0.08	0.85±0.16	0.90±0.13	0.81±0.30	0.86±0.10	0.68±0.27	0.66±0.27
3	KNN	0.82±0.11	0.88±0.15	0.74±0.19	0.94±0.07	0.79±0.15	0.66±0.18	0.63±0.21
	NB	0.82±0.13	0.79±0.20	0.94±0.15	0.73±0.33	0.83±0.13	0.65±0.29	0.60±0.30
	DT	0.78±0.14	0.76±0.15	0.85±0.21	0.73±0.28	0.78±0.15	0.54±0.35	0.51±0.34
	SVM	0.87±0.11	0.85±0.16	0.90±0.17	0.80±0.31	0.86±0.12	0.61±0.33	0.67±0.30
	LR	0.88±0.10	0.86±0.15	0.93±0.11	0.80±0.30	0.88±0.10	0.71±0.30	0.69±0.30
4	KNN	0.83±0.09	0.82±0.14	0.88±0.15	0.79±0.19	0.83±0.07	0.66±0.22	0.63±0.22
	NB	0.85±0.08	0.80±0.10	0.93±0.13	0.68±0.27	0.86±0.10	0.63±0.26	0.61±0.26
	DT	0.86±0.15	0.84±0.18	0.87±0.17	0.85±0.17	0.85±0.16	0.70±0.31	0.69±0.31
	SVM	0.85±0.11	0.83±0.12	0.92±0.12	0.75±0.29	0.86±0.08	0.68±0.33	0.64±0.35
	LR	0.87±0.12	0.86±0.11	0.92±0.12	0.79±0.30	0.88±0.08	0.69±0.37	0.68±0.36
5	KNN	0.75±0.18	0.89±0.18	0.61±0.26	0.91±0.16	0.68±0.23	0.53±0.30	0.49±0.31
	NB	0.66±0.19	0.63±0.22	0.78±0.21	0.56±0.34	0.67±0.18	0.31±0.35	0.29±0.34
	DT	0.74±0.15	0.73±0.14	0.80±0.20	0.62±0.26	0.74±0.13	0.41±0.33	0.40±0.32
	SVM	0.76±0.13	0.77±0.20	0.81±0.26	0.75±0.29	0.73±0.18	0.47±0.33	0.49±0.32
	LR	0.78±0.12	0.80±0.18	0.82±0.25	0.76±0.30	0.76±0.15	0.57±0.26	0.52±0.27
6	KNN	0.88±0.10	0.86±0.19	0.88±0.13	0.88±0.15	0.86±0.13	0.75±0.20	0.73±0.21
	NB	0.88±0.09	0.88±0.15	0.92±0.12	0.81±0.30	0.89±0.09	0.72±0.28	0.70±0.29
	DT	0.85±0.11	0.87±0.14	0.84±0.14	0.85±0.18	0.85±0.12	0.68±0.24	0.66±0.24
	SVM	0.89±0.10	0.89±0.15	0.88±0.15	0.89±0.15	0.87±0.10	0.73±0.22	0.76±0.20
	LR	0.82±0.09	0.83±0.18	0.81±0.13	0.86±0.15	0.81±0.10	0.66±0.18	0.63±0.19
7	KNN	0.89±0.12	0.80±0.19	1.00±0.00	0.83±0.19	0.88±0.12	0.81±0.18	0.79±0.22
	NB	0.86±0.09	0.82±0.19	0.93±0.12	0.84±0.17	0.84±0.10	0.75±0.15	0.71±0.17
	DT	0.87±0.13	0.85±0.16	0.88±0.13	0.87±0.18	0.86±0.13	0.73±0.25	0.71±0.26
	SVM	0.91±0.07	0.83±0.15	0.98±0.05	0.88±0.11	0.89±0.09	0.78±0.21	0.82±0.14
	LR	0.92±0.07	0.88±0.14	0.97±0.06	0.87±0.16	0.91±0.08	0.83±0.13	0.81±0.15
8	KNN	0.93±0.09	0.88±0.15	1.00±0.00	0.85±0.18	0.93±0.10	0.86±0.16	0.84±0.19
	NB	**0.98±0.04**	**0.99±0.04**	**0.99±0.04**	**0.95±0.15**	**0.99±0.03**	**0.94±0.12**	**0.93±0.14**
	DT	0.94±0.08	0.94±0.13	0.96±0.07	0.87±0.30	0.94±0.08	0.83±0.30	0.82±0.30
	SVM	0.96±0.07	0.93±0.13	0.99±0.04	0..95±0.09	0.95±0.08	0.87±0.23	0.91±0.14
	LR	0.97±0.05	0.96±0.09	0.99±0.04	0.97±0.07	0.97±0.05	0.94±0.10	0.93±0.11

AD and HC classification with the NB classifier, with accuracy, precision, sensitivity, specificity, F1-score, MCC, and Kappa score values of 98%, 99%, 99%, 95%, 99%, 0.94, and 0.93, respectively. The second-best results are obtained from FIBF 1 using the DT classifier, with a classification accuracy of 97%. The overall values of precision, sensitivity, specificity, F1-score, MCC value, and Kappa score are 95%, 99%, 97%, 96%, 0.94, and 0.93, respectively. The FIBF-5 shows the lowest performance accuracy of 66% for the NB classifier with the eyes closed EEG dataset.

Dataset II

To assess the effectiveness of the proposed FHESA method, Dataset II is also employed. The performance is evaluated using five classifiers for AD and HC classification. Figure 3.12 illustrates a comparative analysis of accuracy for different FIBFs using several ML classifiers on eyes-open and eyes-closed EEG data.

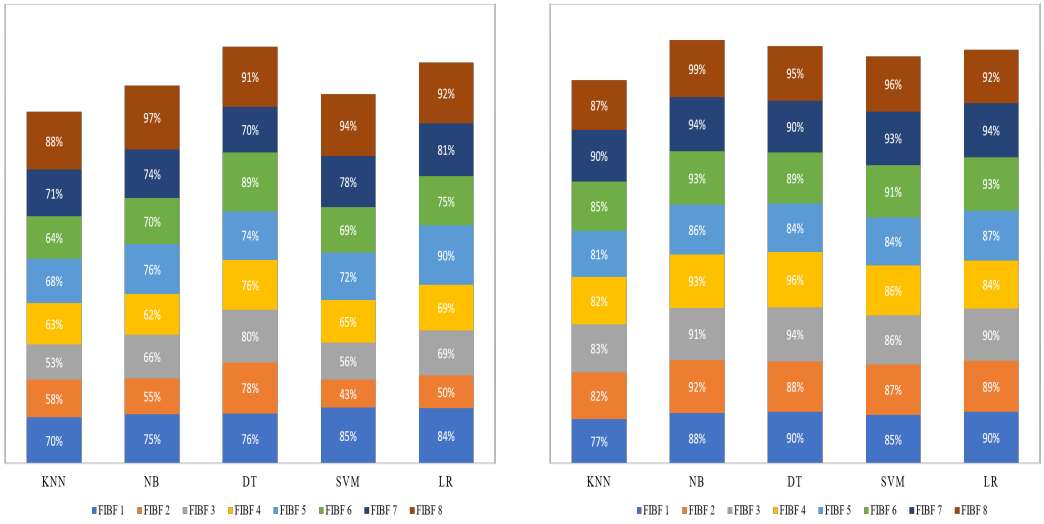

(a) Eyes-open EEG data

(b) Eyes-closed EEG data

Figure 3.12: Comparative analysis of accuracy for different FIBFs for AD detection on Dataset II

On comparing the accuracies of all FIBFs, the findings indicate that FIBF 8 produced the highest average accuracies among all FIBFs. Figure 3.13 illustrates the comparative analysis of performances among various ML classifiers using eyes-open and eyes-closed EEG data for FIBF 8. The results of the classifiers show that the NB

classifier gives the most accurate results for AD and HC classification, with accuracy, precision, sensitivity, specificity, F1-score, MCC, and Kappa score values of 97%, 97%, 99%, 93%, 97%, 0.91, and 0.90 respectively on eyes-open EEG recordings and 99%, 99%, 100%, 95%, 99%, 0.97, and 0.96 respectively on eyes-closed EEG recordings.

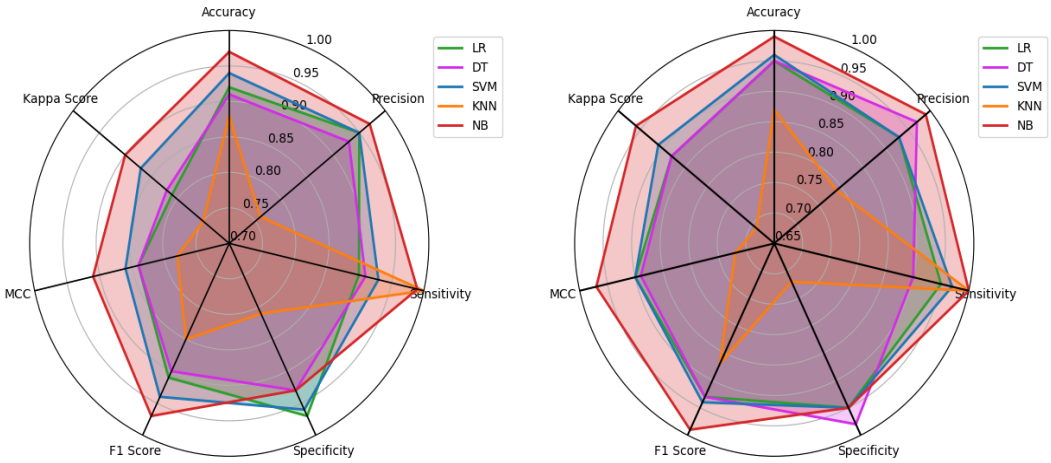

(a) Eyes-open EEG data

(b) Eyes-closed EEG data

Figure 3.13: Comparative analysis of performances among various ML classifiers for AD detection using FIBF 8 (Dataset-II)

The performance analysis indicates that the proposed FHESA approach is adaptable since it does not negatively affect the accuracies when applied to two distinct datasets. The FIBF 8 provides adequate results for AD and HC classification in both datasets.

3.3.4.3 Analyzing the Different Brain Regions and EEG Electrodes

The EEG acquisition system comprises many electrodes located on the scalp. The human brain is divided into different lobes. The frontal lobe (responsible for problem-solving, planning, thinking, judgment, and motor functions), the parietal lobe (manages sensation, handwriting, and body position), the occipital lobe (contains the brain's visual processing system), and the temporal lobe (involved with memory and hearing). The unusual changes observed in these lobes may provide valuable insights into brain structure. Therefore, individually, the specific brain region analyses are carried out for the frontal, central, occipital, parietal, and temporal regions. Table 3.15

illustrates the performance report for lobe-wise closed-eyes EEG data. The results depict that the temporal lobe electrodes provide an accuracy of 97% and the precision, sensitivity, specificity, F1-score, MCC, and Kappa score for ten-fold cross-validation 99%, 95%, 95%, 96%, 0.92, and 0.91, respectively.

Table 3.15: Performance analysis of different brain regions for AD detection.

Brain Region	Electrodes	Evaluation parameters						
		A_c	P_r	S_n	S_p	F_1^{sr}	MCC	K_{sr}
Temporal	T3, T4, T5, T6	0.97±0.05	0.99±0.04	0.95±0.11	0.95±0.15	0.96±0.07	0.92±0.12	0.91±0.14
Frontal	Fp1, Fp2, F3, F4, F7, F8	0.91±0.09	0.89±0.16	0.94±0.12	0.88±0.18	0.90±0.11	0.83±0.16	0.80±0.19
Parital	P3, P4, Pz	0.94±0.08	0.94±0.13	0.95±0.10	0.87±0.30	0.93±0.09	0.82±0.30	0.81±0.30
Occipital	O1, O2	0.92±0.10	0.91±0.16	0.95±0.10	0.84±0.31	0.92±0.11	0.79±00.30	0.77±0.31
Central	C3, C4, Cz	0.88±0.13	0.89±0.16	0.94±0.13	0.79±0.32	0.90±0.12	0.72±0.34	0.69±0.35

To identify which channel provides distinguishable information for AD detection. The impact of each channel is analyzed. Figure 3.14 depicts the varied performance of each channel for eyes-open and eyes-closed EEG data. Results demonstrate that, in both scenarios, the proposed FHESA model obtained the maximum classification accuracy by channel T5, scoring 93% for the eyes-open dataset and 95% accuracy for the eyes-closed dataset. The T5 electrode is situated in the temporal region. The analysis performed on different channels and different brain region electrodes confirms the importance of highly contributing channels. To obtain a better understanding of the brain regions involved in the identification of AD, topographic maps are generated. Figure 3.15 illustrates the topographic maps presenting the accuracy of various channels. Experimental results obtained for distinct datasets show that the proposed FHESA methodology is consistent and accurate for AD detection.

3.3.4.4 Statistical Analysis

To confirm the statistical significance of our model's performance, we performed some hypothesis tests. The ANOVA and Friedman tests are used to identify changes

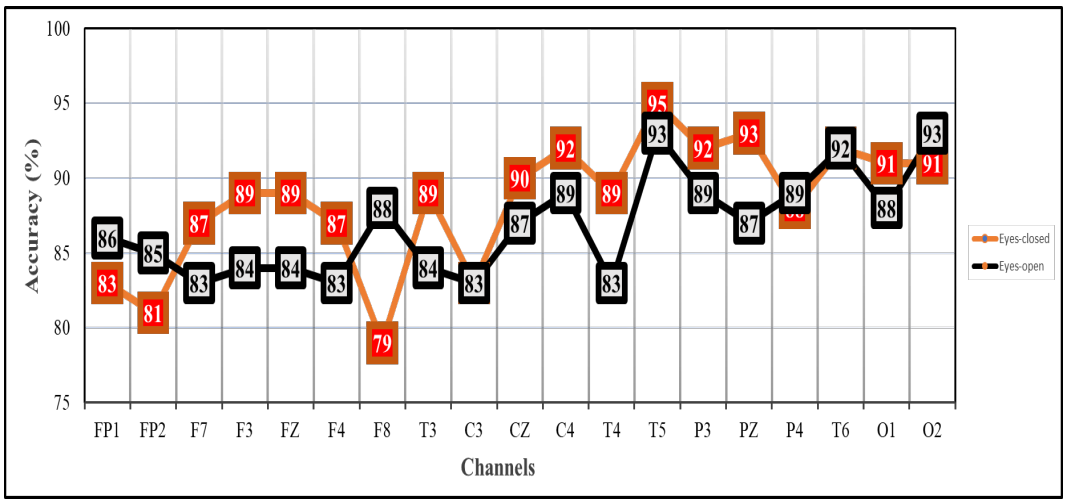

Figure 3.14: Channel-wise performance obtained for AD detection

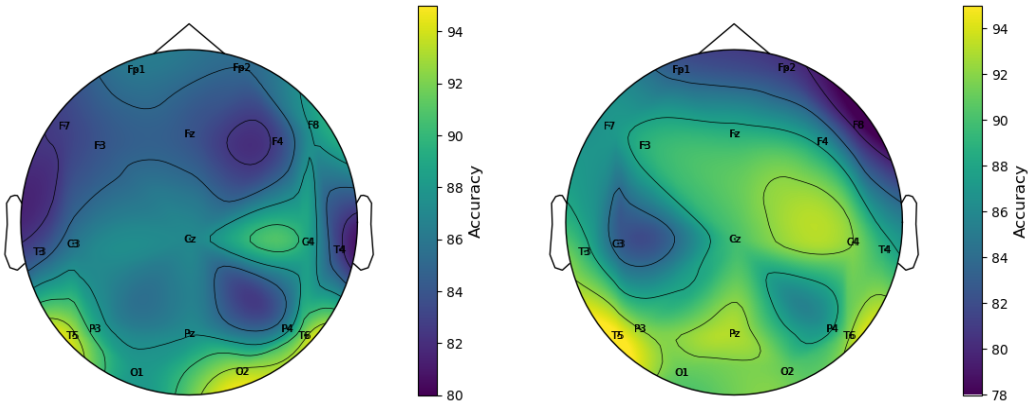

(a) Eyes-open EEG data

(b) Eyes-closed EEG data

Figure 3.15: Topographic map obtained for the EEG channels

in classification accuracy between models. The ANOVA test is primarily used to see if there are statistically significant differences in the means of three or more independent groups, and the Friedman test, a non-parametric alternative to ANOVA, is useful for analyzing more than two related groups. We used ANOVA and the Friedman test to compare the accuracy score of five models: KNN, NB, DT, SVM, and LR. For the eyes-open dataset, the ANOVA test yielded an F-statistic of 4.830 and a p-value of 0.003, with a large effect size of $\eta^2 = 0.300$, indicating substantial group differences. The corresponding Friedman test supported this result with a chi-square statistic of 11.556 and a p-value of 0.021. Similarly, for the eyes-closed dataset, ANOVA

produced an F-statistic of 2.627 and a p-value of 0.047, and the Friedman test yielded a chi-square value of 11.926 and a p-value of 0.018 with an effect size of $\eta^2 = 0.189$, suggesting a moderate effect, indicating statistically significant differences in model accuracies. These findings are consistent across both parametric and non-parametric methods, reinforcing the robustness of the observed performance differences among models.

3.3.5 Discussion

The FHESA method is introduced to detect AD using EEG signals. The influence of various channels and analysis of brain areas across various lobes are conducted to identify significant regions affected by AD. Two different datasets comprising EEG recordings were used in this work. The FDM is employed to decompose the EEG recordings into a group of FIBFs. Thereafter, significant features are extracted using the HT method and applied as inputs to various ML classifiers for the classification of AD and HC.

The FHESA method is contrasted with the existing state-of-the-art approaches employing the EEG dataset. Table 3.16 illustrates the performance comparison of the FHESA method with existing state-of-the-art techniques using EEG signals for AD detection. The features from the EEG signal were directly extracted in [137, 202]. Biagetti et al. [137] employed a Robust Principal Component Analysis (R-PCA) method for extracting significant features from 13 participants' EEG recordings for AD and HC classifications. Four different ML classifiers were used to classify these features. The Gaussian SVM attained a maximum accuracy of 93.18% for AD classification. As EEG signals are highly non-stationary, the system's performance is limited by the analysis of features derived directly from EEG. Different decomposition techniques: EMD, DWT, VMD, TQWT , and wavelet transform were applied to identify representative and hidden qualities in order to achieve the required performance [51–53, 56–59]. Oltu et al. [51] utilized DWT to extract EEG into different sub-bands and then used Burg's approach to evaluate Power Spectral Density (PSD) and coherence across each sub-band. Descriptive statistics, such as the sum and

variance, are used as input features. They tested this approach on 35 subjects using the bagged trees classifier and attained 96.5% accuracy. Puri et al. [57] extracted nine IMFs from each EEG wave using EMD. From these IMFs, ten distinct features were extracted. The LS-SVM classifier was trained and tested using these features and obtained a maximum classification accuracy of 92.9% for IMF-4 employing ten-fold cross-validation.

Table 3.16: Performance comparison of the FHESA method with existing state-of-the-art techniques using EEG signals for AD detection

Author	Year	Method	Classifier	Evaluation parameters				
				A_c (%)	S_n (%)	S_p (%)	P_r (%)	F_1^{sr} (%)
Biagetti et al. [137]	2021	R-PCA	Gaussian SVM	93.18	-	-	-	-
Oltu et al. [51]	2021	DWT+PSD+Coherenc	Bagged trees	96.5	96.21	97.96	-	-
Safi and Safi [52]	2021	DWT+Hjorth parameters	KNN	97.64	95.40	98.81	-	-
Sharma et al. [53]	2021	Wavelet transform	SVM	87.59	-	-	-	-
Perez-Valero [202]	2022	Self driven analysis pipeline	MLP	95	-	-	-	88
Cura et al. [54]	2022	STFT	SVM	92	-	-	-	-
Fouladi et al. [55]	2022	CWT	Modified CNN	92.7	91.26	-	70.48	79.57
Araujo et al. [136]	2022	Discrete wavelet packet transform	SVM	81	-	-	-	-
Puri et al. [56]	2022	TQWT+non linear features	EBT	96.20	90.49	97.50	-	-
Puri et al. [57]	2022	EMD+Hjorth Parameters	LS-SVM	92.90	94.32	94.34	94.33	94.32
Alves et al. [183]	2022	Matrix of connection	CNN	92	83	-	100	-
Fouad et al. [58]	2023	Wavelet transform+ statistical parameters	Naive Bayes	96.55	94.54	96.29	98.11	-
Xia et al. [184]	2023	Overlapping sliding windows	DPCNN	97.66	98	-	-	97.83
Imani [242]	2023	LMCN	ANN	98	100	87	100	98
Goker [243]	2023	Multitaper method	Logit Boost	93.04	92.75	93.33	93.43	93.09
Miltiadous [185]	2023	Band power and Coherence features	Dual input convolutional encoder	83.28	78.81	87.94	-	84.12
Nour et al. [186]	2024	Deep ensemble learning	2D-CNN	97	96	-	96	98
Aslan [59]	2024	VMD+statistical features	Rotation Forest	98.42	98	-	98	98

Author	Year	Method	Classifier	Evaluation parameters				
			Classifier	A_c (%)	S_n (%)	S_p (%)	P_r (%)	F_1^{sr} (%)
Kachare et al. [187]	2024	-	Lightweight CNN	98.50	100	97.55	-	-
Khosravi et al. [60]	2024	DWT+STFT	BiLSTM	96.52	-	-	-	-
Rezaee and Zhu [61]	2025	DWT+STFT	CascadeNet	98.84	98.76	-	98.67	98.71
Jain et al. [244]	2025	Synchrosqueezing	InceptionV3	98.50	94.59	81.02	94.73	79.12
Proposed	**2025**	**FHESA**	**NB**	**99**	**100**	**99**	**98**	**99**
		FHESA	**NB**	**98**	**99**	**95**	**99**	**99**
		FHESA	**NB**	**97**	**97**	**99**	**93**	**97**
		FHESA	**NB**	**99**	**99**	**100**	**95**	**99**

- Not reported

Safi and Safi [52] used several signal decomposition techniques, such as DWT and EMD, for decomposing EEG signals. Specific characteristics, like variance, kurtosis, skewness, Shannon entropy, and Hjorth parameters, were then retrieved from the decomposed signals. The accuracy of AD identification from EEG signals was improved by DWT in conjunction with the Hjorth parameters and attained an accuracy of 97.64%. Aslan et al. [59] employed VMD and extracted statistical features from decomposed signals and achieved 98.42% classification accuracy. Compared to traditional signal processing techniques, the decomposition approaches may be more advantageous when handling non-stationary EEG signals. Time-frequency analysis techniques STFT, SynchroSqueezing Transform (SST), and CWT employed in [54, 55]. Cura et al. [54] employed time-frequency representation (TFR) and deep feature extraction-based models for AD detection. High-resolution SST and STFT were used to obtain the TFR of EEG segments. To extract deep features, the SST and STFT magnitudes were utilized. For AD classification, the STFT-based deep feature extraction strategy produced superior classification results compared to the SST method.

Numerous studies have been conducted to identify AD through the analysis of EEG signals utilizing deep learning techniques [183–186, 242]. Xia et al. [184] employed a deep pyramid CNN to diagnose AD. Sliding window augmentation of the 1-D EEG data was used to overcome the problem of restricted data size. Imani

et al. [242] detected AD by combining CNN and bidirectional LSTM, known as the LMCN fusing framework. CNN was used to explore the relationships between EEG signals and LSTM networks to analyze temporal sequences. A fully connected neural network was then utilized to integrate the regional and temporal data. The LMCN framework provided 98% accuracy for AD detection. Miltiadous [185] deployed a dual-input convolution encoder network (DICE-Net) for AD detection. The band power and coherence features derived from the EEG signal were taken out and fed into the DICE-net. The DICE-Net contains a feed-forward layer, a transformer encoder, and convolution layers. Using LOSO validation, DICE-net obtained an accuracy of 83.28% for AD detection. Kachare et al. [187] developed a lightweight CNN model to distinguish the EEG signal of AD and HC and obtain 98.50% classification accuracy. In [60, 61, 244], 1D EEG data were converted into 2D time-frequency representations by STFT and Synchrosqueezing transform. After being translated into 2D representations, CascadNet and InceptionV3 were used to distinguish the 2D representation into AD and HC class. Nour et al. [186] classified AD using a 2-D CNN and deep ensemble learning (DEL) approach. Using five-fold cross-validation, the integrated system provided an average accuracy of 97.9% for AD detection. Although DL methods attained improved accuracy, their real-time applications are limited since they need a larger amount of data and take a longer time to train. Table 3.16 indicates that, in terms of accuracy, precision, sensitivity, specificity, and F-1 score, the proposed FHESA method performed more accurately in the AD classification. The proposed FHESA method has the following benefits: it is accurate (obtained the greatest classification accuracy), stable (provides the same performance with different datasets), resilient (tested using ten-fold cross-validation on two datasets), and effective.

3.4 Summary

This chapter presents three studies aimed at enhancing the accuracy and efficiency by employing robust feature selection techniques for brain disease detection.

✓ The first study investigates the use of EEG signals for early detection of PD,

where statistical and Hjorth features are extracted, and the Kruskal–Wallis test with an extra tree classifier is used for selecting the most discriminative attributes. Various machine learning classifiers are evaluated, achieving a maximum accuracy of 98% using the decision tree model.

- ✓ The second study explores a speech-based approach for PD detection, proposing a two-stage stacked ensemble model that integrates K-Nearest Neighbor, Decision Tree, and Naïve Bayes classifiers. Feature selection using the extra tree method and data balancing via SMOTE leads to an improved detection accuracy of 98.31%, outperforming traditional single-model approaches.
- ✓ The third study extends the optimization framework to Alzheimer's Disease detection using EEG signals. A Fourier Decomposition Method and Hilbert Transform-based EEG Signal Analysis (FHESA) technique is introduced to extract non-linear and non-stationary features from EEG data. The proposed method achieves 98% and 99% accuracy on two independent datasets, demonstrating its robustness and generalization capability.

Chapter 4

Design and Analysis of an Algorithm for the Classification of Neurological Disorders

This chapter presents a computational framework for the identification and classification of neurological disorders, specifically on AD and FTD. To address diagnostic challenges arising from overlapping clinical phenotypes, a wavelet scattering transform-based deep learning framework (WavDemNet) is proposed. The framework employs wavelet scattering transform (WST) to extract noise-robust, multi-scale time–frequency features, which are subsequently processed by a 1-D convolutional neural network (CNN) for discriminative pattern learning and precise classification.

4.1 WavDemNet: Wavelet Scattering Transform-based Dementia Identification and Classification Network.

4.1.1 Introduction

Dementia is a broader term that describes a set of symptoms characterized by a significant decline in cognitive abilities, such as memory, reasoning, problem-solving, communication skills, etc. AD and FTD are the two most prevalent forms of neurodegenerative dementia, each posing unique challenges for patients, caregivers, and the medical community. Although diagnostic criteria for both conditions are well-established, achieving an early and accurate diagnosis remains difficult due to overlapping clinical symptoms, particularly in the initial stages [245]. For instance, both AD and FTD may manifest as memory impairments, changes in behavior, or

difficulty with language, making it challenging to distinguish between them without advanced diagnostic tools. The lack of a cure for either condition is a reflection of the incomplete understanding of their underlying pathological mechanisms [246].

FTD is the third most frequent form of dementia in all age groups, following AD and Lewy body dementia [247]. AD is mainly associated with the accumulation of amyloid-beta plaques and tau tangles in the brain. Whereas, FTD involves the degeneration of the frontal and temporal lobes, often linked to abnormal deposits of proteins such as TDP-43 or tau. Despite these distinctions, early similarities in clinical presentation often lead to misdiagnosis, delayed treatment, and inappropriate management strategies. These challenges not only hinder the potential for timely interventions but also exacerbate the psychological stress and financial burden on patients and their families [248].

4.1.2 Proposed Methodology

This work proposes a hybrid framework that leverages WST for invariant and multi-scale feature extraction, and deep learning for classification, to enhance robustness and discriminative performance in dementia detection and classification. Figure 4.1 illustrates the block diagram of the proposed WavDemNet for dementia identification and classification.

4.1.2.1 Data Acquisition and Pre-processing

The EEG data used in this work is obtained from the OpenNeuro repository [249]. It includes EEG recordings from 88 participants: 36 with AD, 23 with FTD, and 29 HCs. Nineteen scalp electrodes were employed according to the International 10–20 standard system. The recordings were collected according to the established clinical protocols. Participants were seated with their eyes closed to maintain a calm and stable state conducive to accurate data collection. The EEG signals were captured at a sampling rate of 500 Hz, with a resolution of 10 μV/mm. The average recording time for the AD group was approximately 13.5 minutes, 12 minutes for the FTD, and 13.8 minutes for the HC. This data is publicly available, and its detailed information

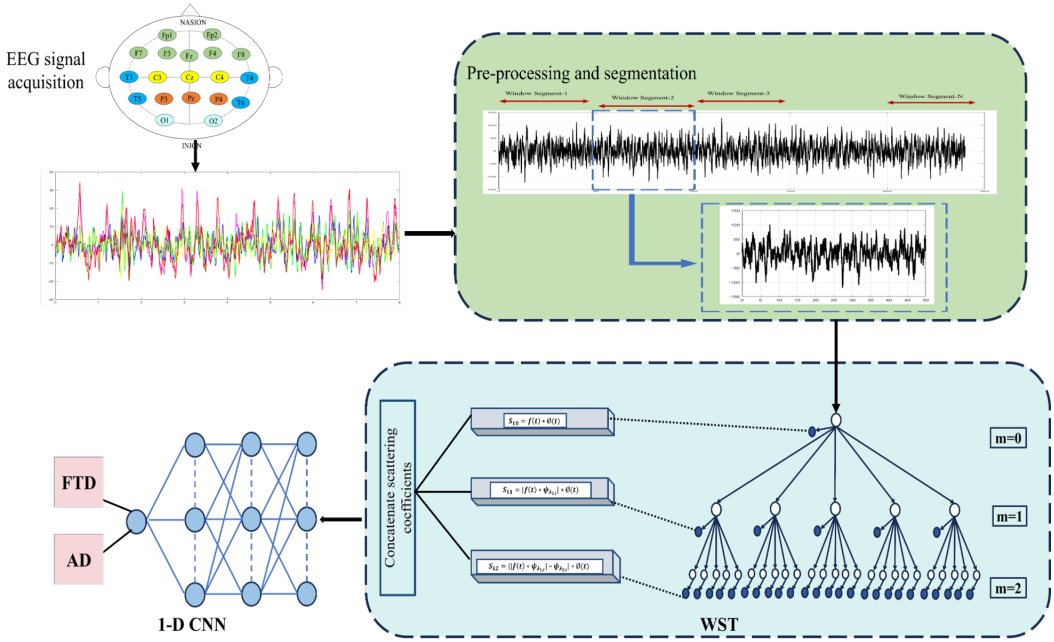

Figure 4.1: Block diagram of the proposed WavDemNet for dementia identification and classification

can be found in [250]. To pre-process the data, the EEG signals were filtered using a Bandpass filter at frequencies ranging from 0.5 to 45 Hz. The artifact subspace reconstruction approach was used to eliminate transitory or high-magnitude artifacts. Independent component analysis was used to eliminate muscle, jaw, and eye-blink artifacts. Table 4.1 presents an extensive overview of the data.

Table 4.1: Overview of OpenNeuro EEG data

Class	AD	FTD	HC
Total subjects	36	23	29
Male	12	14	18
Female	24	9	11
Age	66.4±7.9	63.6±8.2	67.9±5.4
MMSE score	17.75±4.5	22.17±8.22	30±0

4.1.2.2 Wavelet Scattering Transform

WST is a wavelet-based technique that produces stable, accurate, and translation-invariant signals, making it appropriate for extracting the features from non-stationary

data. WST uses wavelet functions and a low-pass scaling function to obtain a low-variance representation of real-valued data [251]. WST decomposes the input signal into consecutive layers in a hierarchical tree structure, with the output from each layer serving as the input for the next. Each layer performs three core operations: convolution with complex wavelets, a non-linear modulus operation, and average pooling using a scaling function.

Let $f(t)$ represent the signal to be analyzed. The scattering transform computes a series of coefficients by iteratively applying the following three operations:

- Convolution with a complex wavelet $\psi_\lambda(t)$, which captures localized frequency content.
- Modulus non-linearity $|.|$, which removes phase information while preserving energy and stability.
- Low-pass filtering with a scaling function $\phi(t)$, which introduces local translation invariance by averaging.

The zeroth-order scattering coefficient is computed by convolving the signal with the scaling function as,

$$S_{L0} = f(t) * \phi(t) \tag{4.1}$$

Convolution can extract low-frequency features from signals, but it also results in the loss of high-frequency information. The high-frequency components in the signal can be extracted via the wavelet modulus. Subsequently convolution with complex wavelets ψ_λ yields the first-order wavelet modulus coefficients W_{M_1}.

$$W_{M_1} = \left| f(t) * \psi_{\lambda_{1,i}} \right| \tag{4.2}$$

In order to determine the first-order wavelet scattering coefficient, the first-order wavelet modulus coefficients are averaged using scaling functions $\phi(t)$ as,

$$S_{L1} = \left| f(t) * \psi_{\lambda_{1,i}} \right| * \phi(t) = W_{M_1} * \phi(t) \tag{4.3}$$

The second-order coefficients recover information lost during the averaging step of the first-order by capturing interactions between frequency components at different

scales.

$$W_{M_2} = \left| \left| f(t) * \psi_{\lambda_{1,i}} \right| * \psi_{\lambda_{2,i}} \right| \tag{4.4}$$

So, the second-order wavelet scattering coefficients are represented as,

$$S_{L2} = \left| \left| f(t) * \psi_{\lambda_{1,i}} \right| * \psi_{\lambda_{2,i}} \right| * \phi(t) = W_{M_2} * \phi(t) \tag{4.5}$$

As the scattering order increases, the energy of the coefficients decreases rapidly, reaching less than 1% by the third order [251]. Thus, in this work, we utilized a second-order scattering network. For the second-order WST network, the quality factor, $Q1$, was adjusted to 8, and $Q2$ was 1 wavelets per octave.

4.1.2.3 Dementia Identification and Classification Network

The proposed WavDemNet structure in this work combines WST and 1-D CNN to effectively extract robust and discriminative features from the EEG signal for dementia identification and classification. A 1-D CNN designed for efficient disease classification using extracted scattering coefficients as input. The WST is a mathematically grounded feature extractor that captures both spectral and temporal information from time-series signals, providing translation-invariant and stable representations. These features are used in place of raw signals to enhance model performance and reduce training complexity. The neural network architecture begins with a standard convolutional block followed by batch normalization and max pooling, effectively reducing feature dimensionality while preserving important patterns. The model further includes three progressively deeper convolutional blocks with increased filter sizes to capture more abstract representations. A dropout layer was incorporated after each convolutional block to improve generalization and mitigate overfitting. Following these layers, the output is flattened and passed through two fully connected layers with L2 regularization and dropout. To predict class probabilities sigmoid activation function was applied at the output layer as shown in Figure 4.2. The WavDemNet requires less memory overhead and computational demand, which helps to ensure efficient execution during training.

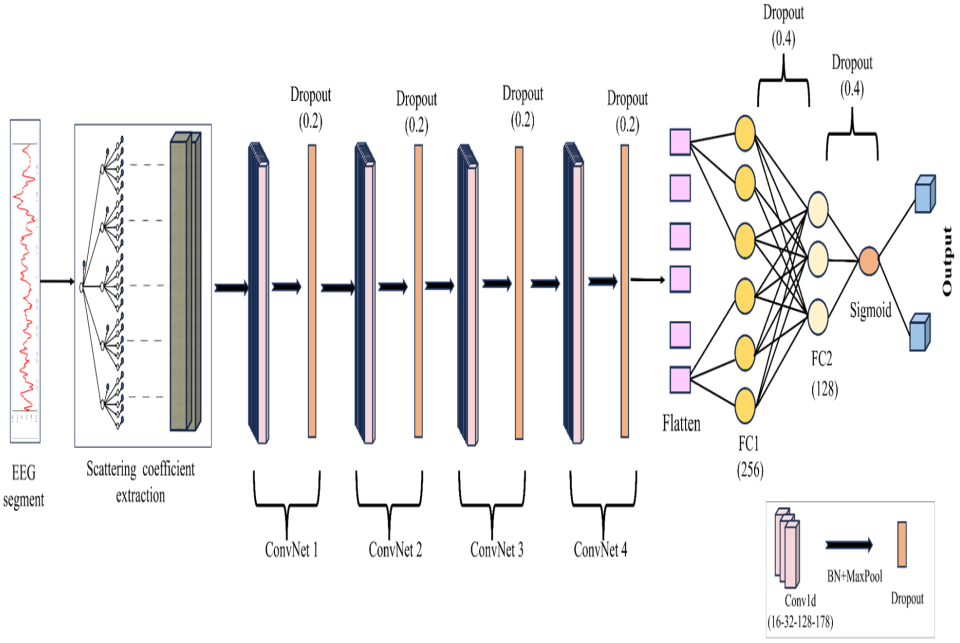

Figure 4.2: Architecture of the proposed WavDemNet for dementia identification and classification

4.1.2.4 Network Parameter Optimization

Adam optimizer was used for model training, with an initial learning rate (l_r) of 10^{-4}. A batch size of 64 was used over a training window of up to 80 epochs. To prevent overfitting and encourage efficient convergence, two adaptive callbacks were implemented: EarlyStopping, with a patience of 10 epochs and restoration of best weights, and ReduceLROnPlateau, which reduced the l_r by a factor of 0.5 after 5 stagnant validation epochs. Input features were derived from the WST, enhancing robustness and reducing training complexity. To evaluate generalization performance, 5-fold stratified cross-validation was applied to preserve class proportions across all folds. The algorithm for the proposed WavDemNet for dementia identification and classification is presented as Algorithm 1.

4.1.3 Results

The proposed work intends to develop an accurate model for automatic identification and classification of dementia by analyzing EEG signals. To analyze the

Algorithm 1 Dementia Identification and Classification Using Proposed WavDemNet

Require: EEG signals

Ensure: Classification of EEG signals [AD or FTD]

Step 1: Preprocessing

Load EEG signal

Read an EEG channel

Segment EEG into non-overlapping windows $f_1, f_2, \ldots, f_N$

Step 2: Feature Extraction using WST

for each EEG segment f_i **do**

  Initialize wavelet scattering parameters (F_s, Q, scale)

  Compute zeroth-order coefficient: $S_{L0} = f(t) * \phi(t)$

  Compute first-order coefficient: $S_{L1} = |f(t) * \psi_{\lambda_{1,i}}| * \phi(t)$

  Compute second-order coefficient: $S_{L2} = ||f(t) * \psi_{\lambda_{1,i}}| * \psi_{\lambda_{2,i}}| * \phi(t)$

  Concatenate scattering coefficients: $S_L = (S_{L0}, S_{L1}, S_{L2})$

end for

Step 3: Classification using 1D CNN

Form $X \in \mathbb{R}^{N \times D}$ from all S_L

Reshape X to $N \times D \times 1$

for each fold $i = 1$ to 5 **do**

  Split X, Y into training and test sets

  Define and compile 1-D CNN model

  Train on training set

  Predict on test set

  Evaluate performance

end for

return Average classification performance over folds

signals, a 5-minute segment was chosen for each participant, as the smallest recording time was 5.1 minutes. The data was divided into 50-second epochs for a total of six epochs per subject. Each epoch had 25,000 samples, with a sampling rate of 500 Hz. The epochs were then processed through a wavelet scattering network, with each epoch producing a feature matrix. The features were then applied to the CNN model for optimal results. The model's performance is evaluated by a 5-fold stratified cross-validation approach, ensuring equal distribution of classes across all folds. The effectiveness of the proposed WavDemNet is evaluated using evaluation parameters like accuracy, sensitivity, precision, and F-1 score.

The EEG signal processing was done in two steps, for the identification and classification of neurological activity. In the first stage, the model performed binary classification to differentiate between EEG signals from healthy and dementia patients. This stage acted as an initial screening method to identify signals that may indicate unusual brain activity. The model demonstrated robust performance, achieving an average accuracy of 89.37%, along with a precision of 89.26%, a sensitivity of 95.65%, and an F1-score of 92.35%. The second stage focused exclusively on dementia classification. The subset of signals identified as demented underwent further diagnostic refinement, wherein the model classified them into AD and FTD categories. This stage offered more detailed characterization of pathological EEG activity and yielded strong results: an accuracy of 88.96%, precision of 88.38%, sensitivity of 94.30%, and an F1-score of 91.24%. Figure 4.3 presents the confusion matrix for Demented vs HC and AD vs FTD classes. The matrix demonstrated how effectively the proposed WavDemNet distinguished demented and HC as well as AD and FTD groups.

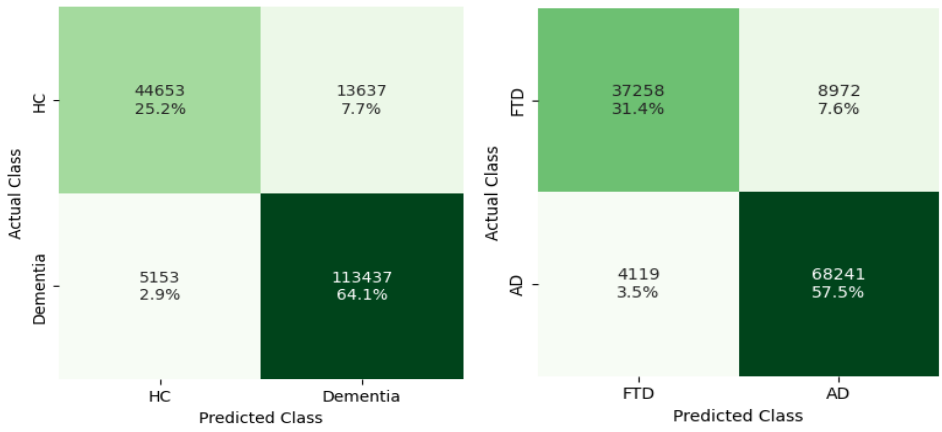

(a) (b)

Figure 4.3: Confusion matrix for (a) Dementia identification, (b) Dementia classification

In addition to diagnosing and classifying dementia, we evaluated the proposed WavDemNet performance by expanding its use to other diagnostic classification tasks. We specifically tested its ability to discriminate persons with AD from HC, as well as

those with FTD from HC. These additional evaluations were conducted to illustrate the generalizability and robustness of our method. Table 4.2 presents the classification performance of the proposed WavDemNet across different diagnostic groups.

Table 4.2: Experimental results of the proposed WavDemNet for different diagnostic groups

Evaluation parameters	Diagnostic Groups			
	AD vs HC	FTD vs HC	AD vs FTD	Dementia vs HC
A_c (%)	88.33±0.25	88.99±0.06	88.96±0.12	89.37±0.20
S_n (%)	86.81±0.77	82.04±0.25	94.30±0.25	95.65±0.58
P_r (%)	91.68±0.70	92.21±0.16	88.38±0.13	89.27±0.57
F_1^{sr} (%)	89.17±0.25	86.83±0.09	91.24±0.10	92.35±0.11

Furthermore, to validate the proposed WavDemNet's effectiveness, a comparison with many well-established classical ML techniques was performed. Figure 4.4 depicts a comparative analysis of identification performance between the proposed WavDemNet and three baseline ML models: NB, KNN, and RF. With an accuracy of 84.4%, Random Forest outperformed KNN (84.03%) and NB (48.96%).

Figure 4.5 presents the classification performance comparison between the proposed WavDemNet and three conventional classifiers: NB, KNN, and RF for dementia classification. Among the baseline models, RF delivered the highest performance with an Accuracy of 83.90%, followed by KNN (83.51%) and NB (53.82%). The results of this comparison indicate the higher performance of WavDemNet across key evaluation measures for dementia identification and classification.

4.1.4 Discussion

Accurate identification and classification of dementia is essential for effective treatment, individualized care, and informed support. An inaccurate diagnosis can lead to inefficient or hazardous therapies, inappropriate care plans, and significant

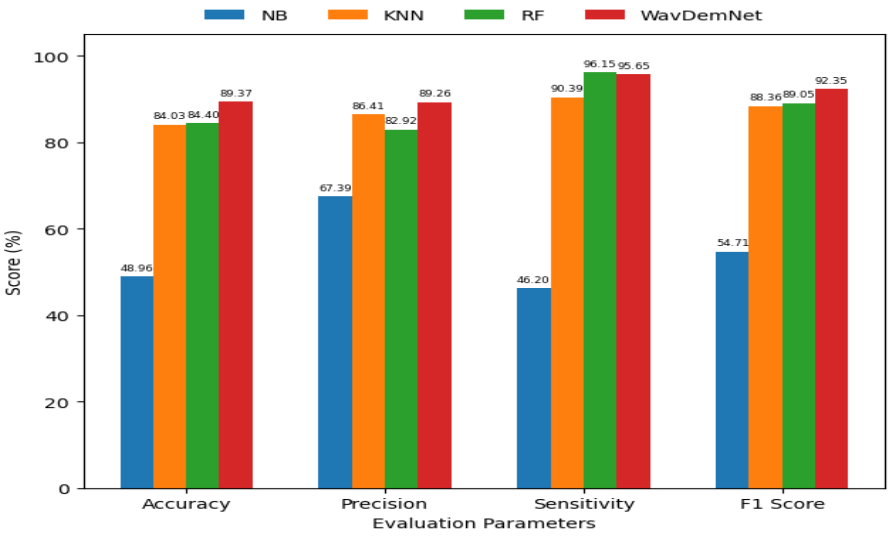

Figure 4.4: Performance comparison of WavDemNet with baseline ML models for dementia identification

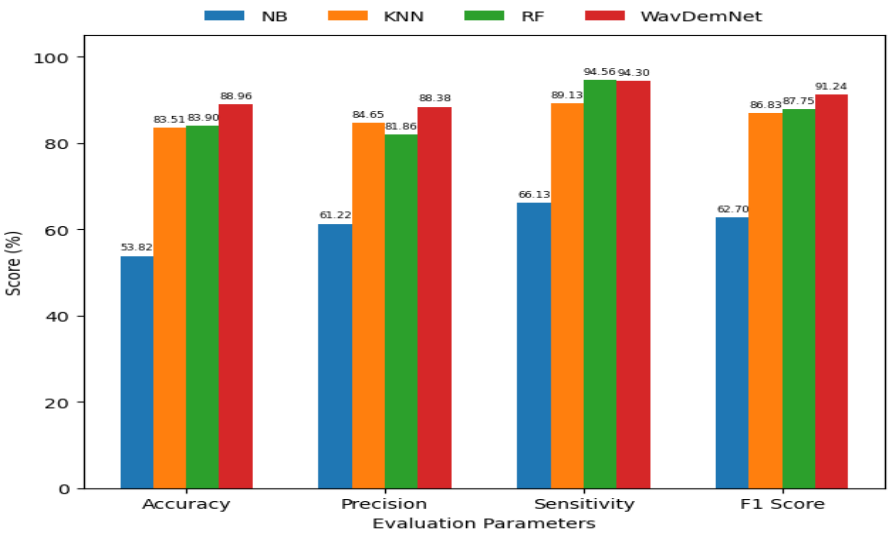

Figure 4.5: Performance comparison of WavDemNet with baseline ML models for dementia classification

emotional and financial stress for patients and their caregivers. EEG signals demonstrate enormous potential for enhancing early identification and categorization of dementia. In this work, WST is employed to extract robust and informative scattering coefficients from EEG signals. These coefficients effectively capture the multiscale temporal and frequency characteristics of the signals. These coefficients serve as input

Table 4.3: The performance comparison of the proposed WavDemNet with existing state-of-the-art methods on the OpenNeuro dataset

Year	Author	Methodology	Task	Evaluation parameters			
				A_c (%)	S_n (%)	P_r (%)	F_1^{sr} (%)
2025	Stefanou et al. [196]	FFT Spectrogram + CNN	Dementia vs HC	80.69	84.31	84.31	83.18
			AD vs HC	79.45	76.06	77.32	77.60
			FTD vs HC	72.85	67.94	71.33	67.85
2024	Zheng et al. [140]	Multi-threshold recurrence rate plot+SVM	Dementia vs HC	86.36	93.22	-	-
			AD vs FTD	72.88	94.44	-	-
			AD vs HC	87.69	97.22	-	-
			FTD vs HC	82.69	73.91	-	-
2023	Si et al. [252]	Frequency-based multi-layer network + GNB	AD vs FTD	81.1	81	71.2	78.9
2023	Mootoo et al. [141]	Graph feature extraction + SVM	Dementia vs HC	85	-	-	-
2023	Miltiadous et al. [185]	DICE-net	AD vs HC	83.28	78.81	-	84.21
			FTD vs HC	74.96	60.62	64.01	62.27
2023	Chen et al. [217]	Dual-branch network (CNN+visual transformer)	AD vs FTD	79.81	-	-	
			AD vs HC	87.33	84.56	-	-
			FTD vs HC	82.98	81.66	-	-
	Proposed	**WavDemNet**	**Dementia vs HC**	**89.37**	**95.65**	**89.26**	**92.35**
			AD vs FTD	**88.96**	**94.30**	**88.38**	**91.24**
			AD vs HC	**88.33**	**86.81**	**91.67**	**89.17**
			FTD vs HC	**88.99**	**82.04**	**92.21**	**86.83**

- Not reported

features to a CNN, which is then trained to identify and distinguish dementia.

Numerous methods have been developed for identifying dementia. Table 4.3 presents a comparative analysis of the proposed WavDemNet with existing approaches described in the literature on the same data. Stefanou et al. [196] used FFT to obtain the spectrogram of EEG signals. The CNN model was used to extract relevant information from these spectrograms to identify dementia and obtained 80.69% accuracy. The features from the EEG signal were directly extracted in [140, 141, 252]. As EEG signals are highly non-stationary, the system's performance is limited by the analysis of features derived directly from the EEG. Miltiadous et al. [185] extracted band power and coherence features from the EEG signal. These features were used to train a dual-input CNN encoder (DICE-Net) for classification. Chen et al. [217] employed a dual-branch network using a CNN and a visual transformer (VIT) to extract texture features and global semantic information from EEG signals, respectively, and attained 81.56% classification accuracy for AD and FTD classification. However, due to their complexity and processing demands, these models are generally ineffective in practical applications. The WavDemNet employed in this work overcomes the constraints of EEG-based analysis by combining the advantages of wavelet-based feature extraction with a fixed, hierarchical architecture. This architecture allows for the extraction of robust, multi-resolution features while significantly reducing model complexity and processing demands. These scattering coefficients are then sent into the CNN, which does deep feature learning and classification, taking advantage of its capacity to model nonlinear and spatial-temporal correlations in data. It is evident from the comparison table that our proposed WavDemNet outperforms the other methods in terms of recognition accuracy, not only for the identification of dementia but also for dementia classification.

4.2 Summary

In this chapter, a robust and end-to-end approach for dementia identification and classification using WavDemNet is presented. The proposed WavDemNet framework integrates WST and CNN. WST extracts discriminative signal features from EEG data,

capturing stable, translation-invariant representations across several time-frequency scales. These features efficiently represent the modest neurological abnormalities found in AD and FTD. A 1D-CNN architecture was then used to learn high-level abstractions from these features, allowing for robust classification by detecting distinct neurophysiological patterns specific to each condition. The proposed WavDemNet attained 89.45% accuracy for dementia identification and 88.40% for AD and FTD classification on the OpenNeuro dataset. Furthermore, a comparison of the WavDemNet architecture with state-of-the-art approaches was performed, which demonstrated its effectiveness and reliability in EEG-based dementia classification. .

Chapter 5

Development of an Automated Algorithm for Early Diagnosis of Brain Diseases

---

In this chapter, an automated algorithmic framework is developed for the early diagnosis of PD through two complementary studies. The first study introduces a speech-based diagnostic framework that employs the Superlet Transform (SLT) to convert one-dimensional speech signals into two-dimensional spectrograms, which are then analyzed using deep neural network architectures for accurate PD detection. The second study extends this approach to gait-based analysis, proposing a super-resolution time–frequency framework for the detection and evaluation of PD severity.

5.1 High-Resolution Superlet Transform based Techniques for Parkinson's Disease Detection using Speech Signal

5.1.1 Introduction

According to studies, early symptoms of PD in 90% of patients include vocal cord damage [253]. These vocal impairments occur initially in PD. There is reduced loudness, vocal tremor, and breathiness in PD patients while speaking. The speech symptoms in PD patients are depicted as dysarthria. Dysarthria is a speech disorder for which the lack of muscle control is the primary cause, and it occurs when the parts of the brain that control speaking abilities become inactive. Hypokinetic dysarthria occurs due to damage in the basal ganglia [254]. People with PD suffer from phonatory

impairment, prosodic impairment, and articulatory impairment. Phonatory impairment refers to the reduction in vocal loudness, prosodic impairment implies pause abnormalities, syllabic stress, and monopitch, while articulatory impairment signifies speech disfluency. In this work, we have proposed a time-frequency spectrogram image-based framework for PD detection using speech signals. Time-frequency domain analysis combines frequency and time information to show how the spectral content of signals varies over time.

5.1.2 Proposed Methodology

The proposed work aims to develop an automated algorithm for early diagnosis of PD using speech signals. The proposed framework utilizes SLT and DNN for PD detection. Figure 5.1 depicts the framework for PD detection using speech signals.

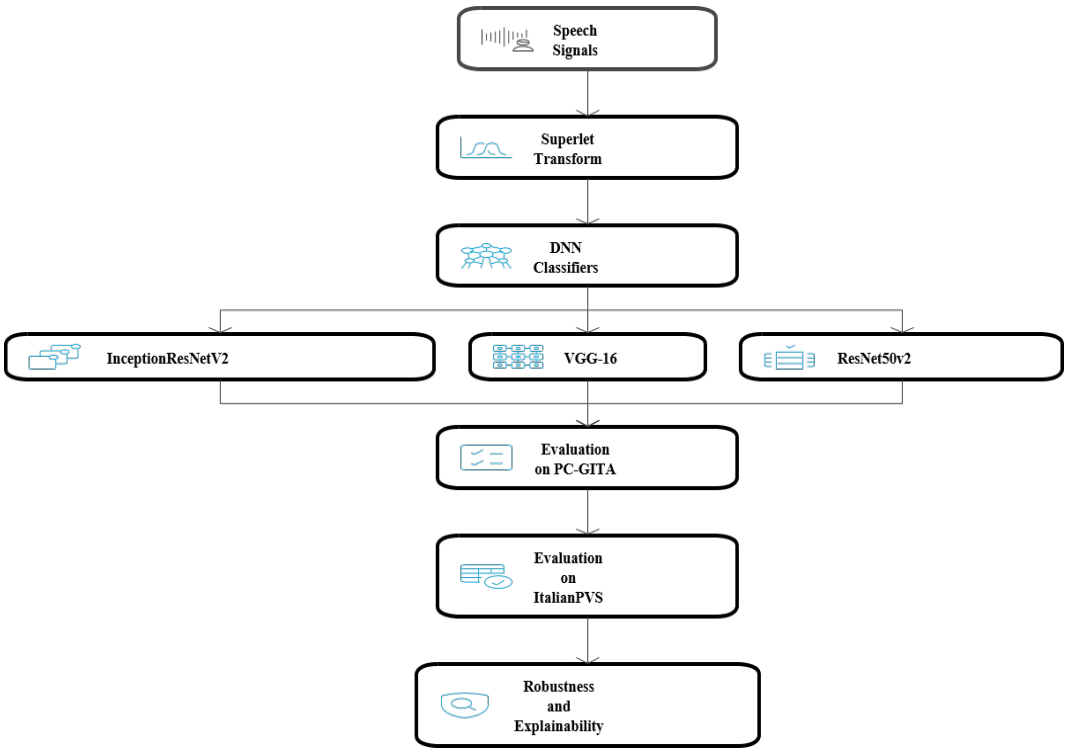

Figure 5.1: Block Diagram of PD detection framework using speech signals

5.1.2.1 Dataset Description

Dataset 1: The PC-GITA dataset [41] contains voice recordings of HC and PD patients. This dataset includes different words, vowels, reading texts, sentences, and monologues. The PC-GITA dataset comprises 100 Spanish native speakers, where 50 speakers were healthy, and the rest 50 speakers were PD patients. HC and PD patients include 25 males and 25 females. For evaluation purposes, three speech task aspects, namely phonation, articulation, and prosody, were analyzed.

1. Phonation can be defined as the production and utterance of speech sounds. For its analysis, three repetitions of five Spanish vowels were used, and these vowels were uttered by changing the tone of each vowel from low to high.
2. Articulation is the formation of comprehensible and well-defined sounds in speech. Its evaluation is done using three repetitions of five vowels uttered in a sustainable manner and a rapid repetition of a set of different words.
3. Prosody refers to the pattern of stress and intonation in a language. For its evaluation, different tasks such as repetition of complex sentences, simple sentences, spontaneous speech, and reading dialogue were performed.

The speech recordings were taken in a noise-controlled environment, and the sampling frequency was 44.1 kHz with 16-bit resolution. A detailed description of the PC-GITA dataset is reported in Table 5.1.

Table 5.1: PC-GITA dataset description

Data	PD	HC	Gender
Sustainable Vowels (/a/, /e/, /i/, /o/, /u/)	150	150	75M, 75F
Modulated Vowels (/a/, /e/, /i/, /o/, /u/)	50	50	50M, 50F
DDK analysis (/petaka/, /ta/, /ka/)	50	50	50M, 50F
Words (/apto/, /globo/, /petaka/)	50	50	50M, 50F

Dataset 2: The ItalianPVS dataset [255] contains voice recordings from 22 HC and 28 PD patients. Each recording session took place in a controlled environment at a 16 kHz sampling frequency. All the subjects completed the following reading tasks while

recording: two phonations of each vowel /a/, /e/, /i/, /o/, /u/, syllable /pa/ and /ka/, two readings of a phonetically balanced text, and two readings of phonetically balanced words and phrases. A detailed description of the ItalianPVS dataset is reported in Table 5.2.

Table 5.2: ItalianPVS dataset description

	PD	HC
Number of subjects	28	22
Male	19	10
Female	9	12
Age	40-80 years	60-70 years

5.1.2.2 Superlet Transform

Superlet (SL) uses a set of wavelets with increased bandwidth and combines geometrics to obtain an excellent temporal resolution of wavelength and attain frequency resolution in the high-frequency range [256]. The STFT performs a time-frequency analysis of the signal and is applied for obtaining the representations that procure time as well as the frequency content of the signal. As a result of Heisenberg's uncertainty principle, the output of temporal and frequency resolution is uniform, so the features generated by STFT cannot attain an immediate localization of both frequency and time. As STFT uses a fixed window length and basis function, it cannot capture events with different durations. The CWT tries to eliminate or reduce the limitations of STFT and provides better temporal resolution at greater frequencies, while an alleviation in frequency resolution can be noticed. Hence, the Discrete Wavelet Transform (DWT) was used, in which the frequencies were represented as a power of two. STFT and CWT both come with a few constraints. The STFT caters to good frequency resolution yet lacks relative temporal resolutions at higher frequencies, and the CWT provides good relative temporal resolution in the entire spectrum, but the frequency resolution deteriorates with an increase in frequency. The SLT furnishes a novel spectral estimation that provides the transient oscillation state of the signals and caters to a TF spectrogram, having a high resolution in temporal and frequency

localizations as compared to STFT and CWT.

SL uses various wavelets to obtain a better TF resolution. Wavelets having minimum cycles deliver a good temporal and degraded frequency resolution, while the wavelets having maximum cycles deliver good frequency resolution but degraded temporal resolution. SLT blends both suitable frequency resolutions and good temporal resolutions to provide a super-resolution. The SLT has been utilized for different biomedical signal processing applications, like cardiac arrhythmia detection, heart rate estimation, and seizure detection [257–260] and electrical signal processing like power system fault recognition [261].

The SLT utilizes Morlet as a mother wavelet, which symbolizes a multi-resolution spectro-temporal representation. The Morlet wavelet is one of the most complex wavelets as given in Eq. (5.1),

$$\phi(t) = \left(e^{-jf_0 t} - e^{\frac{-f_0^2}{2}}\right) e^{\frac{-t^2}{2}} \tag{5.1}$$

Here, f_0 is the central frequency of the mother wavelet. The Morlet wavelet deals with a form quite like the Gabor transform. The imperative disparity that both hold is that in Morlet, the window function can be scaled by the scaling parameter. On the other hand, the size is already fixed for the window in the Gabor transform. The modified Morlet applied in SL is defined in Eq. (5.2) as,

$$\Psi_{f_0,n}(t) = \frac{1}{B_n\sqrt{2\Pi}} e^{\frac{-t^2}{2B_n^2}} e^{j2\Pi f_0 t} \tag{5.2}$$

B_n is the displacement parameter that regulates the time variance of the wavelet, described in Eq. (5.3),

$$B_n = \frac{n}{D \times f_0} \tag{5.3}$$

It is inversely proportional to the frequency, i.e., a smaller value of B_n provides a broader frequency response, and a larger value will provide a narrower frequency response. So, the value of B_n is adjusted in such a way that the wave covers complete cycles (n) within the standard deviation (D) of the Gaussian envelope [256].

SL uses various wavelets with f_0 to provide a better TF representation. The

mathematical representation of SL is given in Eq. (5.4),

$$SL_{f_0,w} = \{\Psi_{f_0,n} | n = n_1, n_2, ..., n_w\} \tag{5.4}$$

Here, w is the order of SL, which portrays the wavelets used in SL. While n_1, n_2,$\cdots$, n_w represent the number of cycles for each wavelet in the SL. The selection of the number of cycles in wavelets in SL can be done additively or multiplicatively. In this work, the multiplicity is used to select the number of cycles as given in Eq. (5.5)

$$n_i = n \times i \tag{5.5}$$

Here, $i = 1, 2, 3, \cdots, w$. Eq. (5.6) describes the response of SL to the speech signal $s(t)$ that can be expressed by the geometric mean of the individual wavelet response.

$$R[SL_{f_0,w}] = \sqrt[w]{\prod_{i=1}^{w} R[\Psi_{f_0,n_i}]} \tag{5.6}$$

Here, Ψ_{f_o,n_i} is the response of i^{th} wavelet of s(t).

For Morlet, it is defined as,

$$R[\Psi_{f_0,n_i}] = \sqrt{2}.s * \Psi_{f_0,n_i} \tag{5.7}$$

Here, s is the speech signal, and * represents the complex convolution. SLTs are similar to CWT, except that SLT uses SLs in place of wavelets used in CWT. A CWT can be described as an SLT including SLs of order 1. The SLTs with higher order (i.e., >1) provide a sharper representation of the signal and are less redundant compared to the CWT. For wide frequency, Adaptive SLT (ASLT) is preferred. An ASLT begins at a low order and elevates the order as a function of frequency to amplify TF illustration throughout the whole frequency domain. Accordingly, the use of ASLT, with an order greater than one, helps in gaining an improved TF illustration of the signal.

Time-Frequencies analysis of speech signal: SLT is well suited for studying transient oscillation occurrences in non-stationary signals. SLT employs numerous wavelets to achieve higher TF resolution while being less leaky than a single wavelet, which makes it more sustainable to apply to non-stationary speech signals. The speech signals and TF analysis of speech signals for PD patients and HC using STFT, CWT,

and SLT are depicted in Figure 5.2. TF analysis methods like STFT and CWT are utilized by researchers to analyze speech signals for PD detection. SLT has several advantages over these methods.

5.1.2.3 Deep Neural Network (DNN)

DNN is a combination of multiple hidden layers. DNN is essentially a collection of neurons organized in a succession of layers. These neurons function parallelly. In DNN, these neurons successively receive the neuron activations as input from the previous layer and thus, perform a simple computation. An input layer, a hidden layer, and an output layer are included in a basic neural network. DNN is characterized by the stacking of multiple neural networks. Through training, a DNN learns how to carry out specific tasks and acquires knowledge about the strength of connections between its units. The identical task is then carried out on new data using the trained DNN [262].

Learning Rate (LR) is a tuning parameter, used in these DNN models for controlling the weights of the neural network model concerning the loss gradient. It contains values between 10^{-6} to 1. For a reduction in the overfitting problem, the dropout parameter is applied. Activation functions are also used later to raise the neural network capabilities of each convolutional layer. In this work, ReLu and softmax activation functions are used. ReLu generates an output x if $x > 0$ or 0 if $x < 0$, which suggests that the neurons with positive values are activated while those with negative values remain inactive. Further, Softmax works for the prediction of the class pertaining to the highest probability in classification problems for the given input classes.

InceptionResNetV2: It is a CNN architecture, trained on the ImageNet dataset. It is a 164-layer deep architecture. In InseptionResNetV2, the input image of 229×229×3 is implemented to the first convolutional layer. In this model, a combination of multiple-sized convolutional filters and residual connections is carried out [263]. The use of residual connections helps in avoiding derogation problems related to deep structures while also reducing the training period. InceptionResNetV2 was developed

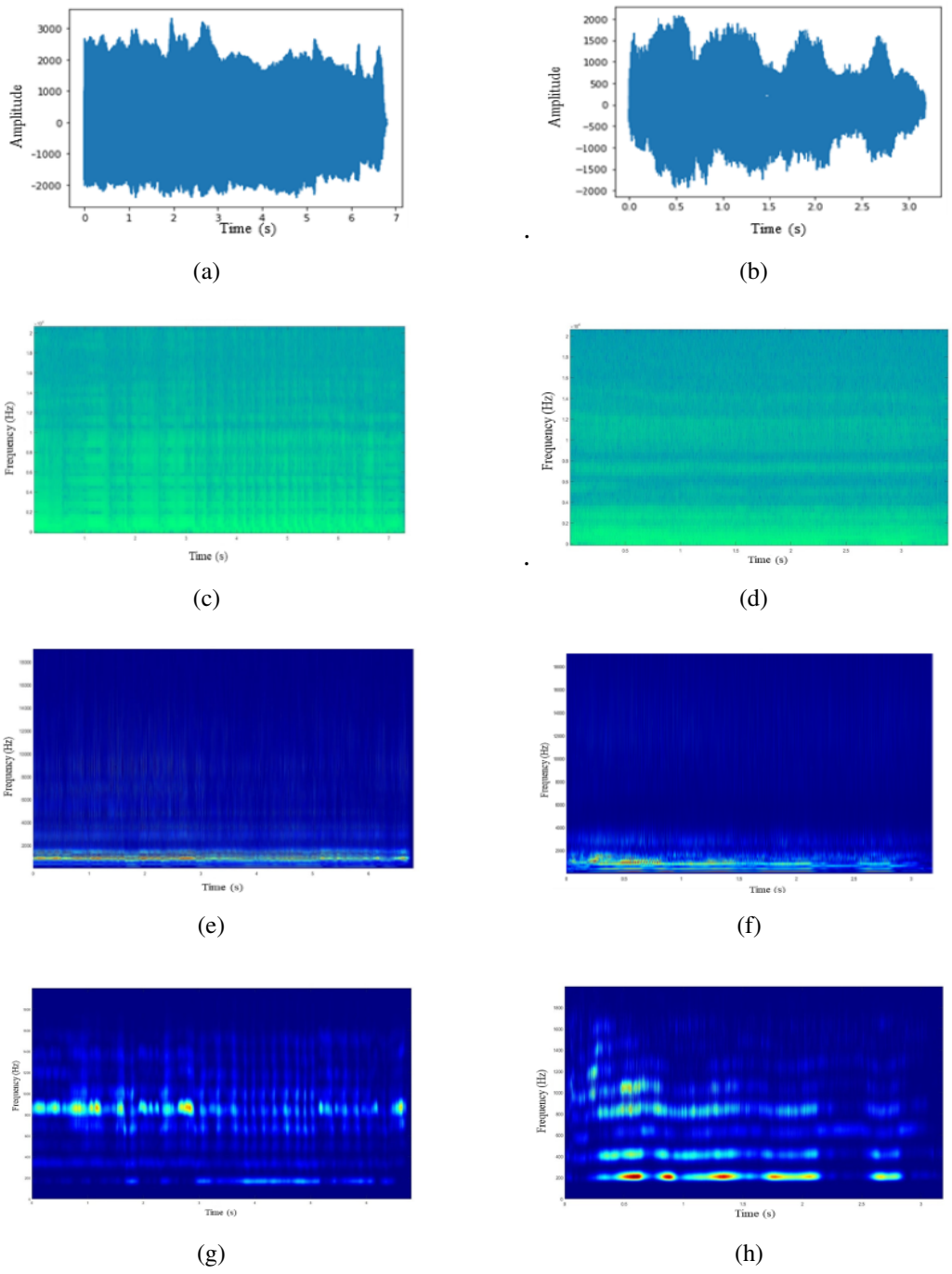

Figure 5.2: The representation for speech signal (a) Time domain representation of speech signal for HC, (b) Time domain representation of speech signal for PD, (c) STFT representation for HC, (d) STFT representation for PD, (e) CWT representation for HC, (f) CWT representation for PD, (g) SLT representation for HC, (h) SLT representation for PD

by the Google team in 2016 for learning and extraction of features signifying facial age and performing an age-based classification. This model also has been effective for classifying images with taking residual networks into consideration.

ResNet: It is considered one of the most prominent deep neural networks. As the depth of the CNN model increases, training error also increases simultaneously. With the help of ResNet, this problem can be overcome as ResNet uses less filters and provides less complexity compared to other DNN structures. ResNet50V2 is a modified version of ResNet50 [264]. It clears the input path to attain output in an identity connection form. It uses batch normalization and ReLU activation to the input before the multiplication with the weight matrix. The usage of batch normalization before each weight layer is the key difference between ResNetV2 and ResnetV1.

VGG-16: The VGG model finds its inception in the year 2014 by Simonyan and Zisserman [265]. The VGG model with 16 layers (VGG-16) is a uniform architecture with an input image of 224×224×3. It is fed to the first convolutional layer. It consists of 3x3 convolutions and a number of filters. It is commonly trained for the extraction of features from images. With its public availability, VGGNet has been used for weight configuration and extraction of features. The VGG-16 network contains 13 convolutional layers, five max-pooling layers, and three fully-connected layers.

The steps involved in the proposed method are explained in Algorithm 1.

5.1.3 Results

To evaluate the performance of this work, different parameters like accuracy, sensitivity, selectivity, precision, and F1 score are taken into consideration. The performance of the DNNs for PD detection is evaluated using 10-fold cross-validation. Table 5.3 shows the results obtained for the sustainable vowels of the PC-GITA dataset with InceptionResNetV2, ResNet50V2, and VGG-16. The VGG-16 model provides the best results for the sustainable vowel /a/ with 88% accuracy. In comparison to ResNet50V2 and InceptionResNetV2, the proposed method with VGG-16 provides better results for sustainable vowels in terms of most of the evaluation parameters.

Algorithm 1: Algorithm of the proposed method using SLT for PD detection

Input: Speech signals obtained from PC-GITA and ItalianPVS dataset

Output: Classification of speech signals [PD or HC]

1: Generation of Spectrogram

(i) Apply the input speech signal

(ii) Assign mother wavelet parameters such as, central frequency (f_0), time spread parameter (B_n)

$$\Psi_{f_0,n}(t) = \frac{1}{B_n\sqrt{2\Pi}} e^{\frac{-t^2}{2B_n^2}} e^{j2\Pi f_0 t}$$

(iii) Selection of SL by taking multiple wavelets.

$$SL_{f_0,w} = \{\Psi_{f_0,n} | n = n_1, n_2, ..., n_w\}$$

(iv) Determine the number of cycles in the wavelet using the multiplicative rule.

$$n_i = n \times i$$

(v) Generation of spectrogram by taking the geometric mean of each wavelet response

$$R[\Psi_{f_0,n_i}] = \sqrt{2}.s * \Psi_{f_0,n_i}$$

2: Use the 2-D spectrogram image data as input to different DNNs.

3: Use the DNNs (VGG-16, InceptionResNetV2, and ResNet50V2) to extract the features and classify the speech signals into PD and HC classes.

Table 5.3: Results obtained using SLT-based method for sustainable vowels of the PC-GITA dataset

Evaluation Parameter	Deep Neural Network	Sustainable Vowel				
		a	e	i	o	u
Accuracy	VGG-16	**0.88±0.11**	**0.80±0.11**	**0.81±0.09**	**0.86±0.10**	**0.82±0.07**
	ResNet50V2	0.81±0.06	0.76±0.08	0.70±0.08	0.77±0.10	0.76±0.10
	IncecptionResNetV2	0.77±0.07	0.70±0.13	0.62±0.11	0.73±0.10	0.65±0.08
Sensitivity	VGG-16	**0.89±0.16**	**0.89±0.09**	**0.80±0.15**	**0.86±0.15**	0.75±0.18
	ResNet50V2	0.87±0.11	0.78±0.18	0.67±0.14	0.84±0.13	**0.83±0.14**
	IncecptionResNetV2	0.79±0.16	0.76±0.15	0.74±0.14	0.80±0.14	0.57±0.14
Specificity	VGG-16	**0.88±0.12**	0.72±0.24	**0.79±0.17**	**0.86±0.10**	**0.88±0.11**
	ResNet50V2	0.75±0.10	**0.73±0.22**	0.73±0.18	0.70±0.20	0.69±0.19
	IncecptionResNetV2	0.74±0.15	0.65±0.20	0.50±0.22	0.67±0.14	0.75±0.18
Precision	VGG-16	**0.89±0.11**	**0.79±0.15**	**0.83±0.14**	**0.87±0.09**	**0.89±0.10**
	ResNet50V2	0.79±0.06	0.77±0.11	0.74±0.15	0.77±0.12	0.75±0.12
	IncecptionResNetV2	0.76±0.17	0.69±0.16	0.61±0.12	0.71±0.09	0.70±0.10
F-1 Score	VGG-16	**0.88±0.11**	**0.83±0.09**	**0.80±0.11**	**0.86±0.10**	**0.80±0.13**
	ResNet50V2	0.82±0.05	0.75±0.11	0.68±0.09	0.79±0.08	0.78±0.09
	IncecptionResNetV2	0.76±0.13	0.71±0.13	0.66±0.09	0.75±0.10	0.61±0.10

Table 5.4: Results obtained using SLT-based method for modulated vowels of the PC-GITA dataset

Evaluation Parameter	Deep Neural Network	Modulated Vowel				
		a	e	i	o	u
Accuracy	VGG-16	**0.88±0.20**	**0.83±0.13**	**0.86±0.14**	**0.90±0.10**	**0.92±0.09**
	ResNet50V2	0.74±0.19	0.75±0.13	0.75±0.14	0.89±0.10	0.84±0.14
	IncecptionResNetV2	0.71±0.23	0.71±0.14	0.67±0.17	0.68±0.10	0.66±0.16
Sensitivity	VGG-16	**0.94±0.18**	**0.81±0.21**	**0.92±0.18**	**0.93±0.11**	**0.92±0.11**
	ResNet50V2	0.86±0.17	0.76±0.23	0.86±0.24	0.86±0.23	0.89±0.14
	IncecptionResNetV2	0.59±0.34	0.80±0.17	0.64±0.27	0.62±0.25	0.60±0.26
Specificity	VGG-16	0.82±0.20	**0.91±0.18**	**0.80±0.21**	0.89±0.17	**0.91±0.16**
	ResNet50V2	0.68±0.32	0.81±0.26	0.58±0.32	**0.93±0.12**	0.78±0.22
	IncecptionResNetV2	**0.89±0.14**	0.59±0.27	0.74±0.15	0.74±0.18	0.76±0.18
Precision	VGG-16	**0.85±0.20**	**0.90±0.20**	**0.82±0.17**	0.90±0.13	**0.95±0.08**
	ResNet50V2	0.76±0.23	0.83±0.19	0.69±0.20	**0.93±0.12**	0.80±0.17
	IncecptionResNetV2	0.81±0.25	0.65±0.18	0.69±0.21	0.73±0.17	0.75±0.22
F-1 Score	VGG-16	**0.89±0.18**	**0.81±0.15**	**0.86±0.16**	**0.90±0.09**	**0.93±0.08**
	ResNet50V2	0.77±0.15	0.75±0.11	0.74±0.19	0.86±0.17	0.84±0.14
	IncecptionResNetV2	0.62±0.28	0.71±0.16	0.63±0.21	0.63±0.16	0.61±0.18

Results obtained for modulated vowels of the PC-GITA dataset are summarized in Table 5.4. For modulated vowels /a/, /e/, /i/, /o/, and /u/ the accuracy achieved by VGG-16 is 88%, 83%, 86%, 90%, and 92%, respectively. The modulated vowel 'u' yields the best outcomes with VGG-16 DNN. Table 5.5 illustrates the results of the DDK analysis of the PC-GITA dataset. The results demonstrate that for PD detection using DDK analysis /petaka/ the VGG-16 DNN provides the best results with 84% accuracy, 84% sensitivity, 87% specificity, 85% precision, and 83% F-1 score.

The results for the isolated words of the PC-GITA dataset are presented in Table 5.6. For word /globo/ accuracy, sensitivity, specificity, precision, and F-1 score achieved are 87%, 83%, 90%, 90%, and 85%, respectively. The results demonstrate that on the PC-GITA dataset, modulated vowels outperformed all other speech exercises, and VGG-16 DNN exceeds other ResNet50V2 and InceptionResNetV2 for PD detection.

The performance of the proposed method is also evaluated on the ItalianPVS dataset. The maximum accuracy attained in the ItalianPVS dataset is 96% for vowel /a/ and vowel /o/. The results obtained are illustrated in Table 5.7. Figure 5.3 shows

Table 5.5: Results obtained using SLT-based method for DDK analysis of PC-GITA dataset

Evaluation Parameter	Deep Neural Network	DDK Analysis		
		Ta	Ka	Petaka
Accuracy	VGG-16	**0.83±0.17**	0.83±0.17	**0.84±0.19**
	ResNet50V2	0.66±0.20	**0.83±0.13**	0.77±0.14
	IncecptionResNetV2	0.68±0.16	0.77±0.13	0.72±0.15
Sensitivity	VGG-16	**0.85±0.19**	**0.85±0.23**	**0.84±0.22**
	ResNet50V2	0.67±0.25	0.82±0.22	0.72±0.13
	IncecptionResNetV2	0.65±0.24	0.80±0.16	0.74±0.24
Specificity	VGG-16	**0.82±0.17**	0.82±0.20	**0.87±0.21**
	ResNet50V2	0.74±0.23	**0.85±0.14**	**0.87±0.21**
	IncecptionResNetV2	0.67±0.24	0.78±0.18	0.69±0.22
Precision	VGG-16	**0.84±0.14**	0.81±0.24	0.85±0.24
	ResNet50V2	0.72±0.26	**0.81±0.21**	**0.87±0.22**
	IncecptionResNetV2	0.72±0.20	0.78±0.18	0.72±0.22
F-1 Score	VGG-16	**0.83±0.15**	0.81±0.21	**0.83±0.21**
	ResNet50V2	0.63±0.21	**0.81±0.19**	0.76±0.13
	IncecptionResNetV2	0.66±0.17	0.77±0.12	0.69±0.20

the confusion matrix obtained by VGG-16 for the ItalianPVS vowel /a/ and/o.

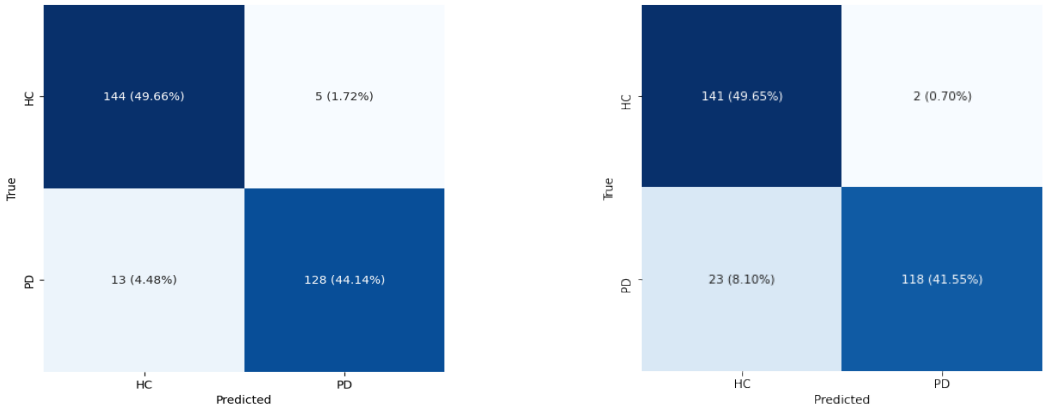

(a) /a/ (b) /o/

Figure 5.3: Confusion matrix obtained using SLT-based method for vowel dataset (a) /a/, (b) /o/

Table 5.6: Results obtained using SLT-based method for isolated words of the PC-GITA dataset

Evaluation Parameter	Deep Neural Network	Isolated Words		
		Apto	Globo	Petaka
Accuracy	VGG-16	**0.83±0.21**	**0.87±0.15**	**0.84±0.16**
	ResNet50V2	0.77±0.17	0.76±0.17	0.82±0.22
	IncecptionResNetV2	0.69±0.13	0.74±0.14	0.65±0.16
Sensitivity	VGG-16	0.79±0.19	0.83±0.23	**0.96±0.07**
	ResNet50V2	**0.81±0.19**	**0.91±0.17**	0.83±0.21
	IncecptionResNetV2	0.69±0.24	0.74±0.23	0.56±0.22
Specificity	VGG-16	**0.87±0.25**	**0.90±0.13**	0.74±0.28
	ResNet50V2	0.68±0.27	0.66±0.26	**0.81±0.27**
	IncecptionResNetV2	0.65±0.29	0.72±0.14	0.78±0.17
Precision	VGG-16	**0.88±0.22**	**0.90±0.16**	0.80±0.21
	ResNet50V2	0.75±0.17	0.71±0.21	**0.84±0.21**
	IncecptionResNetV2	0.71±0.19	0.73±0.17	0.70±0.23
F-1 Score	VGG-16	**0.82±0.20**	**0.85±0.18**	**0.86±0.14**
	ResNet50V2±	0.77±0.16	0.77±0.16	0.83±0.20
	IncecptionResNetV2	0.66±0.17	0.72±0.19	0.60±0.20

5.1.4 Discussion

Speech is one of the many motor and non-motor functions that PD can impact. According to studies, early symptoms of PD in 90% of patients include vocal cord damage [253]. Thus, speech assessment appears to be an appealing prospective biomarker for PD detection. The proposed work uses the high-resolution SLT technique to obtain the TF spectrogram of the speech signal. The DNN approach is utilized to classify these spectrograms into PD and HC classes. In order to assess the proposed method's performance, the outcomes of the proposed work are contrasted with existing techniques like Hilbert spectrum analysis, EMD, CWT, and STFT. Table 5.8 provides a summary of some significant research focused on the detection of PD using speech signals.

Table 5.7: Results obtained using SLT-based method for the ItalianPVS dataset

Evaluation Parameter	Deep Neural Network	Vowels	
		a	o
Accuracy	VGG-16	**0.96±0.04**	**0.96±0.05**
	ResNet50V2	0.95±0.07	0.95±0.06
	IncecptionResNetV2	0.86±0.08	0.88±0.08
Sensitivity	VGG-16	0.93±0.08	0.93±0.10
	ResNet50V2	**0.97±0.05**	**0.94±0.09**
	IncecptionResNetV2	0.89±0.08	0.93±0.07
Specificity	VGG-16	**0.99±0.02**	**1.00±0.00**
	ResNet50V2	0.94±0.10	0.97±0.07
	IncecptionResNetV2	0.83±0.17	0.85±0.13
Precision	VGG-16	**0.99±0.02**	**1.00±0.00**
	ResNet50V2	0.93±0.11	0.97±0.06
	IncecptionResNetV2	0.84±0.13	0.86±0.11
F-1 Score	VGG-16	**0.96±0.04**	**0.96±0.06**
	ResNet50V2	0.95±0.07	0.95±0.06
	IncecptionResNetV2	0.86±0.08	0.89±0.07

Table 5.8: Comparison of the SLT-based method with existing methods for PD detection

Autor	Dataset	Speech Task	Method	Accuracy
Karan et al. [139]	PC-GITA	Sustainable vowel and Isolated words	IEDCC features used with SVM classifier	81 to 90%
Upadhya et al. [182]	Indian speech dataset	Vowel	Modified MFCC Mel scaled filter with neural networks	83.8%
Rueda et al. [48]	PC-GITA	Sustained vowel 'a'	Two stage filter-wrapper feature selection method with SVM classifier	70%
Vásquez-Correa et al. [63]	PC-GITA	DDK analysis	Articulation and EMD features	76%
Narendra et al. [207]	PC-GITA	Sustainable vowel	Iterative adaptive inverse filtering and quasi-closed phase glottal inverse filtering methods SVM classifier	68.56%
Karan et al. [118]	PC-GITA	Sustainable vowel	STFT and CWT-based TF representation with stacked based autoencoder and SVM classifier	87% with STFT 82% with CWT.

Autor	Dataset	Speech Task	Method	Accuracy
Vásquez-Correa et al. [119]	PC-GITA, German speech recordings, and Czech data	-	TF representations based on STFT with CNN	77.3%
Proposed method	**PC-GITA**	**Sustainable vowel, Modulated vowel, Isolated words, and DDK analysis**	**High resolution SLT with VGG-16**	**92%**
Proposed method	**ItalianPVS**	**Vowels**	**High resolution SLT with VGG-16**	**96%**

Karan et al. [139] utilized the Hilbert spectrum features to characterize non-linearities and non-stationarities of the speech signal. A new feature, the instantaneous energy deviation cepstral coefficient (IEDCC), was introduced, which extracted relevant information and exceeded the traditional acoustic features, with accuracy ranging from 81 to 90%. Upadhya et al. [182] proposed an improved Mel scale filter with a radial basis network on the Indian speech dataset and exhibited a classification accuracy of 83.8%. The methods reported in [48,63,118,119,207] provided an accuracy of 70%, 76%, 68.56%, 87% and 77.3%. The existing studies have been done with different feature extraction and selection techniques. The proposed technique outperforms the reported PD detection techniques with a maximum accuracy of 92% on the PC-GITA dataset and 96% on the ItalianPVS dataset. The proposed method effectively reduces the system complexity as it does not require any additional pre-processing and feature extraction steps.

5.2 A Robust Super Resolution Time-Frequency Framework for Parkinson's Disease Severity Assessment using Gait Signal

5.2.1 Introduction

The walking and running patterns of an individual are represented by their gait, which can be governed by complex neural networks, including cortical regions that regulate cognition and movement activities. PD patients' gait patterns exhibit a range

of impairments and abnormalities since the disease affects both the brain's motor and cognitive functioning [266]. In the early stages of PD, the step length is short, and the gait is sluggish. However, these irregularities of gait are age-related and can result from a multitude of illnesses; they are not specific indicators of PD. PD patients have more specific symptoms, such as decreased arm swing and motion regularity, and increased interlimb asymmetry, which is commonly unilateral in the initial stages. In the mild-to-moderate stage, patients show progressively more significant gait difficulties. The deficits and irregularities of gait patterns worsen for patients with advanced PD. Freezing of gait (FOG) is usually in people with advanced PD stages, although a study has shown that it can also occur in persons with early-stage PD [267].

With the rapid growth of technology, various gait analysis systems have been developed. Wearable devices have been used for constantly monitoring gait performance and identifying FOG occurrences. Also, provide help to PD patients with on-demand cueing at the most advantageous moment to overcome gait disruption [268]. Wearable devices make it easier for professionals to keep track of the symptoms and activities of patients. Due to their portability, ease of affordability, ease of use, and minimal impact on patients' health, wearable devices are considered the perfect choice for monitoring [266]. The most widely used wearable devices are equipped with sensors, like inertial measurement units (IMUs), and insole force- or pressure-based sensors, which are used to monitor the ground reaction force. These sensors' outputs can help with studies of gait, body movement, and tremors that aid in the diagnosis of PD. Gait analysis utilizing sensors is a quick, simple, and inexpensive methodology in contrast to other PD diagnosis approaches. To identify PD, a number of decision-support techniques have been used. These techniques are intended to aid in the early identification and diagnosis of PD by finding typical patterns or irregularities in signals that are symptomatic of the patient's condition.

5.2.2 Methodology

This work proposes a robust super-resolution time-frequency framework (RoSuReTFF) for PD detection and severity assessment using gait signals. The proposed

methodology consists of the following steps: (i) dataset acquisition; (ii) data segmentation; (iii) extraction of TFR and data construction; (iv) providing such TFRs to the CNN model in order to extract features; and lastly (iv) TFR spectrogram categorization into multi and binary classes. Figure 5.4 depicts the block diagram of the proposed RoSuReTFF for PD detection and severity assessment.

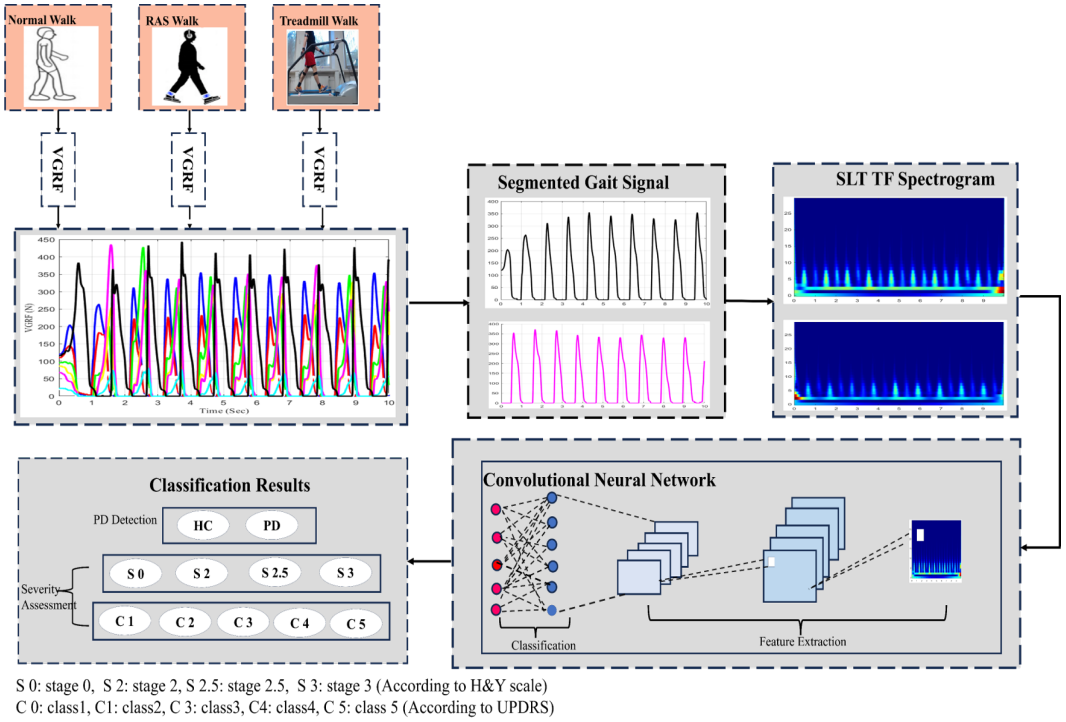

Figure 5.4: Block diagram of the RoSuReTFF method for PD detection using gait signals

5.2.2.1 Dataset

The data utilized in this study is acquired from Physionet [40]. This dataset consists of three independent studies: Ga [269], Ju [270], and Si [271]. The gate patterns were collected from 93 PD patients and 72 HCs. The demographics of both PD patients and HC are shown in Table 5.9.

The Ga data set includes gate patterns from typical walking on level ground, the Ju data includes the gate cycle for walking at a comfortable speed with rhythmic auditory stimulation, and the Si data includes gate time series data from treadmill

Table 5.9: Demographics of PD patients and HC in the Physionet dataset

Dataset	Class	Age	Group	
			Male	Female
Ga	HC	57.9±6.7	10	8
	PD	61.6±8.8	20	9
Ju	HC	39.31±18.51	12	14
	PD	66.80±10.85	16	13
Si	HC	64.5±6.8	18	11
	PD	67.2±9.1	22	13

walking. Eight separate sensors were put in the insole of each subject's foot and used to calculate the vertical ground reaction force (VGRF) in Newtons as a function of time. The coordinate position of the pressure sensors on the sole is illustrated in Figure 5.5. The subjects' VGRF readings were taken at 100 Hz for an approximately two-minute walk.

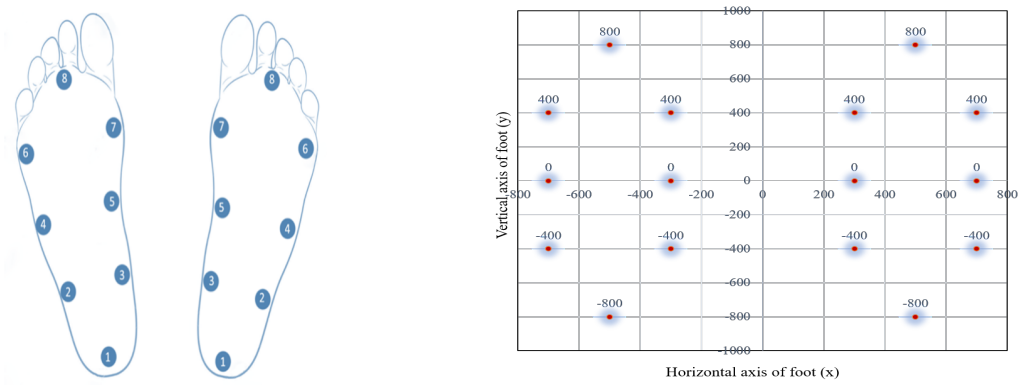

Figure 5.5: The coordinate position of the VGRF sensor positioning underneath each sole

The dataset also contains two signals reflecting the summation of eight sensor outputs, for the left and right foot, respectively. The severity level of PD was graded by the UPDRS and the H&Y scale. Table 5.10 and Table 5.11 present the division of subjects with their level of severity based on the UPDRS and H&Y scale, respectively. The first twenty and last ten seconds of gait signals were already removed from this dataset to reduce the starting and end impacts. The proposed RoSuReTFF employs the sum of all VGRF signals from the PD patients and HC as input.

Table 5.10: Division of subjects based on severity level using UPDRS scale

Dataset	Class 1	Class 2	Class 3	Class 4	Class 5
Ga	18	0	8	11	10
Ju	25	2	15	8	4
Si	29	0	5	11	17

Table 5.11: Division of subjects based on severity level using H&Y scale

Dataset	Severity 0	Severity 2	Severity 2.5	Severity 3
Ga	18	15	8	6
Ju	25	12	13	4
Si	29	29	6	0

5.2.2.2 Data Segmentation

To examine the foot force signal more precisely, the gait signals are divided into equal time segments. Since gait signals are non-stationary, aperiodic, and have fluctuating signal strength over time. To acquire representative data for a certain period of time, the data of each participant is separated into 10-second intervals (1000 samples) with no overlap.

5.2.2.3 Extraction of TFR and Data Construction

Gait signals are nonlinear, non-stationary, and noisy in nature. The non-linear aspect of gait is because it is coordinated by the brain's synchronized activity. The non-linear nature of gait makes it challenging to analyze. To gain a comprehensive understanding of the signals, the signals must be translated from one domain to another. Transformation techniques enable the simultaneous capture of time-domain signal information into the frequency domain. The spectrum fluctuation of the gait signal over time can be captured using TFR. In this work, SLT is utilized to convert the signal into a high-resolution TFR. Data is divided into 10-second window segments (1000 samples without overlapping) to capture dynamic changes in gait characteristics. The complete dataset comprised 3236 windows, with 2242 designated for PD and 994 for HC. The TFR consolidated essential information from the time and frequency domain analysis. Additionally, offers an extensive amount of information about the

time-specificity of power increases in various frequency bands. Figure 5.6 depicts the time-domain visualization of the signals from PD stages 1, 2, 3, 4, and 5 on the UPDRS scale, and the corresponding time-domain signals represented as TFR. The TFR illustrates that, for varying degrees of PD severity, the spectrograms exhibit variation in the spectrum component.

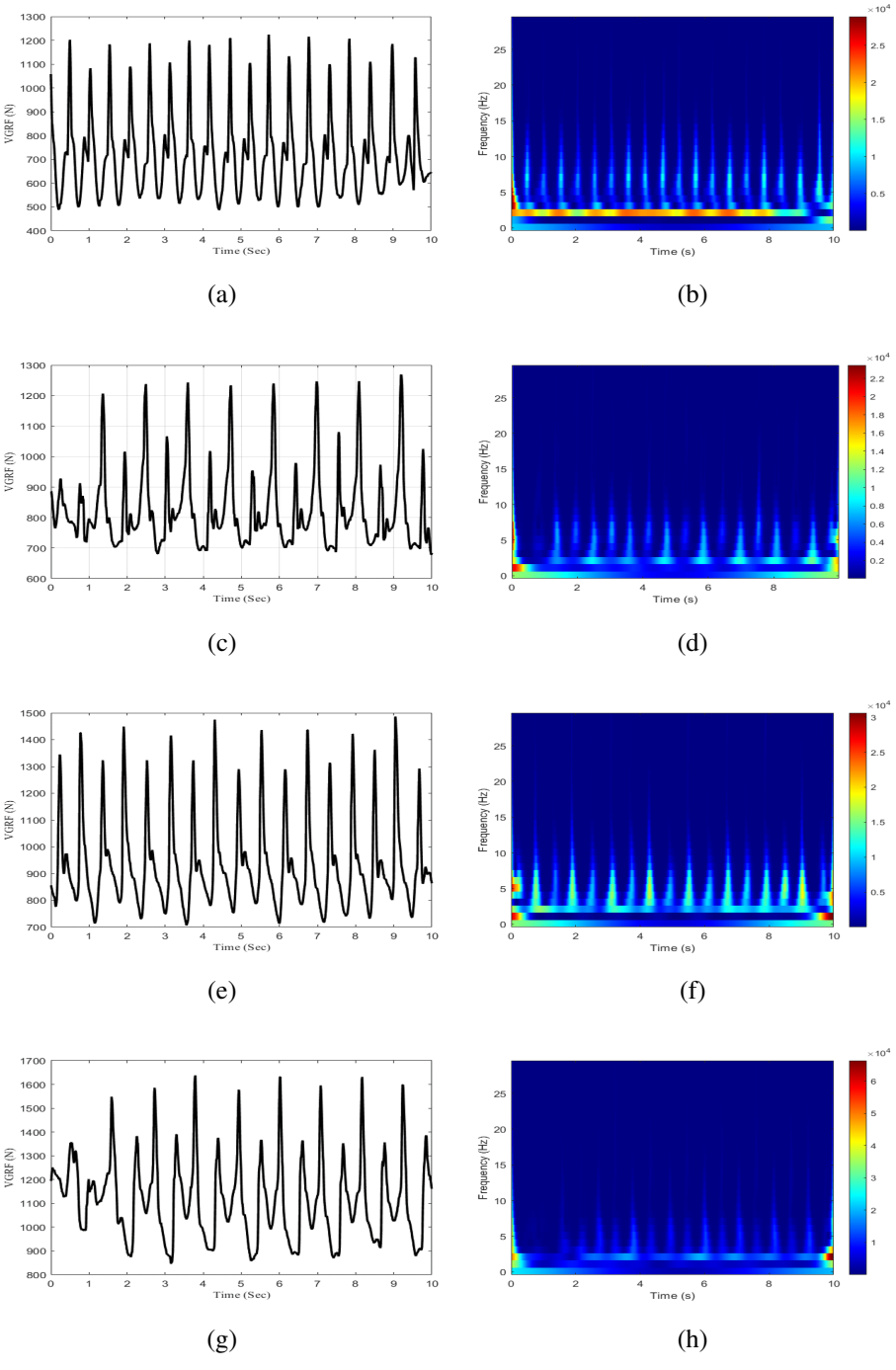

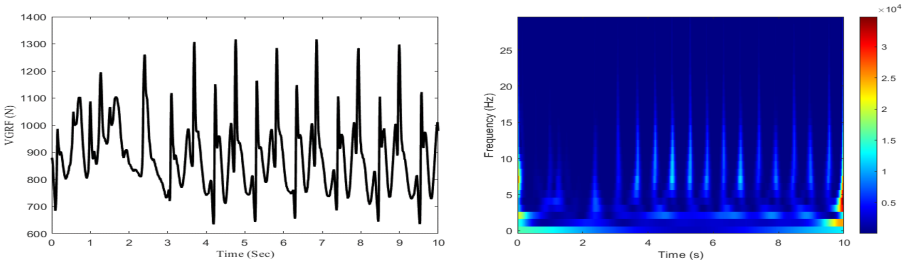

(a) (b)

Figure 5.6: Time-domain visualization of PD stages (class 1-5), with their respective SLT-based TFR

5.2.2.4 Deep Learning Approach: VGG-19

To automate the diagnosis and prognosis of PD, a CNN is utilized to identify latent abnormal patterns in gait signals using the TF spectrogram. CNNs are frequently used in classification, object recognition, picture segmentation, and other domains due to their ability to automatically learn complicated information. However, building an in-depth model necessitates a significant amount of computational power and data. This study employs the VGG-19 model to classify the gait patterns. The VGG-19 model comprises sixteen convolution layers (for feature extraction), and three fully connected layers for classification [265]. The layers utilized for feature extraction are divided into five groups, each of which is followed by a max-pooling layer. The VGG-19 deep CNN model is capable of extracting the hidden representation from the TFRs. The extracted relevant information improves the model's generalization capacity for classification. Figure 5.7 illustrates the architecture of the VGG-19 deep CNN model for PD detection and severity assessment.

5.2.3 Results

To assess the effectiveness of the proposed RoSuReTFF, evaluation criteria like accuracy, sensitivity, precision, specificity, and F-1 score are employed. A 5-fold cross-validation is used to ensure the experiment's dependability and reduce bias. The data is organized into five folds. One of the five folds is tested during each

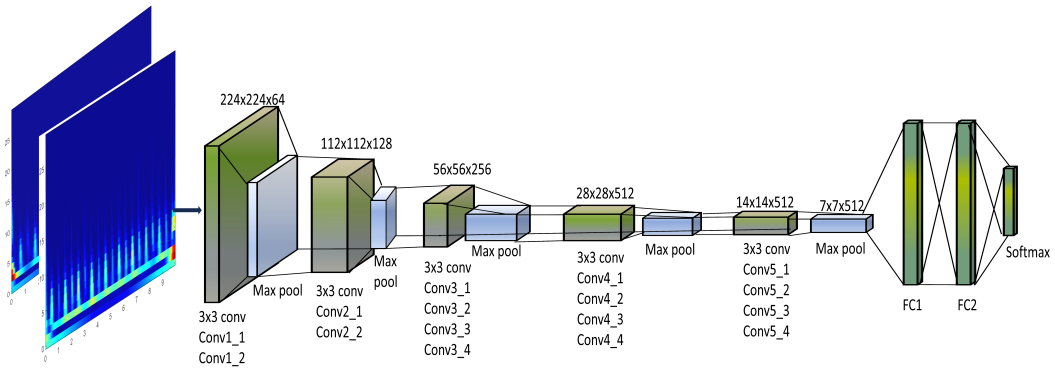

Figure 5.7: Detailed architecture of the VGG-19 deep CNN model for PD detection and severity assessment

cross-validation session, while the remaining four are used to train the classification model. The final result is expressed as the average of the five folds.

5.2.3.1 Performance Analysis for PD Detection

The proposed framework's performance is evaluated using gait signal training and testing for binary and multiclass severity classification using the VGG-19 model. The batch size and number of epochs for the model are set to 16 and 50, respectively. To scale each weight's learning rate, the adaptive moment estimation (Adam) optimizer with a learning rate of 10^{-5} is employed. The input signal for the VGG-19 model is determined by the window size used during gait signal segmentation. The input TFR for HC and PD classes in the Ga, Ju, and Si datasets are 447,900; 199,922; and 348,420, respectively for the ten-second window segment. These TFRs are applied to VGG-19 for PD detection. Table 5.12 presents the outcomes of the proposed RoSuReTFF for binary classification tasks on the Ga, Ju, Si, and combined datasets.

The proposed framework yields an average accuracy of 97.85% for the Ga dataset, 95.63% for the Ju dataset, and 97.26% for the Si dataset. The three datasets (Ga, Ju, and Si) are also merged and fed into the proposed PD detection model. The combined dataset obtained an average accuracy of 96.13%. Figure 5.8 displays the confusion metrics on these datasets using the proposed RoSuReTFF for PD classification.

Table 5.12: Experimental results of the RoSuReTFF method for PD detection

Evaluation parameters	Dataset			
	Ga	Ju	Si	Ga+Ju+Si
Accuracy (%)	97.85±1.06	95.63±0.94	97.26±1.45	96.13±0.49
Sensitivity (%)	99.32±0.41	98.15±0.88	97.85±1.16	97.14±0.72
Precision (%)	97.50±1.15	96.61±1.44	97.18±1.73	97.27±0.41
Specificity (%)	94.85±2.41	83.92±7.16	96.55±2.15	93.86±0.98
F-1 score (%)	98.41±0.78	97.36±0.54	97.51±1.31	97.21±0.35

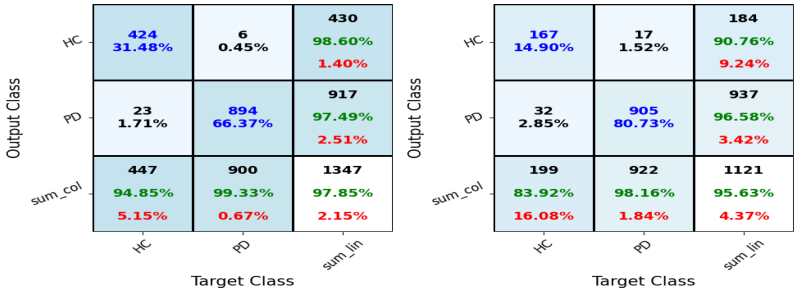

(a) Ga

(b) Ju

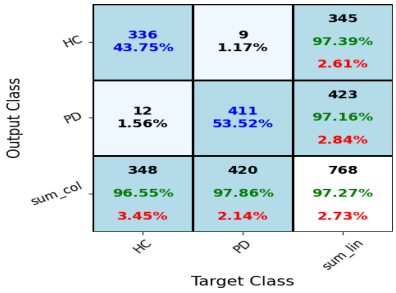

(c) Si

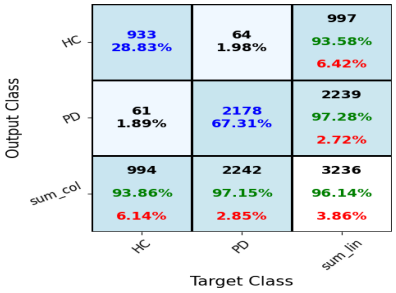

(d) Ga+Ju+Si

Figure 5.8: Confusion matrix (a) Ga dataset, (b) Ju dataset, (c) Si dataset, (d) Ga+Ju+Si (combined) dataset for PD detection

For the Ga dataset, it is observed that 424 TFRs are accurately categorized as HC. It is accurate to classify 894 TFRs as PD patients. For the Ju dataset, it is observed that 167 TFRs are correctly labeled as HC and 905 TFRs as PD patients. For the Si dataset, 336 TFRs are correctly identified as HC, and 411 TFRs are correctly labeled as PD patients. For the combined dataset, out of 2242 PD TFRs 2178 are accurately identified as PD. Table 5.13 presents the comparison of the proposed

framework to the state-of-the-art approaches used to detect PD on the same dataset. The proposed RoSuReTFF outperforms the existing methods for PD detection. Table 5.13 indicates that for both combined and individual datasets (Ga, Ju, and Si) the proposed RoSuReTFF outperforms the existing method for PD detection.

Table 5.13: Comparison of the RoSuReTFF method with other existing approaches for PD detection

Author	Method	Dataset									
		Ga		Ju		Si		Ga+Ju+Si			
		A_c (%)	S_n (%)	A_c (%)	S_n (%)	A_c (%)	S_n (%)	A_c (%)	S_n (%)	S_p (%)	P_r (%)
Lee and Lim (2012) [117]	WT+NEWFM	-	-	-	-	-	-	77.33	65.48	81.10	-
Daliri (2013) [120]	STFT+SVM	-	-	-	-	-	-	91.20	91.71	89.92	-
Ertugrul et al. (2016) [206]	1DLBP+MLP	-	-	-	-	-	-	88.88	88.9	82.2	-
Perumal and Sankar (2016) [272]	Linear discriminant analysis	92.25	-	92.5	-	90	-	-	-	-	-
Zhao et al. (2018) [195]	DNN	-	-	-	-	-	-	90.3	96.2	76.7	-
Khoury et al. (2019) [91]	Time domain features+KNN	86.05	86.34	90.91	85.35	81.25	81.67	-	-	-	-
Masoumi et al. (2021) [121]	CWT+DNN	84.62	-	81.82	-	76.92	–	88.47	-	-	-
Ozel et al. (2021) [122]	Statistical fetaures+KNN	92.92	-	90.69	-	76.56	-	92.96	-	-	-
Zhong et al. (2022) [273]	RFdGAD	-	-	-	-	-	-	93.8	-	-	-
Nguyen et al. (2022) [221]	1-D Transformer	-	-	-	-	-	-	95.2	98.1	86.8	-
Sharma et al. (2023) [194]	1-D CNN	-	-	-	-	-	-	90.47	90	90.9	-
Dong et al. (2023) [274]	Optical flow	-	-	-	-	-	-	93.3	94.6	91.7	-
Proposed	**RoSuReTFF**	**97.85**	**99.32**	**95.63**	**98.15**	**97.26**	**97.85**	**96.13**	**97.14**	**93.86**	**97.27**

- Not reported

5.2.3.2 Performance Analysis for PD Severity Assessment

Due to the progressive nature of PD, it is essential to assess the severity of patients in order to monitor their recovery and give tailored treatment to each individual. Thus, we have also evaluated our approach for estimating PD severity levels. To diagnose the severity level of PD, H&Y and UPDRS scales are most widely utilized.

5.2.3.3 Performance Analysis for PD Severity Assessment using H&Y Scale

To depict the severity of PD, the H&Y scale includes 8 stages. Stage 0 denotes no evidence of PD, Stage 1 denotes the disease's symptoms are limited to one side of the body; Stage 1.5 denotes the disease's symptoms are present on one side in addition to the neck and spine; Stage 2 denotes the disease's symptoms are seen on both sides of the body, although balance is unaffected; Stage 2.5 denotes the disease's mild symptoms appear on both sides of the body; Stage 3 denotes balance impairment, and mild to moderate discomfort in both legs; Stage 4 indicates severe impairment, although the patient may walk without assistance; and Stage 5 denotes individuals who are bedridden without assistance or who require a wheelchair [275].

The Physionet dataset employed PD Stages 0, 2, 2.5, and 3 for the H&Y scale. The severity assessment model for the H&Y scale maintained the detection model's network topology. The last layer is substituted by a fully connected layer containing four neurons and utilizing a softmax activation function. For the ten-second window segment, the TFRs obtained for PD Stage 0, PD Stage 2, PD Stage 2.5, and PD Stage 3 are as follows: Ga dataset: 447 (PD Stage 0), 492 (PD Stage 2), 240 (PD Stage 2.5), and 168 (PD Stage 3); Ju dataset: 199 (PD Stage 0), 354 (PD Stage 2), 459 (PD Stage 2.5), and 109 (PD Stage 3); Si dataset: 348 (PD Stage 0), 336 (PD Stage 2), and 84 (PD Stage 2.5). The average classification accuracy of the Ga dataset is 93.76%, for the Ju dataset 95.06%, and for the Si dataset 94.53%. Additionally, the three datasets are integrated and fed into the VGG-19 model for classifying PD severities. The combined dataset obtained an average classification accuracy of 93.60%. Table 5.14 illustrates the performance outcomes of the proposed RoSuReTFF for PD severity classification on the H&Y scale.

Table 5.14: Experimental results of the RoSuReTFF method for PD severity assessment on H&Y scale

Dataset	Class	Evaluation parameters					
		Accuracy (%)	Sensitivity (%)	Precision (%)	Specificity (%)	F-1 score (%)	Overall Accuracy (%)
Ga	Stage 0	97.69±0.79	95.97±1.66	97.09±1.93	98.55±0.96	96.51±1.19	93.76±1.55
	Stage 2	95.61±1.29	93.49±2.11	94.45±1.67	96.83±0.95	93.97±1.81	
	Stage 2.5	97.54±0.76	95.41±2.76	91.40±3.70	98.01±0.92	93.29±2.03	
	Stage 3	96.65±1.10	86.27±5.35	87.20±5.73	98.15±1.03	86.57±4.35	
Ju	Stage 0	96.34±0.95	89.98±6.69	89.96±4.64	97.72±1.21	89.67±2.81	95.09±1.09
	Stage 2	96.87±0.74	96.32±1.12	94.01±2.61	97.13±1.37	95.12±1.11	
	Stage 2.5	97.50±1.04	96.07±2.62	97.81±1.50	98.49±1.06	96.90±1.32	
	Stage 3	99.46±0.43	96.32±3.41	98.17±2.23	99.80±0.24	97.22±2.28	
Si	Stage 0	97.00±0.51	95.11±0.71	98.23±1.09	98.56±0.89	96.64±0.55	94.53±0.66
	Stage 2	95.57±0.96	97.02±1.33	93.18±1.70	94.44±1.57	95.05±1.01	
	Stage 2.5	96.48±0.97	82.05±8.54	86.00±6.79	98.24±1.10	83.53±4.72	
Ga+Ju+Si	Stage 0	96.67±0.72	93.66±1.78	95.39±1.51	97.99±0.67	94.51±1.20	93.60±1.74
	Stage 2	96.19±1.11	94.56±1.81	91.22±3.21	96.78±1.31	92.88±1.97	
	Stage 2.5	96.13±1.52	94.19±3.32	94.61±2.24	97.16±1.20	94.38±2.27	
	Stage 3	98.20±0.25	88.09±3.72	90.71±2.65	99.15±0.28	89.34±1.63	

5.2.3.4 Performance Analysis for PD Severity Assessment using UPDRS Scale

The UPDRS scale assesses 42 points encompassing cognitive, functional, and behavioral aspects of PD. A higher score on the UPDRS scale indicates a more severe level of illness.

Maachi et al. [176] distributed the severity of PD into five categories based on the UPDRS score as follows:

- Class 1: UPDRS score < 5
- Class 2: 5 $\leq$ UPDRS score < 15
- Class 3: 15 $\leq$ UPDRS score < 25
- Class 4: 25 $\leq$ UPDRS score < 35
- Class 5: 35 $\leq$ UPDRS score

For the ten-second window segment, the TFRs for Class 1, Class 2, Class 3, Class4, and Class 5 in the Ga, Ju, and Si datasets are as follows: Ga dataset: 447 (Class1),

204 (Class3), 348 (Class4), and 348 (Class5); Ju dataset: 199 (Class1), 40 (Class2), 510 (Class3), 266 (Class4), and 106 (Class5); Si dataset: 348 (Class1), 60 (Class3), 132 (Class4), and 204 (Class5).

Table 5.15: Experimental results of the RoSuReTFF method for PD severity assessment on UPDRS scale

Dataset	Class	Evaluation parameters					
		Accuracy (%)	Sensitivity (%)	Precision (%)	Specificity (%)	F-1 score (%)	Overall Accuracy (%)
Ga	Class 1	97.32±0.78	96.19±2.85	95.82±1.67	97.89±0.89	95.97±1.24	93.24±1.50
	Class 3	97.39±1.06	90.68±5.43	92.71±6.97	98.60±1.38	91.38±3.36	
	Class 4	96.13±0.50	93.39±1.91	91.92±2.91	97.09±1.15	92.59±0.87	
	Class 5	95.62±1.17	90.81±2.65	92.29±3.59	97.29±1.43	91.48±2.13	
Ju	Class 1	96.25±1.06	86.97±9.25	91.91±3.05	98.25±0.79	88.93±4.03	95.36±1.82
	Class 2	99.64±0.34	100.00±0.00	91.38±7.62	99.62±0.34	95.42±4.69	
	Class 3	97.32±0.92	97.45±1.33	96.73±1.91	97.22±1.67	97.07±0.99	
	Class 4	98.75±0.86	97.35±1.92	97.48±3.24	99.18±1.07	97.37±1.76	
	Class 5	98.75±0.71	94.37±3.47	92.75±4.51	99.21±0.50	93.52±3.59	
Si	Class 1	97.31±1.53	98.27±1.42	96.16±2.87	96.46±2.82	97.17±1.55	95.70±1.82
	Class 3	98.92±1.38	96.67±4.08	91.58±1.09	99.12±1.16	93.89±7.75	
	Class 4	97.98±1.03	92.36±5.9	96.15±2.28	99.18±0.51	94.18±3.35	
	Class 5	97.17±1.71	93.13±3.24	96.60±4.28	98.70±1.71	94.78±3.09	
Ga+Ju+Si	Class 1	97.10±0.55	95.27±1.99	95.37±1.34	97.92±0.65	95.31±0.92	94.20±1.22
	Class 2	99.96±0.06	97.50±4.99	100.00±0.0	100±0.00	98.66±2.67	
	Class 3	97.69±0.77	94.96±2.49	95.45±0.97	98.56±0.29	95.19±1.67	
	Class 4	97.07±0.87	94.24±0.54	93.24±3.46	97.93±1.20	93.76±1.69	
	Class 5	96.57±0.59	91.49±1.87	91.77±1.51	97.88±0.40	91.62±1.47	

The final layer of the VGG-19 model is replaced with a fully connected layer consisting of five neurons and a softmax activation function. The validation is carried out by a five-fold cross-validation. The model's batch size is set to 16, and the number of epochs is set to 50. The effectiveness of the proposed method for PD severity assessment on the UPDRS scale is illustrated in Table 5.15.

The proposed approach achieves an overall accuracy of 93.24% for the Ga dataset, 95.36% for the Ju dataset, and 95.70% for the Si dataset. Nonetheless, the model achieves 94.20% accuracy for the combined dataset. Figure 5.9 (a) displays the confusion matrix obtained from the proposed approach for PD severity assessment

using the H&Y scale, and Figure 5.9 (b) depicts the confusion matrix obtained from the proposed approach for PD severity assessment using the UPDRS scale on the combined dataset.

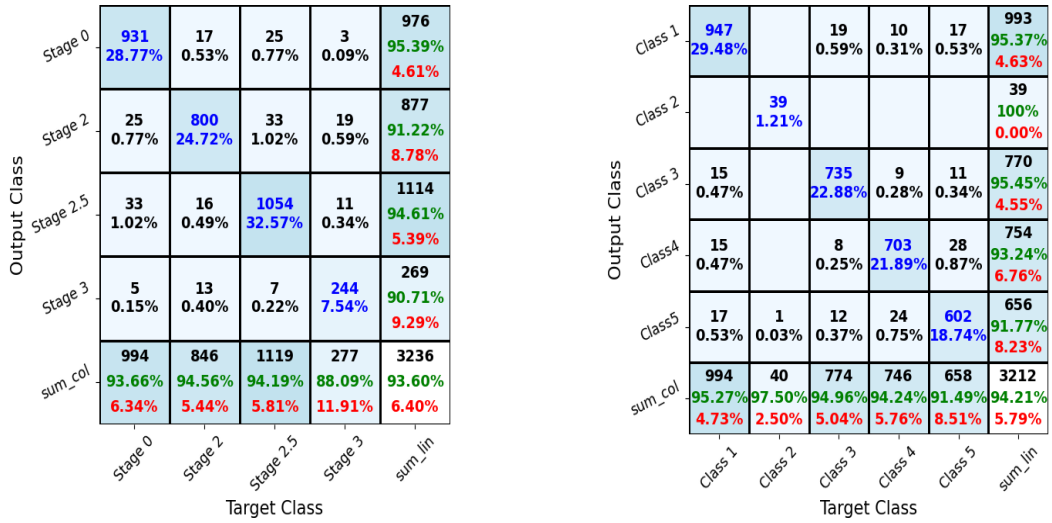

(a) H&Y (b) UPDRS

Figure 5.9: Confusion matrix for PD severity assessment on the combined dataset (a) H&Y (b) UPDRS

Table 5.16: The performance comparison of the RoSuReTFF method with existing techniques for PD severity assessment

Autor	Method	Rating Scale	Evaluation parameters		
			A_c (%)	S_n (%)	P_r (%)
Maachi et al. (2020) [176]	1D-CNN	UPDRS	85.3	85.3	87.3
Veeraragavan et al. (2020) [276]	ANN	H&Y	76.08	-	-
Naimi et al. (2023) [219]	Hybrid ConvNet-Transformer	H&Y	87.89	85.25	87
Dong et al. (2023) [274]	Optical flow	H&Y	91.4	85.5	-
Dong et al. (2023) [175]	1D-Convnet	UPDRS	92.3	92.2	92.8
Proposed	**RoSuReTFF**	**H&Y**	**93.60**	**92.62**	**92.98**
Proposed	**RoSuReTFF**	**UPDRS**	**94.21**	**94.69**	**95.16**

Table 5.16 presents the comparison of the proposed framework to the state-of-the-art approaches used for PD severity assessment on the same dataset. The outcomes

demonstrate that the proposed RoSuReTFF outperforms the existing methods for PD severity assessment.

5.2.3.5 Ablation Study

An ablation study is carried out to assess the impact of different components and configurations on the overall performance of our proposed method for PD detection. Specifically, we examined the effect of different TFR techniques, including SLT, Smoothed Pseudo Wigner-Ville Distribution (SPWVD), and Wavelet synchrosqueezed transform (WSST). Within SLT, we explore the influence of various parameters on the performance of the proposed framework. This study helps to better understand how various parameters affect the model's overall performance.

Table 5.17: Ablation study using different evaluation parameters for PD detection

Model	Method	Parameters	BS	Optimizer	Evaluation parameters				
					A_c (%)	S_n (%)	S_p (%)	P_r (%)	F_1^{sr} (%)
A	SPWVD+VGG-19	-	16	Adam	93.87±1.69	95.93±0.96	89.29±6.28	95.23±2.53	95.61±1.13
B	WSST+VGG-19	-	16	Adam	95.48±1.62	97.23±2.09	91.55±6.70	96.28±2.67	96.76±1.11
C	SLT+AlexNet	Additivity (m=3)	16	Adam	81.39±1.88	94.23±3.23	52.41±11.71	81.92±3.20	87.53±0.96
D	SLT+ResNet-50	Additivity (m=3)	16	Adam	95.64±1.08	97.01±1.25	92.55±0.86	96.70±0.40	96.86±0.79
E	SLT+VGG-19	Additivity (m=3)	32	Adam	94.49±0.68	96.96±1.96	88.93±2.97	95.21±0.11	96.06±0.53
F	SLT+VGG-19	Additivity (m=5)	16	Adam	95.30±1.57	96.38±3.22	92.85±3.06	96.81±1.28	96.60±1.24
G	SLT+VGG-19	Multiplicity (m=3)	16	Adam	95.33±0.61	97.10±0.19	96.23±0.13	91.34±0.32	96.64±0.47
H	SLT+VGG-19	Multiplicity (m=5)	16	Adam	94.61±2.11	95.85±4.01	91.84±4.12	96.43±1.69	96.06±1.68
I	SLT+VGG-19	Additivity (m=3)	64	Adam	95.95±0.91	97.40±1.63	96.77±0.69	92.64±1.71	97.11±0.69
J	SLT+VGG-19	Additivity (m=3)	16	RMSprop	68.75±7.02	56.51±11.00	96.37±3.20	97.46±2.04	70.85±8.58
K	**SLT+VGG-19**	**Additivity (m=3)**	**16**	**Adam**	**96.13±0.49**	**97.14±0.72**	**93.86±0.98**	**97.27±0.41**	**97.20±0.35**

As additivity or multiplicative laws in SL influence the number of wavelength cycles, we evaluated SLT with both multiplicity (Mul) and additivity (Add) to find the

number of cycles in the wavelet. Furthermore, we test our method across multiple neural network architectures, including ResNet50 and AlexNet, to determine the optimal architecture for PD detection.

Additionally, we investigate how variations in training parameters, such as batch size (BS), and optimizer (Adam, RMSprop), affect model performance. This comprehensive study allows us to determine the impact of each component and configuration, providing a deeper understanding of their roles in the overall effectiveness of the proposed method. Table 5.17 depicts the progressive development of the proposed method on different evaluation parameters. The ablation study demonstrates that the SLT (additivity m=3), combined with the VGG-19 architecture, consistently delivered the optimal performance, achieving an accuracy of 96.13% for PD detection.

5.3 Summary

This chapter explored two complementary studies aimed at improving the detection and assessment of PD using advanced time-frequency analysis and deep learning techniques.

- ✓ In the first study, a novel hybrid approach combining the Superlet Transform (SLT) with Deep Neural Networks (DNNs) was proposed for the automatic detection of PD from speech signals. The SLT was employed to transform non-stationary one-dimensional speech signals into high-resolution time-frequency spectrograms, which effectively capture the key spectral characteristics of speech. These spectrograms were then used as input to three deep learning models, VGG-16, ResNet50V2, and InceptionResNetV2 for PD classification. Experimental evaluation on the PC-GITA and ItalianPVS datasets, using a 10-fold cross-validation scheme, achieved accuracies of 92% and 96%, respectively. Among the tested models, VGG-16 demonstrated superior performance, outperforming several existing state-of-the-art techniques, including EMD, CWT, and STFT-based methods.
- ✓ The second study focused on assessing PD severity through gait analysis. A super-resolution time-frequency framework, integrating the Superlet Transform

with a VGG-19 convolutional neural network, was developed using gait data from the Physionet dataset. The SLT generated high-quality time-frequency spectrograms from gait signals, which served as direct input to the deep model. Unlike traditional methods that rely on multiple vertical ground reaction force channels and extensive feature engineering, the proposed framework provides an end-to-end, computationally efficient approach. Experimental findings confirmed its robustness and accuracy in evaluating PD severity, highlighting its potential for real-world clinical applications.

Chapter 6

Conclusion, Future Directions and Social Impact

This chapter presents a comprehensive overview of the findings from both theoretical and experimental studies. It integrates the key insights obtained throughout the endeavor, emphasizing how the theoretical framework supports and explains the experimental findings. Furthermore, the chapter includes the future scope and identifies prospective areas for improvement. Finally, it addresses the social impact of this work.

6.1 Conclusion

This research work began with the primary goal of designing and developing techniques for identifying and classifying brain diseases, with a focus on neurodegenerative disorders such as AD and PD. These disorders worsen over time and have no permanent cure. Early and reliable diagnosis of these disorders remains a significant challenge, as existing diagnostic techniques are generally based on subjective clinical evaluations and have limited ability to identify subtle, early-stage abnormalities. To address this difficulty, the study employs several biosignaling modalities, including EEG, speech, and gait data, to identify and categorize these diseases. This thesis establishes three major objectives for the diagnosis and categorization of brain disorders. To fulfill these objectives, various methods and approaches have been developed and implemented, as summarised below:

- ✓ EEG signals are considered a valuable tool for the early detection of PD, as they capture subtle changes in brain activity associated with the disorder. In

this work, statistical features (mean, variance, skewness, and kurtosis) and Hjorth parameters (Hjorth activity, mobility, and complexity) are extracted from different EEG channels. These features provide an accurate representation of EEG signals by capturing both amplitude and frequency properties. The relevant set of features was selected using KW test and ETC. The KW test identifies features that differ statistically significantly between PD patients and HCs, whereas the ETC assesses feature importance to select the most discriminative qualities. After feature selection, various ML classifiers were trained and evaluated to distinguish PD from HCs. DT classifier achieved the highest performance,with accuracy, precision, sensitivity, and F-1 score of 98%, 97%, 99%, and 98%, respectively. The results demonstrates that the selected EEG features are highly effective in capturing the neural changes associated with PD.

- ✓ Speech impairment is one of the earliest and most consistent indicators of PD, making speech-based diagnostic systems a promising tool for early detection. For this purpose, a two-stage stacked ensemble model is developed. At first, the speech features are preprocessed, and the class imbalance problem is addressed using SMOTE to generate synthetic samples for the minority class. To obtain the optimal set of features, ETC is used. For PD prediction, firstlly three base classifiers are used. These classifiers learn patterns from the specified characteristics independently, and their predictions are then combined by a meta-classifier in the second stage to generate the final prediction. This framework leverages the complementary strengths of the base models and achieves an accuracy of 98.31%, sensitivity of 96.55%, and AUC of 98.27%, significantly outperforming traditional single-model approaches and demonstrating the effectiveness of combining feature selection, data balancing, and ensemble learning for accurate PD detection using speech attributes.
- ✓ Accurately identifying the brain regions and EEG channels most impacted by AD is critical for reliable diagnosis and meaningful interpretation. AD is a progressive disorder that affects neuronal connections and alters rhythmic brain activity, particularly in certain cortical areas. To detect these, EEG signals

from the frontal, temporal, parietal, and occipital lobes are examined. For this purpose, a Fourier Decomposition and Hilbert Transform-based EEG Signal Analysis (FHESA) method is developed. FHESA enables efficient classification and localization of AD-related dysfunction, facilitating early and precise disease detection. Two distinct datasets are used to validate the effectiveness of the proposed FHESA method. Five classifiers, namely KNN, NB, DT, SVM, and LR, are employed for model evaluation. The best classification performance is achieved by the NB classifier. The proposed FHESA approach detected AD with 98% (closed-eyes EEG recording) and 99% (open-eyes EEG recording) accuracy on Dataset I and 99% (closed-eyes EEG recording) and 97% (open-eyes EEG recording) accuracy on Dataset II. Also analyzed the influence of various channels and performed brain area analysis at various lobes to identify significant regions affected by AD. The results depict that the temporal lobe electrodes provide an accuracy of 97% and the precision, sensitivity, specificity, F1-score, MCC, and Kappa score for ten-fold cross-validation 99%, 95%, 95%, 96%, 0.92, and 0.91, respectively.

- ✓ Accurate identification and classification of neurological disorders, such as dementia, are crucial for early diagnosis and effective treatment. To address this, WavDemNet is proposed. It integrates the WST to extract stable, discriminative time–frequency features from EEG signals and a 1D CNN to learn high-level abstractions for reliable classification. By capturing subtle neurophysiological differences associated with AD and FTD, WavDemNet achieved 89.45% accuracy for dementia identification and 88.40% for AD–FTD classification on the OpenNeuro dataset, outperforming existing state-of-the-art EEG-based methods.
- ✓ Traditional assessment methods rely heavily on subjective clinical evaluation, which can be inconsistent and time-consuming. So, an automated end-to-end framework is developed for the early diagnosis of PD. For speech-based diagnosis, speech recordings are preprocessed and transformed using the SLT to create high-resolution time–frequency spectrograms. These spectrograms are then analyzed by DNN to detect PD by identifying subtle changes in voice

patterns, which serve as early biomarkers of the disease. The VGG-16 model with SLT achieved an overall accuracy of 92% with sensitivity, specificity, precision, and F-1 score of 92%, 91%, 95%, and 93%, respectively. The proposed method also achieved an accuracy of 96% on the ItalianPVS dataset.

- ✓ A robust super-resolution time-frequency framework (Ro- SuReTFF) is developed to detect and assess the severity level of PD using gait signals. Gait patterns are converted into TFR to capture fine motor abnormalities. The proposed work achieved an overall accuracy of 96.13% for PD detection, 94.20% for severity evaluation on the UPDRS scale, and 93.60% for severity evaluation on the H&Y scale. The outcomes indicate that the proposed approach outperforms the state-of-the-art methods for PD detection and severity assessment.

In order to identify and classify brain diseases, EEG signals, speech signals, and gait patterns are utilized in this thesis. For PD detection, EEG signals and speech signals are considered. Extracted the relevant and optimized set of features from these signals to obtain efficient detection accuracy. PD severity assessment is performed using gait signals, and an automated algorithm has been developed that eliminates the need for any additional pre-processing or feature extraction steps. For AD detection, the influence of various channels was analyzed, and brain area analysis at various lobes was performed to identify significant regions affected by AD using EEG signals. Additionally, for identifying and classifying neurological disorders, AD and FTD are considered as both diseases are types of dementia and have overlapping symptoms. To address diagnostic challenges arising from overlapping clinical phenotypes, a wavelet scattering transform-based deep learning framework is developed to solve this problem.

6.2 Limitations of the Study

This work yields valuable insights, but also has several limitations as mentioned below:

A Two-Stage Ensemble Approach for the Analysis of Parkinson's Disease Using Speech Signals considers only cepstrum coefficients and special features extracted

from audio signals; however, other features, such as acoustic and statistical data, can also be investigated. The proposed method is intended for three base learners, which can be expanded, and alternative combinations of base learners can be tested to improve classification performance. Furthermore, the suggested method may be used for bigger datasets containing voice signals that vary in tone, pitch, ethnicity, language, and environmental noise.

An additional constraint we encountered concerns the collection of datasets on different neurological diseases. Multi-disease brain data is limited due to data fragmentation, privacy constraints, high collection costs, lack of standardization, and class imbalance. Most datasets focus on single diseases, making multi-disease analysis and model generalization challenging.

PD detection and severity assessment rely on high-performance GPU hardware for efficient training and inference, thereby increasing computational costs and potentially limiting deployment in low-resource settings. Future work will focus on incorporating explainable AI techniques and optimizing model architectures to reduce computational complexity while enhancing transparency and clinical applicability.

6.3 Future Directions and Social Impact

The objective of this endeavor is to build and develop algorithms for identifying and classifying brain diseases, with a focus on neurodegenerative disorders. Future research will focus on improving the model's resilience by considering a broader range of brain disorders. This work could also be expanded to encompass the detection of numerous neurological problems, as well as the development of a real-time application that will assist medical practitioners in promptly and correctly distinguishing between different neurological disorders using a wider range of signaling modalities. We also intend to combine signaling data with clinical, genetic, and demographic information to obtain more comprehensive diagnostic insights. Additional work will focus on establishing explainable AI methods to increase model interpretability, ensuring that clinicians understand and trust the model's decision-making process.

This work has the potential to revolutionize the detection and treatment of brain disorders, which would have a significant socioeconomic impact. The following are the main areas of impact:

- ✓ **Early Detection:** Identifying disorders at the initial stage enables therapies that can delay or even prevent the symptoms. Earlier diagnosis is frequently associated with improved long-term outcomes and better quality of life.
- ✓ **Helps in Treatment:** Early diagnosis allows for the use of disease-modifying medications before irreversible harm occurs. Treatment at an earlier stage is typically more effective and less intrusive.
- ✓ **Improved Decision Making:** Early detection of brain diseases allows patients and their carers to make more informed decisions about healthcare, lifestyle, and financial planning.
- ✓ **Real time monitoring:** Patients may receive adaptive treatment based on their continuously monitored and customized health.
- ✓ **Associated Care:** The patients' need for a caregiver is minimized, lowering the pressure on support services.

Bibliography

[1] C. P. Ferri, M. Prince, C. Brayne, H. Brodaty, L. Fratiglioni, M. Ganguli, K. Hall, K. Hasegawa, H. Hendrie, Y. Huang, *et al.*, "Global prevalence of dementia: a delphi consensus study," *The lancet*, vol. 366, no. 9503, pp. 2112–2117, 2005.

[2] N. Goenka and S. Tiwari, "Deep learning for alzheimer prediction using brain biomarkers," *Artificial Intelligence Review*, vol. 54, no. 7, pp. 4827–4871, 2021.

[3] E. Nichols, C. E. Szoeke, S. E. Vollset, N. Abbasi, F. Abd-Allah, J. Abdela, M. T. E. Aichour, R. O. Akinyemi, F. Alahdab, S. W. Asgedom, *et al.*, "Global, regional, and national burden of alzheimer's disease and other dementias, 1990–2016: a systematic analysis for the global burden of disease study 2016," *The Lancet Neurology*, vol. 18, no. 1, pp. 88–106, 2019.

[4] U. Petti, S. Baker, and A. Korhonen, "A systematic literature review of automatic alzheimer's disease detection from speech and language," *Journal of the American Medical Informatics Association*, vol. 27, no. 11, pp. 1784–1797, 2020.

[5] B. Winblad, P. Amouyel, S. Andrieu, C. Ballard, C. Brayne, H. Brodaty, A. Cedazo-Minguez, B. Dubois, D. Edvardsson, H. Feldman, *et al.*, "Defeating alzheimer's disease and other dementias: a priority for european science and society," *The Lancet Neurology*, vol. 15, no. 5, pp. 455–532, 2016.

[6] M. Dolatshahi, A. Salehipour, A. Saghazadeh, H. Sanjeari Moghaddam, V. Aghamollaii, A. Fotouhi, and A. Tafakhori, "Thyroid hormone levels in alzheimer disease: a systematic review and meta-analysis," *Endocrine*, vol. 79, no. 2, pp. 252–272, 2023.

[7] R. Dhapola, S. S. Hota, P. Sarma, A. Bhattacharyya, B. Medhi, and D. H. Reddy, "Recent advances in molecular pathways and therapeutic implications

targeting neuroinflammation for alzheimer's disease," *Inflammopharmacology*, pp. 1–13, 2021.

[8] A. Association, "2019 alzheimer's disease facts and figures," *Alzheimer's & dementia*, vol. 15, no. 3, pp. 321–387, 2019.

[9] M. A. Ebrahimighahnavieh, S. Luo, and R. Chiong, "Deep learning to detect alzheimer's disease from neuroimaging: A systematic literature review," *Computer methods and programs in biomedicine*, vol. 187, p. 105242, 2020.

[10] M. Fernandez-Alvarez, M. Atienza, and J. L. Cantero, "Effects of non-modifiable risk factors of alzheimer's disease on intracortical myelin content," *Alzheimer's Research & Therapy*, vol. 14, no. 1, p. 202, 2022.

[11] X.-X. Zhang, Y. Tian, Z.-T. Wang, Y.-H. Ma, L. Tan, and J.-T. Yu, "The epidemiology of alzheimer's disease modifiable risk factors and prevention," *The journal of prevention of Alzheimer's disease*, vol. 8, no. 3, pp. 313–321, 2021.

[12] A. Sharma, S. Rudrawar, S. B. Bharate, and H. R. Jadhav, "Recent advancements in the therapeutic approaches for alzheimer's disease treatment: current and future perspective," *RSC Medicinal Chemistry*, vol. 16, no. 2, pp. 652–693, 2025.

[13] J. Jankovic, "Parkinson's disease: clinical features and diagnosis," *Journal of neurology, neurosurgery & psychiatry*, vol. 79, no. 4, pp. 368–376, 2008.

[14] D. B. Miller and J. P. O'Callaghan, "Biomarkers of parkinson's disease: present and future," *Metabolism*, vol. 64, no. 3, pp. S40–S46, 2015.

[15] E. Naghsh, M. F. Sabahi, and S. Beheshti, "Spatial analysis of eeg signals for parkinson's disease stage detection," *Signal, Image and Video Processing*, vol. 14, no. 2, pp. 397–405, 2020.

[16] E. R. Dorsey and B. R. Bloem, "The parkinson pandemic—a call to action," *JAMA neurology*, vol. 75, no. 1, pp. 9–10, 2018.

[17] B. Brakedal, L. Toker, K. Haugarvoll, and C. Tzoulis, "A nationwide study of the incidence, prevalence and mortality of parkinson's disease in the norwegian population," *npj Parkinson's Disease*, vol. 8, no. 1, p. 19, 2022.

[18] G. E. Gillies, I. S. Pienaar, S. Vohra, and Z. Qamhawi, "Sex differences in parkinson's disease," *Frontiers in neuroendocrinology*, vol. 35, no. 3, pp. 370–384, 2014.

[19] C. Ahlrichs and M. Lawo, "Parkinson's disease motor symptoms in machine learning: A review," *arXiv preprint arXiv:1312.3825*, 2013.

[20] S. Gupta and S. Shukla, "Non-motor symptoms in parkinson's disease: Opening new avenues in treatment," *Current Research in Behavioral Sciences*, vol. 2, p. 100049, 2021.

[21] G. M. Earhart and M. J. Falvo, "Parkinson disease and exercise," *Comprehensive Physiology*, vol. 3, no. 2, pp. 833–848, 2013.

[22] S. Cerri, L. Mus, and F. Blandini, "Parkinson's disease in women and men: what's the difference?," *Journal of Parkinson's disease*, vol. 9, no. 3, pp. 501–515, 2019.

[23] R. Xia and Z.-H. Mao, "Progression of motor symptoms in parkinson's disease," *Neuroscience bulletin*, vol. 28, pp. 39–48, 2012.

[24] M. J. Armstrong and M. S. Okun, "Diagnosis and treatment of parkinson disease: a review," *Jama*, vol. 323, no. 6, pp. 548–560, 2020.

[25] U. Raghavendra, U. R. Acharya, and H. Adeli, "Artificial intelligence techniques for automated diagnosis of neurological disorders," *European neurology*, vol. 82, no. 1-3, pp. 41–64, 2019.

[26] A. A. Bhurane, S. Dhok, M. Sharma, R. Yuvaraj, M. Murugappan, and U. R. Acharya, "Diagnosis of parkinson's disease from electroencephalography signals using linear and self-similarity features," *Expert Systems*, vol. 39, no. 7, p. e12472, 2022.

[27] C. Sridhar, S. Bhat, U. R. Acharya, H. Adeli, and G. M. Bairy, "Diagnosis of attention deficit hyperactivity disorder using imaging and signal processing techniques," *Computers in Biology and Medicine*, vol. 88, pp. 93–99, 2017.

[28] Z. K. Senturk, "Early diagnosis of parkinson's disease using machine learning algorithms," *Medical hypotheses*, vol. 138, p. 109603, 2020.

[29] A. A. Lima, M. F. Mridha, S. C. Das, M. M. Kabir, M. R. Islam, and Y. Watanobe, "A comprehensive survey on the detection, classification, and challenges of neurological disorders," *Biology*, vol. 11, no. 3, p. 469, 2022.

[30] Y. J. Bae, J.-M. Kim, C.-H. Sohn, J.-H. Choi, B. S. Choi, Y. S. Song, Y. Nam, S. J. Cho, B. Jeon, and J. H. Kim, "Imaging the substantia nigra in parkinson disease and other parkinsonian syndromes," *Radiology*, vol. 300, no. 2, pp. 260–278, 2021.

[31] N. Weiskopf, R. Veit, M. Erb, K. Mathiak, W. Grodd, R. Goebel, and N. Birbaumer, "Physiological self-regulation of regional brain activity using real-time functional magnetic resonance imaging (fmri): methodology and exemplary data," *Neuroimage*, vol. 19, no. 3, pp. 577–586, 2003.

[32] T. Katayama, J. Sawada, K. Takahashi, and O. Yahara, "Cerebrospinal fluid biomarkers in parkinson's disease: a critical overview of the literature and meta-analyses," *Brain sciences*, vol. 10, no. 7, p. 466, 2020.

[33] I. Aouraghe, G. Khaissidi, and M. Mrabti, "A literature review of online handwriting analysis to detect parkinson's disease at an early stage," *Multimedia Tools and Applications*, vol. 82, no. 8, pp. 11923–11948, 2023.

[34] C. R. Jack Jr, M. A. Bernstein, N. C. Fox, P. Thompson, G. Alexander, D. Harvey, B. Borowski, P. J. Britson, J. L. Whitwell, C. Ward, *et al.*, "The alzheimer's disease neuroimaging initiative (adni): Mri methods," *Journal of Magnetic Resonance Imaging: An Official Journal of the International Society for Magnetic Resonance in Medicine*, vol. 27, no. 4, pp. 685–691, 2008.

[35] D. S. Marcus, T. H. Wang, J. Parker, J. G. Csernansky, J. C. Morris, and R. L. Buckner, "Open access series of imaging studies (oasis): cross-sectional mri data in young, middle aged, nondemented, and demented older adults," *Journal of cognitive neuroscience*, vol. 19, no. 9, pp. 1498–1507, 2007.

[36] A. M. Lanzi, A. K. Saylor, D. Fromm, H. Liu, B. MacWhinney, and M. L. Cohen, "Dementiabank: Theoretical rationale, protocol, and illustrative analyses," *American Journal of Speech-Language Pathology*, vol. 32, no. 2, pp. 426–438, 2023.

[37] K. A. Ellis, A. I. Bush, D. Darby, D. De Fazio, J. Foster, P. Hudson, N. T. Lautenschlager, N. Lenzo, R. N. Martins, P. Maruff, *et al.*, "The australian imaging, biomarkers and lifestyle (aibl) study of aging: methodology and baseline characteristics of 1112 individuals recruited for a longitudinal study of alzheimer's disease," *International psychogeriatrics*, vol. 21, no. 4, pp. 672–687, 2009.

[38] A. P. Rockhill, N. Jackson, J. George, A. Aron, N. C. Swann, *et al.*, "uc san diego resting state eeg data from patients with parkinson's disease," *Available:*, 2020.

[39] K. Marek, D. Jennings, S. Lasch, A. Siderowf, C. Tanner, T. Simuni, C. Coffey, K. Kieburtz, E. Flagg, S. Chowdhury, *et al.*, "The parkinson progression marker initiative (ppmi)," *Progress in neurobiology*, vol. 95, no. 4, pp. 629–635, 2011.

[40] A. L. Goldberger, L. A. Amaral, L. Glass, J. M. Hausdorff, P. C. Ivanov, R. G. Mark, J. E. Mietus, G. B. Moody, C.-K. Peng, and H. E. Stanley, "Physiobank, physiotoolkit, and physionet: components of a new research resource for complex physiologic signals," *circulation*, vol. 101, no. 23, pp. e215–e220, 2000.

[41] J. R. Orozco-Arroyave, J. D. Arias-Londono, J. F. Vargas-Bonilla, and E. Nöth, "Analysis of speech from people with parkinson's disease through nonlin-

ear dynamics," in *International conference on nonlinear speech processing*, pp. 112–119, Springer, 2013.

[42] C. R. Pereira, D. R. Pereira, F. A. Silva, J. P. Masieiro, S. A. T. Weber, C. Hook, and J. P. Papa, "A new computer vision-based approach to aid the diagnosis of parkinson's disease," *Computer Methods and Programs in Biomedicine*, vol. 136, pp. 79–88, 2016.

[43] A. Tagaris, D. Kollias, and A. Stafylopatis, "Assessment of parkinson's disease based on deep neural networks," in *Engineering Applications of Neural Networks: 18th International Conference, EANN 2017, Athens, Greece, August 25–27, 2017, Proceedings*, pp. 391–403, Springer, 2017.

[44] P. Drotár, J. Mekyska, I. Rektorová, L. Masarová, Z. Smékal, and M. Faundez-Zanuy, "Analysis of in-air movement in handwriting: A novel marker for parkinson's disease," *Computer methods and programs in biomedicine*, vol. 117, no. 3, pp. 405–411, 2014.

[45] S. García, S. Ramírez-Gallego, J. Luengo, J. M. Benítez, and F. Herrera, "Big data preprocessing: methods and prospects," *Big Data Analytics*, vol. 1, no. 1, pp. 1–22, 2016.

[46] S. Khalid, T. Khalil, and S. Nasreen, "A survey of feature selection and feature extraction techniques in machine learning," in *2014 science and information conference*, pp. 372–378, IEEE, 2014.

[47] F. O. López-Pabón, T. Arias-Vergara, and J. R. Orozco-Arroyave, "Cepstral analysis and hilbert-huang transform for automatic detection of parkinson's disease," *TecnoLógicas*, vol. 23, no. 47, pp. 91–106, 2020.

[48] A. Rueda, J. C. Vásquez-Correa, C. D. Rios-Urrego, J. R. Orozco-Arroyave, S. Krishnan, and E. Nöth, "Feature representation of pathophysiology of parkinsonian dysarthria.," in *INTERSPEECH*, pp. 3048–3052, 2019.

[49] B. Karan, S. S. Sahu, and K. Mahto, "Parkinson disease prediction using intrinsic mode function based features from speech signal," *Biocybernetics and Biomedical Engineering*, vol. 40, no. 1, pp. 249–264, 2020.

[50] R. Lamba, T. Gulati, and A. Jain, "A hybrid feature selection approach for parkinson's detection based on mutual information gain and recursive feature elimination," *Arabian Journal for Science and Engineering*, vol. 47, no. 8, pp. 10263–10276, 2022.

[51] B. Oltu, M. F. Akşahin, and S. Kibaroğlu, "A novel electroencephalography based approach for alzheimer's disease and mild cognitive impairment detection," *Biomedical Signal Processing and Control*, vol. 63, p. 102223, 2021.

[52] M. S. Safi and S. M. M. Safi, "Early detection of alzheimer's disease from eeg signals using hjorth parameters," *Biomedical Signal Processing and Control*, vol. 65, p. 102338, 2021.

[53] N. Sharma, M. H. Kolekar, and K. Jha, "Eeg based dementia diagnosis using multi-class support vector machine with motor speed cognitive test," *Biomedical Signal Processing and Control*, vol. 63, p. 102102, 2021.

[54] O. K. Cura, G. C. Yilmaz, H. S. Ture, and A. Akan, "Deep time-frequency feature extraction for alzheimer's dementia eeg classification," in *2022 Medical Technologies Congress (TIPTEKNO)*, pp. 1–4, IEEE, 2022.

[55] S. Fouladi, A. A. Safaei, N. Mammone, F. Ghaderi, and M. Ebadi, "Efficient deep neural networks for classification of alzheimer's disease and mild cognitive impairment from scalp eeg recordings," *Cognitive Computation*, vol. 14, no. 4, pp. 1247–1268, 2022.

[56] D. Puri, S. Nalbalwar, A. Nandgaonkar, and A. Wagh, "Alzheimer's disease detection from optimal electroencephalogram channels and tunable q-wavelet transform," *Indo. Journal of Elec. Engg and Comp. Sci*, vol. 25, no. 3, pp. 1420–1428, 2022.

[57] D. Puri, S. Nalbalwar, A. Nandgaonkar, P. Kachare, J. Rajput, and A. Wagh, "Alzheimer's disease detection using empirical mode decomposition and hjorth parameters of eeg signal," in *2022 International Conference on Decision Aid Sciences and Applications (DASA)*, pp. 23–28, IEEE, 2022.

[58] I. A. Fouad and F. E.-Z. M. Labib, "Identification of alzheimer's disease from central lobe eeg signals utilizing machine learning and residual neural network," *Biomedical Signal Processing and Control*, vol. 86, p. 105266, 2023.

[59] Z. Aslan, "A novel computer-aided diagnostic system for alzheimer's diagnosis using variational mode decomposition method," *Circuits, Systems, and Signal Processing*, vol. 43, no. 1, pp. 615–633, 2024.

[60] M. Khosravi, H. Parsaei, K. Rezaee, and M. S. Helfroush, "Fusing convolutional learning and attention-based bi-lstm networks for early alzheimer's diagnosis from eeg signals towards iomt," *Scientific Reports*, vol. 14, no. 1, p. 26002, 2024.

[61] K. Rezaee and M. Zhu, "Diagnose alzheimer's disease and mild cognitive impairment using deep cascadenet and handcrafted features from eeg signals," *Biomedical Signal Processing and Control*, vol. 99, p. 106895, 2025.

[62] L. Moro-Velazquez, J. A. Gómez-García, J. I. Godino-Llorente, J. Villalba, J. R. Orozco-Arroyave, and N. Dehak, "Analysis of speaker recognition methodologies and the influence of kinetic changes to automatically detect parkinson's disease," *Applied Soft Computing*, vol. 62, pp. 649–666, 2018.

[63] J. C. Vásquez-Correa, C. D. Rios-Urrego, A. Rueda, J. R. Orozco-Arroyave, S. Krishnan, and E. Nöth, "Articulation and empirical mode decomposition features in diadochokinetic exercises for the speech assessment of parkinson's disease patients," in *Iberoamerican Congress on Pattern Recognition*, pp. 688–696, Springer, 2019.

[64] R. A. Shirvan and E. Tahami, "Voice analysis for detecting parkinson's disease using genetic algorithm and knn classification method," in *2011 18th Iranian conference of biomedical engineering (ICBME)*, pp. 278–283, IEEE, 2011.

[65] A. Ouhmida, A. Raihani, B. Cherradi, and O. Terrada, "A novel approach for parkinson's disease detection based on voice classification and features selection techniques," *Int. J. Online Eng*, vol. 17, p. 111, 2021.

[66] C. O. Sakar, G. Serbes, A. Gunduz, H. C. Tunc, H. Nizam, B. E. Sakar, M. Tutuncu, T. Aydin, M. E. Isenkul, and H. Apaydin, "A comparative analysis of speech signal processing algorithms for parkinson's disease classification and the use of the tunable q-factor wavelet transform," *Applied Soft Computing*, vol. 74, pp. 255–263, 2019.

[67] P. Ghaheri, H. Nasiri, A. Shateri, and A. Homafar, "Diagnosis of parkinson's disease based on voice signals using shap and hard voting ensemble method," *Computer methods in biomechanics and biomedical engineering*, pp. 1–17, 2023.

[68] Z. Cai, J. Gu, and H.-L. Chen, "A new hybrid intelligent framework for predicting parkinson's disease," *IEEE Access*, vol. 5, pp. 17188–17200, 2017.

[69] B. Karan and S. S. Sahu, "An improved framework for parkinson's disease prediction using variational mode decomposition-hilbert spectrum of speech signal," *Biocybernetics and Biomedical Engineering*, vol. 41, no. 2, pp. 717–732, 2021.

[70] H.-L. Chen, C.-C. Huang, X.-G. Yu, X. Xu, X. Sun, G. Wang, and S.-J. Wang, "An efficient diagnosis system for detection of parkinson's disease using fuzzy k-nearest neighbor approach," *Expert systems with applications*, vol. 40, no. 1, pp. 263–271, 2013.

[71] E. Avuçlu and A. Elen, "Evaluation of train and test performance of machine learning algorithms and parkinson diagnosis with statistical measurements,"

Medical & Biological Engineering & Computing, vol. 58, pp. 2775–2788, 2020.

[72] B. E. Sakar, M. E. Isenkul, C. O. Sakar, A. Sertbas, F. Gurgen, S. Delil, H. Apaydin, and O. Kursun, "Collection and analysis of a parkinson speech dataset with multiple types of sound recordings," *IEEE Journal of Biomedical and Health Informatics*, vol. 17, no. 4, pp. 828–834, 2013.

[73] H.-H. Zhang, L. Yang, Y. Liu, P. Wang, J. Yin, Y. Li, M. Qiu, X. Zhu, and F. Yan, "Classification of parkinson's disease utilizing multi-edit nearest-neighbor and ensemble learning algorithms with speech samples," *Biomedical engineering online*, vol. 15, pp. 1–22, 2016.

[74] M. Alhussein, "Monitoring parkinson's disease in smart cities," *IEEE Access*, vol. 5, pp. 19835–19841, 2017.

[75] Z. Soumaya, B. D. Taoufiq, N. Benayad, K. Yunus, and A. Abdelkrim, "The detection of parkinson disease using the genetic algorithm and svm classifier," *Applied Acoustics*, vol. 171, p. 107528, 2021.

[76] V. Despotovic, T. Skovranek, and C. Schommer, "Speech based estimation of parkinson's disease using gaussian processes and automatic relevance determination," *Neurocomputing*, vol. 401, pp. 173–181, 2020.

[77] Y. Li, C. Liu, P. Wang, H. Zhang, A. Wei, and Y. Zhang, "Envelope multi-type transformation ensemble algorithm of parkinson speech samples," *Applied Intelligence*, pp. 1–22, 2022.

[78] J. W. de Souza, S. S. Alves, E. d. S. Rebouças, J. S. Almeida, and P. P. Rebouças Filho, "A new approach to diagnose parkinson's disease using a structural cooccurrence matrix for a similarity analysis," *Computational Intelligence and Neuroscience*, vol. 2018, 2018.

[79] P. Drotár, J. Mekyska, I. Rektorová, L. Masarová, Z. Smékal, and M. Faundez-Zanuy, "Evaluation of handwriting kinematics and pressure for differential

diagnosis of parkinson's disease," *Artificial intelligence in Medicine*, vol. 67, pp. 39–46, 2016.

[80] U. Gupta, H. Bansal, and D. Joshi, "An improved sex-specific and age-dependent classification model for parkinson's diagnosis using handwriting measurement," *Computer methods and programs in biomedicine*, vol. 189, p. 105305, 2020.

[81] P. Drotár, J. Mekyska, I. Rektorová, L. Masarová, Z. Smékal, and M. Faundez-Zanuy, "Decision support framework for parkinson's disease based on novel handwriting markers," *IEEE Transactions on Neural Systems and Rehabilitation Engineering*, vol. 23, no. 3, pp. 508–516, 2014.

[82] L. S. Bernardo, A. Quezada, R. Munoz, F. M. Maia, C. R. Pereira, W. Wu, and V. H. C. de Albuquerque, "Handwritten pattern recognition for early parkinson's disease diagnosis," *Pattern recognition letters*, vol. 125, pp. 78–84, 2019.

[83] D. Impedovo, G. Pirlo, and G. Vessio, "Dynamic handwriting analysis for supporting earlier parkinson's disease diagnosis," *Information*, vol. 9, no. 10, p. 247, 2018.

[84] C. D. Rios-Urrego, J. C. Vásquez-Correa, J. F. Vargas-Bonilla, E. Nöth, F. Lopera, and J. R. Orozco-Arroyave, "Analysis and evaluation of handwriting in patients with parkinson's disease using kinematic, geometrical, and non-linear features," *Computer methods and programs in biomedicine*, vol. 173, pp. 43–52, 2019.

[85] M. Kamble, P. Shrivastava, and M. Jain, "Digitized spiral drawing classification for parkinson's disease diagnosis," *Measurement: Sensors*, vol. 16, p. 100047, 2021.

[86] J. Chandra, S. Muthupalaniappan, Z. Shang, R. Deng, R. Lin, I. Tolkova, D. Butts, D. Sul, S. Marzouk, S. Bose, *et al.*, "Screening of parkinson's disease using geometric features extracted from spiral drawings," *Brain Sciences*, vol. 11, no. 10, p. 1297, 2021.

[87] M. Gerger and A. Gümüşçü, "Diagnosis of parkinson's disease using spiral test based on pattern recognition," *SCIENCE AND TECHNOLOGY*, vol. 25, no. 1, pp. 100–113, 2022.

[88] R. Lamba, T. Gulati, K. A. Al-Dhlan, and A. Jain, "A systematic approach to diagnose parkinson's disease through kinematic features extracted from handwritten drawings," *Journal of Reliable Intelligent Environments*, pp. 1–10, 2021.

[89] T. D. Pham and H. Yan, "Tensor decomposition of gait dynamics in parkinson's disease," *IEEE Transactions on Biomedical Engineering*, vol. 65, no. 8, pp. 1820–1827, 2017.

[90] E. Abdulhay, N. Arunkumar, K. Narasimhan, E. Vellaiappan, and V. Venkatraman, "Gait and tremor investigation using machine learning techniques for the diagnosis of parkinson disease," *Future Generation Computer Systems*, vol. 83, pp. 366–373, 2018.

[91] N. Khoury, F. Attal, Y. Amirat, L. Oukhellou, and S. Mohammed, "Data-driven based approach to aid parkinson's disease diagnosis," *Sensors*, vol. 19, no. 2, p. 242, 2019.

[92] E. Balaji, D. Brindha, V. K. Elumalai, and K. Umesh, "Data-driven gait analysis for diagnosis and severity rating of parkinson's disease," *Medical Engineering & Physics*, vol. 91, pp. 54–64, 2021.

[93] R. Alkhatib, M. O. Diab, C. Corbier, and M. El Badaoui, "Machine learning algorithm for gait analysis and classification on early detection of parkinson," *IEEE Sensors Letters*, vol. 4, no. 6, pp. 1–4, 2020.

[94] B. Vidya and P. Sasikumar, "Gait based parkinson's disease diagnosis and severity rating using multi-class support vector machine," *Applied Soft Computing*, vol. 113, p. 107939, 2021.

[95] Y. Yan, O. M. Omisore, Y.-C. Xue, H.-H. Li, Q.-H. Liu, Z.-D. Nie, J. Fan, and L. Wang, "Classification of neurodegenerative diseases via topological motion

analysis—a comparison study for multiple gait fluctuations," *IEEE Access*, vol. 8, pp. 96363–96377, 2020.

[96] H. Zhao, R. Wang, Y. Lei, W.-H. Liao, H. Cao, and J. Cao, "Severity level diagnosis of parkinson's disease by ensemble k-nearest neighbor under imbalanced data," *Expert Systems with Applications*, vol. 189, p. 116113, 2022.

[97] O. Cigdem, I. Beheshti, and H. Demirel, "Effects of different covariates and contrasts on classification of parkinson's disease using structural mri," *Computers in biology and medicine*, vol. 99, pp. 173–181, 2018.

[98] N. Amoroso, M. La Rocca, A. Monaco, R. Bellotti, and S. Tangaro, "Complex networks reveal early mri markers of parkinson's disease," *Medical image analysis*, vol. 48, pp. 12–24, 2018.

[99] G. Solana-Lavalle and R. Rosas-Romero, "Classification of ppmi mri scans with voxel-based morphometry and machine learning to assist in the diagnosis of parkinson's disease," *Computer Methods and Programs in Biomedicine*, vol. 198, p. 105793, 2021.

[100] R. Prashanth, S. D. Roy, P. K. Mandal, and S. Ghosh, "Automatic classification and prediction models for early parkinson's disease diagnosis from spect imaging," *Expert Systems with Applications*, vol. 41, no. 7, pp. 3333–3342, 2014.

[101] T. Shiiba, Y. Arimura, M. Nagano, T. Takahashi, and A. Takaki, "Improvement of classification performance of parkinson's disease using shape features for machine learning on dopamine transporter single photon emission computed tomography," *PLoS One*, vol. 15, no. 1, p. e0228289, 2020.

[102] F. Segovia, I. A. Illan, J. M. Gorriz, J. Ramirez, A. Rominger, and J. Levin, "Distinguishing parkinson's disease from atypical parkinsonian syndromes using pet data and a computer system based on support vector machines and bayesian networks," *Frontiers in computational neuroscience*, vol. 9, p. 137, 2015.

[103] R. Prashanth, S. D. Roy, P. K. Mandal, and S. Ghosh, "High-accuracy classification of parkinson's disease through shape analysis and surface fitting in 123i-ioflupane spect imaging," *IEEE journal of biomedical and health informatics*, vol. 21, no. 3, pp. 794–802, 2016.

[104] D. Castillo-Barnes, F. J. Martinez-Murcia, A. Ortiz, D. Salas-Gonzalez, J. RamÍrez, and J. M. Górriz, "Morphological characterization of functional brain imaging by isosurface analysis in parkinson's disease," *International journal of neural systems*, vol. 30, no. 09, p. 2050044, 2020.

[105] F. Segovia, J. M. Górriz, J. Ramírez, F. J. Martínez-Murcia, and D. Castillo-Barnes, "Assisted diagnosis of parkinsonism based on the striatal morphology," *International Journal of neural systems*, vol. 29, no. 09, p. 1950011, 2019.

[106] F. J. Martínez-Murcia, J. M. Górriz, J. Ramírez, I. A. Illán, and C. G. Puntonet, "Texture features based detection of parkinson's disease on datscan images," in *Natural and Artificial Computation in Engineering and Medical Applications: 5th International Work-Conference on the Interplay Between Natural and Artificial Computation, IWINAC 2013, Mallorca, Spain, June 10-14, 2013. Proceedings, Part II 5*, pp. 266–277, Springer, 2013.

[107] D. Shi, X. Yao, Y. Li, H. Zhang, G. Wang, S. Wang, and K. Ren, "Classification of parkinson's disease using a region-of-interest-and resting-state functional magnetic resonance imaging-based radiomics approach," *Brain Imaging and Behavior*, vol. 16, no. 5, pp. 2150–2163, 2022.

[108] C. Salvatore, A. Cerasa, I. Castiglioni, F. Gallivanone, A. Augimeri, M. Lopez, G. Arabia, M. Morelli, M. Gilardi, and A. Quattrone, "Machine learning on brain mri data for differential diagnosis of parkinson's disease and progressive supranuclear palsy," *Journal of neuroscience methods*, vol. 222, pp. 230–237, 2014.

[109] P. D. Barua, S. Dogan, T. Tuncer, M. Baygin, and U. R. Acharya, "Novel automated pd detection system using aspirin pattern with eeg signals," *Computers in Biology and Medicine*, vol. 137, p. 104841, 2021.

[110] S. A. Khoshnevis and R. Sankar, "Classification of the stages of parkinson's disease using novel higher-order statistical features of eeg signals," *Neural Computing and Applications*, vol. 33, pp. 7615–7627, 2021.

[111] P. Chawla, S. B. Rana, H. Kaur, K. Singh, R. Yuvaraj, and M. Murugappan, "A decision support system for automated diagnosis of parkinson's disease from eeg using fawt and entropy features," *Biomedical Signal Processing and Control*, vol. 79, p. 104116, 2023.

[112] A. P. S. De Oliveira, M. A. De Santana, M. K. S. Andrade, J. C. Gomes, M. C. Rodrigues, and W. P. dos Santos, "Early diagnosis of parkinson's disease using eeg, machine learning and partial directed coherence," *Research on Biomedical Engineering*, vol. 36, pp. 311–331, 2020.

[113] S. Hassin-Baer, O. S. Cohen, S. Israeli-Korn, G. Yahalom, S. Benizri, D. Sand, G. Issachar, A. B. Geva, R. Shani-Hershkovich, and Z. Peremen, "Identification of an early-stage parkinson's disease neuromarker using event-related potentials, brain network analytics and machine-learning," *Plos one*, vol. 17, no. 1, p. e0261947, 2022.

[114] S. K. Khare, V. Bajaj, and U. R. Acharya, "Detection of parkinson's disease using automated tunable q wavelet transform technique with eeg signals," *Biocybernetics and Biomedical Engineering*, vol. 41, no. 2, pp. 679–689, 2021.

[115] N. Betrouni, A. Delval, L. Chaton, L. Defebvre, A. Duits, A. Moonen, A. F. Leentjens, and K. Dujardin, "Electroencephalography-based machine learning for cognitive profiling in parkinson's disease: Preliminary results," *Movement Disorders*, vol. 34, no. 2, pp. 210–217, 2019.

[116] X. Zhang, L. Zhang, K. Xu, Y. Yang, R. Zhao, and Y. She, "Optimal channels selection based on abc-svm in parkinsons disease detection using short-time

resting state eeg: X. zhang et al.," *The Journal of Supercomputing*, vol. 81, no. 8, p. 977, 2025.

[117] S.-H. Lee and J. S. Lim, "Parkinson's disease classification using gait characteristics and wavelet-based feature extraction," *Expert Systems with Applications*, vol. 39, no. 8, pp. 7338–7344, 2012.

[118] B. Karan, S. S. Sahu, and K. Mahto, "Stacked auto-encoder based time-frequency features of speech signal for parkinson disease prediction," in *2020 International Conference on Artificial Intelligence and Signal Processing (AISP)*, pp. 1–4, IEEE, 2020.

[119] J. C. Vásquez-Correa, T. Arias-Vergara, C. D. Rios-Urrego, M. Schuster, J. Rusz, J. R. Orozco-Arroyave, and E. Nöth, "Convolutional neural networks and a transfer learning strategy to classify parkinson's disease from speech in three different languages," in *Progress in Pattern Recognition, Image Analysis, Computer Vision, and Applications: 24th Iberoamerican Congress, CIARP 2019, Havana, Cuba, October 28-31, 2019, Proceedings 24*, pp. 697–706, Springer, 2019.

[120] M. R. Daliri, "Chi-square distance kernel of the gaits for the diagnosis of parkinson's disease," *Biomedical Signal Processing and Control*, vol. 8, no. 1, pp. 66–70, 2013.

[121] S. Masoumi, M. Rastgarpour, and N. J. Dabanloo, "Parkinson's disease diagnosis based on vertical ground reaction force signals of gait using deep neural network," in *Progress in Intelligent Decision Science: Proceeding of IDS 2020*, pp. 254–264, Springer, 2021.

[122] E. Özel, R. Tekin, and Y. Kaya, "Implementation of artifact removal algorithms in gait signals for diagnosis of parkinson disease.," *Traitement du Signal*, vol. 38, no. 3, 2021.

[123] B. Venkatesh and J. Anuradha, "A review of feature selection and its methods," *Cybernetics and information technologies*, vol. 19, no. 1, pp. 3–26, 2019.

[124] B. Xue, M. Zhang, W. N. Browne, and X. Yao, "A survey on evolutionary computation approaches to feature selection," *IEEE Transactions on evolutionary computation*, vol. 20, no. 4, pp. 606–626, 2015.

[125] R. Aziz, C. Verma, and N. Srivastava, "Dimension reduction methods for microarray data: a review," *AIMS Bioeng*, vol. 4, no. 1, pp. 179–197, 2017.

[126] K. Balakrishnan and R. Dhanalakshmi, "Feature selection techniques for microarray datasets: a comprehensive review, taxonomy, and future directions," *Frontiers of Information Technology & Electronic Engineering*, vol. 23, no. 10, pp. 1451–1478, 2022.

[127] T. Tuncer, S. Dogan, M. Baygin, P. D. Barua, E. E. Palmer, S. March, E. J. Ciaccio, R.-S. Tan, and U. R. Acharya, "Flp: Factor lattice pattern-based automated detection of parkinson's disease and specific language impairment using recorded speech," *Computers in Biology and Medicine*, vol. 173, p. 108280, 2024.

[128] L. Ali, C. Zhu, M. Zhou, and Y. Liu, "Early diagnosis of parkinson's disease from multiple voice recordings by simultaneous sample and feature selection," *Expert Systems with Applications*, vol. 137, pp. 22–28, 2019.

[129] H.-L. Chen, G. Wang, C. Ma, Z.-N. Cai, W.-B. Liu, and S.-J. Wang, "An efficient hybrid kernel extreme learning machine approach for early diagnosis of parkinson's disease," *Neurocomputing*, vol. 184, pp. 131–144, 2016.

[130] M. Peker, B. Sen, and D. Delen, "Computer-aided diagnosis of parkinson's disease using complex-valued neural networks and mrmr feature selection algorithm," *Journal of healthcare engineering*, vol. 6, no. 3, pp. 281–302, 2015.

[131] C. Tremblay, J. Mei, and J. Frasnelli, "Olfactory bulb surroundings can help to distinguish parkinson's disease from non-parkinsonian olfactory dysfunction," *NeuroImage: Clinical*, vol. 28, p. 102457, 2020.

[132] S. Thapa, S. Adhikari, A. Ghimire, and A. Aditya, "Feature selection based twin-support vector machine for the diagnosis of parkinson's disease," in *2020 IEEE 8th R10 humanitarian technology conference (R10-HTC)*, pp. 1–6, IEEE, 2020.

[133] D. Avci and A. Dogantekin, "An expert diagnosis system for parkinson disease based on genetic algorithm-wavelet kernel-extreme learning machine," *Parkinson's disease*, vol. 2016, 2016.

[134] K. Shyamala and T. Navamani, "Design of an efficient prediction model for early parkinson's disease diagnosis," *IEEE Access*, 2024.

[135] A. M. Elshewey, M. Y. Shams, N. El-Rashidy, A. M. Elhady, S. M. Shohieb, and Z. Tarek, "Bayesian optimization with support vector machine model for parkinson disease classification," *Sensors*, vol. 23, no. 4, p. 2085, 2023.

[136] T. Araújo, J. P. Teixeira, and P. M. Rodrigues, "Smart-data-driven system for alzheimer disease detection through electroencephalographic signals," *Bioengineering*, vol. 9, no. 4, p. 141, 2022.

[137] G. Biagetti, P. Crippa, L. Falaschetti, S. Luzzi, and C. Turchetti, "Classification of alzheimer's disease from eeg signal using robust-pca feature extraction," *Procedia Computer Science*, vol. 192, pp. 3114–3122, 2021.

[138] X. Chen, X. Yao, C. Tang, Y. Sun, X. Wang, and X. Wu, "Detecting parkinson's disease using gait analysis with particle swarm optimization," in *Human Aspects of IT for the Aged Population. Applications in Health, Assistance, and Entertainment: 4th International Conference, ITAP 2018, Held as Part of HCI International 2018, Las Vegas, NV, USA, July 15–20, 2018, Proceedings, Part II 4*, pp. 263–275, Springer, 2018.

[139] B. Karan, S. S. Sahu, J. R. Orozco-Arroyave, and K. Mahto, "Hilbert spectrum analysis for automatic detection and evaluation of parkinson's speech," *Biomedical Signal Processing and Control*, vol. 61, p. 102050, 2020.

[140] H. Zheng, X. Xiong, and X. Zhang, "Multi-threshold recurrence rate plot: A novel methodology for eeg analysis in alzheimer's disease and frontotemporal dementia," *Brain Sciences*, vol. 14, no. 6, p. 565, 2024.

[141] X. S. Mootoo, A. Fours, C. Dinesh, M. Ashkani, A. Kiss, and M. Faltyn, "Detecting alzheimer disease in eeg data with machine learning and the graph discrete fourier transform," *medRxiv*, pp. 2023–11, 2023.

[142] G. James, D. Witten, T. Hastie, and R. Tibshirani, *An introduction to statistical learning*, vol. 112. Springer, 2013.

[143] Z.-H. Zhou, *Ensemble methods: foundations and algorithms*. CRC press, 2012.

[144] N. Aggarwal, G. J. Saxena, S. Singh, and A. Pundir, "Explainable ai approach for early detection of parkinson's disease using ppmi online data," *Neural Computing and Applications*, pp. 1–22, 2024.

[145] K. Bhatt, N. Jayanthi, and M. Kumar, "Automatic detection of parkinson's disease using eeg signals: A machine learning approach," in *2024 IEEE International Conference on Interdisciplinary Approaches in Technology and Management for Social Innovation (IATMSI)*, vol. 2, pp. 1–6, IEEE, 2024.

[146] K. Haritha, M. Judy, K. Papageorgiou, V. C. Georgiannis, and E. Papageorgiou, "Distributed fuzzy cognitive maps for feature selection in big data classification," *Algorithms*, vol. 15, no. 10, p. 383, 2022.

[147] S. Sperandei, "Understanding logistic regression analysis," *Biochemia medica*, vol. 24, no. 1, pp. 12–18, 2014.

[148] M. M. Saritas and A. Yasar, "Performance analysis of ann and naive bayes classification algorithm for data classification," *International journal of intelligent systems and applications in engineering*, vol. 7, no. 2, pp. 88–91, 2019.

[149] B. T. Jijo and A. M. Abdulazeez, "Classification based on decision tree algorithm for machine learning," *evaluation*, vol. 6, no. 7, 2021.

[150] I. K. Veetil, V. Sowmya, J. R. Orozco-Arroyave, and E. Gopalakrishnan, "Robust language independent voice data driven parkinson's disease detection," *Engineering Applications of Artificial Intelligence*, vol. 129, p. 107494, 2024.

[151] J. Goyal, P. Khandnor, and T. C. Aseri, "A hybrid approach for parkinson's disease diagnosis with resonance and time-frequency based features from speech signals," *Expert Systems with Applications*, vol. 182, p. 115283, 2021.

[152] B. Akila and J. J. V. Nayahi, "Parkinson classification neural network with mass algorithm for processing speech signals," *Neural Computing and Applications*, pp. 1–17, 2024.

[153] M. Gazda, M. Hireš, and P. Drotár, "Multiple-fine-tuned convolutional neural networks for parkinson's disease diagnosis from offline handwriting," *IEEE Transactions on Systems, Man, and Cybernetics: Systems*, vol. 52, no. 1, pp. 78–89, 2021.

[154] M. Gil-Martín, J. M. Montero, and R. San-Segundo, "Parkinson's disease detection from drawing movements using convolutional neural networks," *Electronics*, vol. 8, no. 8, p. 907, 2019.

[155] M. Alissa, M. A. Lones, J. Cosgrove, J. E. Alty, S. Jamieson, S. L. Smith, and M. Vallejo, "Parkinson's disease diagnosis using convolutional neural networks and figure-copying tasks," *Neural Computing and Applications*, pp. 1–21, 2022.

[156] L. C. Afonso, G. H. Rosa, C. R. Pereira, S. A. Weber, C. Hook, V. H. C. Albuquerque, and J. P. Papa, "A recurrence plot-based approach for parkinson's disease identification," *Future Generation Computer Systems*, vol. 94, pp. 282–292, 2019.

[157] İ. Cantürk, "Fuzzy recurrence plot-based analysis of dynamic and static spiral tests of parkinson's disease patients," *Neural Computing and Applications*, vol. 33, no. 1, pp. 349–360, 2021.

[158] M. Shaban, "A novel variational mode decomposition based convolutional neural network for the identification of freezing of gait intervals for patients with

parkinson's disease," *Machine Learning with Applications*, vol. 16, p. 100553, 2024.

[159] A. S. Alharthi, A. J. Casson, and K. B. Ozanyan, "Gait spatiotemporal signal analysis for parkinson's disease detection and severity rating," *IEEE Sensors Journal*, vol. 21, no. 2, pp. 1838–1848, 2020.

[160] H. W. Loh, C. P. Ooi, E. Palmer, P. D. Barua, S. Dogan, T. Tuncer, M. Baygin, and U. R. Acharya, "Gaborpdnet: Gabor transformation and deep neural network for parkinson's disease detection using eeg signals," *Electronics*, vol. 10, no. 14, p. 1740, 2021.

[161] M. Shaban and A. W. Amara, "Resting-state electroencephalography based deep-learning for the detection of parkinson's disease," *Plos one*, vol. 17, no. 2, p. e0263159, 2022.

[162] S. K. Khare, V. Bajaj, and U. R. Acharya, "Pdcnnet: An automatic framework for the detection of parkinson's disease using eeg signals," *IEEE Sensors Journal*, vol. 21, no. 15, pp. 17017–17024, 2021.

[163] L. Qiu, J. Li, L. Zhong, W. Feng, C. Zhou, and J. Pan, "A novel eeg-based parkinson's disease detection model using multiscale convolutional prototype networks," *IEEE Transactions on Instrumentation and Measurement*, 2024.

[164] S. L. Oh, Y. Hagiwara, U. Raghavendra, R. Yuvaraj, N. Arunkumar, M. Murugappan, and U. R. Acharya, "A deep learning approach for parkinson's disease diagnosis from eeg signals," *Neural Computing and Applications*, vol. 32, pp. 10927–10933, 2020.

[165] B. Xiao, N. He, Q. Wang, Z. Cheng, Y. Jiao, E. M. Haacke, F. Yan, and F. Shi, "Quantitative susceptibility mapping based hybrid feature extraction for diagnosis of parkinson's disease," *NeuroImage: Clinical*, vol. 24, p. 102070, 2019.

[166] H. Choi, S. Ha, H. J. Im, S. H. Paek, and D. S. Lee, "Refining diagnosis of parkinson's disease with deep learning-based interpretation of dopamine transporter imaging," *NeuroImage: Clinical*, vol. 16, pp. 586–594, 2017.

[167] A. Piccardo, R. Cappuccio, G. Bottoni, D. Cecchin, L. Mazzella, A. Cirone, S. Righi, M. Ugolini, P. Bianchi, P. Bertolaccini, *et al.*, "The role of the deep convolutional neural network as an aid to interpreting brain [18 f] dopa pet/ct in the diagnosis of parkinson's disease," *European Radiology*, vol. 31, pp. 7003–7011, 2021.

[168] O. Karaman, H. Çakın, A. Alhudhaif, and K. Polat, "Robust automated parkinson disease detection based on voice signals with transfer learning," *Expert Systems with Applications*, vol. 178, p. 115013, 2021.

[169] M. Wodzinski, A. Skalski, D. Hemmerling, J. R. Orozco-Arroyave, and E. Nöth, "Deep learning approach to parkinson's disease detection using voice recordings and convolutional neural network dedicated to image classification," in *2019 41st Annual International Conference of the IEEE Engineering in Medicine and Biology Society (EMBC)*, pp. 717–720, IEEE, 2019.

[170] I. Kamran, S. Naz, I. Razzak, and M. Imran, "Handwriting dynamics assessment using deep neural network for early identification of parkinson's disease," *Future Generation Computer Systems*, vol. 117, pp. 234–244, 2021.

[171] A. Naseer, M. Rani, S. Naz, M. I. Razzak, M. Imran, and G. Xu, "Refining parkinson's neurological disorder identification through deep transfer learning," *Neural Computing and Applications*, vol. 32, pp. 839–854, 2020.

[172] E. Arasteh, A. Mahdizadeh, M. S. Mirian, S. Lee, and M. J. McKeown, "Deep transfer learning for parkinson's disease monitoring by image-based representation of resting-state eeg using directional connectivity," *Algorithms*, vol. 15, no. 1, p. 5, 2022.

[173] P. R. Magesh, R. D. Myloth, and R. J. Tom, "An explainable machine learning model for early detection of parkinson's disease using lime on datscan imagery," *Computers in Biology and Medicine*, vol. 126, p. 104041, 2020.

[174] A. Kurmi, S. Biswas, S. Sen, A. Sinitca, D. Kaplun, and R. Sarkar, "An ensemble of cnn models for parkinson's disease detection using datscan images," *Diagnostics*, vol. 12, no. 5, p. 1173, 2022.

[175] C. Dong, Y. Chen, Z. Huan, Z. Li, B. Zhou, and Y. Liu, "Static-dynamic temporal networks for parkinson's disease detection and severity prediction," *IEEE Transactions on Neural Systems and Rehabilitation Engineering*, 2023.

[176] I. El Maachi, G.-A. Bilodeau, and W. Bouachir, "Deep 1d-convnet for accurate parkinson disease detection and severity prediction from gait," *Expert Systems with Applications*, vol. 143, p. 113075, 2020.

[177] X. Yang, Q. Ye, G. Cai, Y. Wang, and G. Cai, "Pd-resnet for classification of parkinson's disease from gait," *IEEE Journal of Translational Engineering in Health and Medicine*, vol. 10, pp. 1–11, 2022.

[178] S. Siuly, S. K. Khare, E. Kabir, M. T. Sadiq, and H. Wang, "An efficient parkinson's disease detection framework: Leveraging time-frequency representation and alexnet convolutional neural network," *Computers in Biology and Medicine*, vol. 174, p. 108462, 2024.

[179] F. J. Martinez-Murcia, J. M. Górriz, J. Ramírez, and A. Ortiz, "Convolutional neural networks for neuroimaging in parkinson's disease: Is preprocessing needed?," *International journal of neural systems*, vol. 28, no. 10, p. 1850035, 2018.

[180] S. Rahman, M. Hasan, A. K. Sarkar, and F. Khan, "Classification of parkinson's disease using speech signal with machine learning and deep learning approaches," *European Journal of Electrical Engineering and Computer Science*, vol. 7, no. 2, pp. 20–27, 2023.

[181] Y. Dai, Z. Tang, Y. Wang, *et al.*, "Data driven intelligent diagnostics for parkinson's disease," *IEEE Access*, vol. 7, pp. 106941–106950, 2019.

[182] S. S. Upadhya, A. Cheeran, and J. H. Nirmal, "Discriminating parkinson diseased and healthy people using modified mfcc filter bank approach," *International Journal of Speech Technology*, vol. 22, no. 4, pp. 1021–1029, 2019.

[183] C. L. Alves, A. M. Pineda, K. Roster, C. Thielemann, and F. A. Rodrigues, "Eeg functional connectivity and deep learning for automatic diagnosis of brain disorders: Alzheimer's disease and schizophrenia," *Journal of Physics: complexity*, vol. 3, no. 2, p. 025001, 2022.

[184] W. Xia, R. Zhang, X. Zhang, and M. Usman, "A novel method for diagnosing alzheimer's disease using deep pyramid cnn based on eeg signals," *Heliyon*, vol. 9, no. 4, 2023.

[185] A. Miltiadous, E. Gionanidis, K. D. Tzimourta, N. Giannakeas, and A. T. Tzallas, "Dice-net: a novel convolution-transformer architecture for alzheimer detection in eeg signals," *IEEE Access*, 2023.

[186] M. Nour, U. Senturk, and K. Polat, "A novel hybrid model in the diagnosis and classification of alzheimer's disease using eeg signals: Deep ensemble learning (del) approach," *Biomedical Signal Processing and Control*, vol. 89, p. 105751, 2024.

[187] P. Kachare, D. Puri, S. B. Sangle, I. Al-Shourbaji, A. Jabbari, R. Kirner, A. Alameen, H. Migdady, and L. Abualigah, "Lcadnet: a novel light cnn architecture for eeg-based alzheimer disease detection," *Physical and Engineering Sciences in Medicine*, vol. 47, no. 3, pp. 1037–1050, 2024.

[188] M. Rey-Paredes, C. J. Pérez, and A. Mateos-Caballero, "Time series classification of raw voice waveforms for parkinson's disease detection using generative adversarial network-driven data augmentation," *IEEE Open Journal of the Computer Society*, 2024.

[189] P. Valarmathi, Y. Suganya, K. Saranya, and S. Shanmuga Priya, "Enhancing parkinson disease detection through feature based deep learning with autoencoders and neural networks," *Scientific Reports*, vol. 15, no. 1, p. 8624, 2025.

[190] D. K. Saha and T. D. Nath, "A lightweight cnn-based ensemble approach for early detecting parkinson's disease with enhanced features," *International Journal of Speech Technology*, pp. 1–15, 2025.

[191] T. Hasib, V. V. Vengadasalam, and R. Kannan, "Early identification of parkinson's disease using time frequency analysis on eeg signals," *Journal of Informatics and Web Engineering*, vol. 4, no. 1, pp. 168–183, 2025.

[192] L. Ali, M.-F. Leung, M. A. Khan, R. Nour, Y. Imrana, and A. V. Vasilakos, "Chiga-net: A genetically optimized neural network with refined deeply extracted features using $\chi 2$ statistical score for trustworthy parkinson's disease detection," *Neurocomputing*, vol. 624, p. 129450, 2025.

[193] M. M. Afonso, D. R. Edla, and R. R. Reddy, "Optimizing parkinson's disease detection: Hybrid s-transform-eeg feature reduction through trajectory analysis," *SN Computer Science*, vol. 6, no. 2, p. 135, 2025.

[194] N. P. Sharma, I. Junaid, and S. Ari, "Early diagnosis of parkinson's disease and severity assessment based on gait using 1d-cnn," in *2023 2nd International Conference on Smart Technologies and Systems for Next Generation Computing (ICSTSN)*, pp. 1–6, IEEE, 2023.

[195] A. Zhao, L. Qi, J. Li, J. Dong, and H. Yu, "A hybrid spatio-temporal model for detection and severity rating of parkinson's disease from gait data," *Neurocomputing*, vol. 315, pp. 1–8, 2018.

[196] K. Stefanou, K. D. Tzimourta, C. Bellos, G. Stergios, K. Markoglou, E. Gionanidis, M. G. Tsipouras, N. Giannakeas, A. T. Tzallas, and A. Miltiadous, "A novel cnn-based framework for alzheimer's disease detection using eeg spectrogram representations," *Journal of Personalized Medicine*, vol. 15, no. 1, p. 27, 2025.

[197] Z.-J. Xu, R.-F. Wang, J. Wang, and D.-H. Yu, "Parkinson's disease detection based on spectrogram-deep convolutional generative adversarial network sample augmentation," *IEEE Access*, vol. 8, pp. 206888–206900, 2020.

[198] M. B. Er, E. Isik, and I. Isik, "Parkinson's detection based on combined cnn and lstm using enhanced speech signals with variational mode decomposition," *Biomedical Signal Processing and Control*, vol. 70, p. 103006, 2021.

[199] N. Chintalapudi, G. Battineni, M. A. Hossain, and F. Amenta, "Cascaded deep learning frameworks in contribution to the detection of parkinson's disease," *Bioengineering*, vol. 9, no. 3, p. 116, 2022.

[200] T.-L. Yang, C.-H. Lin, W.-L. Chen, H.-Y. Lin, C.-S. Su, and C.-K. Liang, "Hash transformation and machine learning-based decision-making classifier improved the accuracy rate of automated parkinson's disease screening," *IEEE Transactions on Neural Systems and Rehabilitation Engineering*, vol. 28, no. 1, pp. 72–82, 2019.

[201] S. Lee, R. Hussein, R. Ward, Z. J. Wang, and M. J. McKeown, "A convolutional-recurrent neural network approach to resting-state eeg classification in parkinson's disease," *Journal of neuroscience methods*, vol. 361, p. 109282, 2021.

[202] E. Perez-Valero, M. Á. Lopez-Gordo, C. M. Gutiérrez, I. Carrera-Muñoz, and R. M. Vílchez-Carrillo, "A self-driven approach for multi-class discrimination in alzheimer's disease based on wearable eeg," *Computer Methods and Programs in Biomedicine*, vol. 220, p. 106841, 2022.

[203] L. Ali, C. Zhu, Z. Zhang, and Y. Liu, "Automated detection of parkinson's disease based on multiple types of sustained phonations using linear discriminant analysis and genetically optimized neural network," *IEEE journal of translational engineering in health and medicine*, vol. 7, pp. 1–10, 2019.

[204] S. J. Priya, A. J. Rani, M. Subathra, M. A. Mohammed, R. Damaševičius, and N. Ubendran, "Local pattern transformation based feature extraction for

recognition of parkinson's disease based on gait signals," *Diagnostics*, vol. 11, no. 8, p. 1395, 2021.

[205] O. C. Yurdakul, M. Subathra, and S. T. George, "detection of parkinson's disease from gait using neighborhood representation local binary patterns," *Biomedical Signal Processing and Control*, vol. 62, p. 102070, 2020.

[206] Ö. F. Ertuğrul, Y. Kaya, R. Tekin, and M. N. Almalı, "Detection of parkinson's disease by shifted one dimensional local binary patterns from gait," *Expert Systems with Applications*, vol. 56, pp. 156–163, 2016.

[207] N. Narendra, B. Schuller, and P. Alku, "The detection of parkinson's disease from speech using voice source information," *IEEE/ACM Transactions on Audio, Speech, and Language Processing*, vol. 29, pp. 1925–1936, 2021.

[208] X. Wang, J. Huang, M. Chatzakou, K. Medijainen, A. Toomela, S. Nõmm, and M. Ruzhansky, "Lstm-cnn: An efficient diagnostic network for parkinson's disease utilizing dynamic handwriting analysis," *Computer Methods and Programs in Biomedicine*, vol. 247, p. 108066, 2024.

[209] Y. Xia, Z. Yao, Q. Ye, and N. Cheng, "A dual-modal attention-enhanced deep learning network for quantification of parkinson's disease characteristics," *IEEE Transactions on Neural Systems and Rehabilitation Engineering*, vol. 28, no. 1, pp. 42–51, 2019.

[210] S. Pragadeeswaran and S. Kannimuthu, "Cosine deep convolutional neural network for parkinson's disease detection and severity level classification using hand drawing spiral image in iot platform," *Biomedical Signal Processing and Control*, vol. 94, p. 106220, 2024.

[211] C. L. Chowdhary and R. Srivatsan, "Non-invasive detection of parkinson's disease using deep learning," 2022.

[212] S. M. Abdullah, T. Abbas, M. H. Bashir, I. A. Khaja, M. Ahmad, N. F. Soliman, and W. El-Shafai, "Deep transfer learning based parkinson's disease detection using optimized feature selection," *IEEE Access*, 2023.

[213] W. Zeng, F. Liu, Q. Wang, Y. Wang, L. Ma, and Y. Zhang, "Parkinson's disease classification using gait analysis via deterministic learning," *Neuroscience letters*, vol. 633, pp. 268–278, 2016.

[214] L. Aversano, M. L. Bernardi, M. Cimitile, and R. Pecori, "Early detection of parkinson disease using deep neural networks on gait dynamics," in *2020 International Joint Conference on Neural Networks (IJCNN)*, pp. 1–8, IEEE, 2020.

[215] S. A. A. Shah, L. Zhang, and A. Bais, "Dynamical system based compact deep hybrid network for classification of parkinson disease related eeg signals," *Neural Networks*, vol. 130, pp. 75–84, 2020.

[216] S. Xu, Z. Wang, J. Sun, Z. Zhang, Z. Wu, T. Yang, G. Xue, and C. Cheng, "Using a deep recurrent neural network with eeg signal to detect parkinson's disease," *Annals of translational medicine*, vol. 8, no. 14, 2020.

[217] Y. Chen, H. Wang, D. Zhang, L. Zhang, and L. Tao, "Multi-feature fusion learning for alzheimer's disease prediction using eeg signals in resting state," *Frontiers in Neuroscience*, vol. 17, p. 1272834, 2023.

[218] X. Huan, H. Zhou, B. Jung, and L. Ma, "Enhancing gait analysis for parkinson's disease detection and severity staging with a parallel conv1d-efficient transformer and bidirectional gru hybrid architecture," *IEEE Access*, 2025.

[219] S. Naimi, W. Bouachir, and G.-A. Bilodeau, "1d-convolutional transformer for parkinson disease diagnosis from gait," *Neural Computing and Applications*, vol. 36, no. 4, pp. 1947–1957, 2024.

[220] M. M. Afonso, D. R. Edla, and D. Ramesh, "Transformers-based deep learning for parkinson's disease detection using electroencephalography and stockwell transform," *Procedia Computer Science*, vol. 258, pp. 4094–4104, 2025.

[221] D. M. D. Nguyen, M. Miah, G.-A. Bilodeau, and W. Bouachir, "Transformers for 1d signals in parkinson's disease detection from gait," in *2022 26th Inter-*

national Conference on Pattern Recognition (ICPR), pp. 5089–5095, IEEE, 2022.

[222] U. Khatri and G.-R. Kwon, "Training vision transformer with gradient centralization optimizer for alzhemier's disease small dataset increase the diagnostic accuracy," *Age*, vol. 79, no. 6.13, pp. 77–30, 2024.

[223] D. kumar Ravikanti and S. Saravanan, "Eegalzheimer'snet: Development of transformer-based attention long short term memory network for detecting alzheimer disease using eeg signal," *Biomedical Signal Processing and Control*, vol. 86, p. 105318, 2023.

[224] L. Huang, X. Ye, M. Yang, L. Pan, and S. hua Zheng, "Mnc-net: Multi-task graph structure learning based on node clustering for early parkinson's disease diagnosis," *Computers in Biology and Medicine*, vol. 152, p. 106308, 2023.

[225] S. Wang, G. Wang, G. Pei, and T. Yan, "An eeg-based approach for parkinson's disease diagnosis using capsule network," in *2022 7th International Conference on Intelligent Computing and Signal Processing (ICSP)*, pp. 1641–1645, IEEE, 2022.

[226] M. Murugappan, W. Alshuaib, A. K. Bourisly, S. K. Khare, S. Sruthi, and V. Bajaj, "Tunable q wavelet transform based emotion classification in parkinson's disease using electroencephalography," *Plos one*, vol. 15, no. 11, p. e0242014, 2020.

[227] N. Kamalakannan, S. P. S. Balamurugan, and K. Shanmugam, "A novel approach for the early detection of parkinson's disease using eeg signal," *Technology (IJEET)*, vol. 12, no. 5, pp. 80–95, 2021.

[228] B. Hjorth, "Eeg analysis based on time domain properties," *Electroencephalography and clinical neurophysiology*, vol. 29, no. 3, pp. 306–310, 1970.

[229] K. Bhatt, N. Jayanthi, and M. Kumar, "Machine learning based optimal feature selection technique for early stage prediction of alzheimer's disease," in *2023*

Third International Conference on Secure Cyber Computing and Communication (ICSCCC), pp. 715–719, IEEE, 2023.

[230] C. O. Sakar and O. Kursun, "Telediagnosis of parkinson's disease using measurements of dysphonia," *Journal of medical systems*, vol. 34, pp. 591–599, 2010.

[231] M. Little, P. Mcsharry, S. Roberts, D. Costello, and I. Moroz, "Exploiting nonlinear recurrence and fractal scaling properties for voice disorder detection," *Nature Precedings*, pp. 1–1, 2007.

[232] H. Liu and L. Yu, "Toward integrating feature selection algorithms for classification and clustering," *IEEE Transactions on knowledge and data engineering*, vol. 17, no. 4, pp. 491–502, 2005.

[233] N. V. Chawla, K. W. Bowyer, L. O. Hall, and W. P. Kegelmeyer, "Smote: synthetic minority over-sampling technique," *Journal of artificial intelligence research*, vol. 16, pp. 321–357, 2002.

[234] Y. Liu, Y. Li, X. Tan, P. Wang, and Y. Zhang, "Local discriminant preservation projection embedded ensemble learning based dimensionality reduction of speech data of parkinson's disease," *Biomedical Signal Processing and Control*, vol. 63, p. 102165, 2021.

[235] Z. Xue, H. Lu, T. Zhang, J. Xu, and X. Guo, "A local dynamic feature selection fusion method for voice diagnosis of parkinson's disease," *Computer Speech & Language*, p. 101536, 2023.

[236] U. Saha, I. U. Ahamed, I. U. Ahamed, and A.-A. Hossain, "Graph convolutional network-based approach for parkinson's disease classification using euclidean distance graphs," in *2024 7th International Conference on Informatics and Computational Sciences (ICICoS)*, pp. 532–537, IEEE, 2024.

[237] A. S. L. O. Campanharo, F. M. Ramos, A. M. Pineda, and L. E. Betting, "Data from: Quantile graphs for eeg-based diagnosis of alzheimer's disease," Jan 2020.

[238] M. L. Vicchietti, F. M. Ramos, L. E. Betting, and A. S. L. O. Campanharo, "Data from: Computational methods of eeg signals analysis for alzheimer's disease classification," Feb 2023.

[239] P. Singh, S. D. Joshi, R. K. Patney, and K. Saha, "The fourier decomposition method for nonlinear and non-stationary time series analysis," *Proceedings of the Royal Society A: Mathematical, Physical and Engineering Sciences*, vol. 473, no. 2199, p. 20160871, 2017.

[240] G. Altan, Y. Kutlu, and N. Allahverdi, "A new approach to early diagnosis of congestive heart failure disease by using hilbert–huang transform," *Computer methods and programs in biomedicine*, vol. 137, pp. 23–34, 2016.

[241] S. Shukla, S. Mishra, and B. Singh, "Empirical-mode decomposition with hilbert transform for power-quality assessment," *IEEE transactions on power delivery*, vol. 24, no. 4, pp. 2159–2165, 2009.

[242] M. Imani, "Alzheimer's diseases diagnosis using fusion of high informative bilstm and cnn features of eeg signal," *Biomedical Signal Processing and Control*, vol. 86, p. 105298, 2023.

[243] H. Göker, "Detection of alzheimer's disease from electroencephalography (eeg) signals using multitaper and ensemble learning methods," *Uludağ Üniversitesi Mühendislik Fakültesi Dergisi*, vol. 28, no. 1, pp. 141–152, 2023.

[244] S. Jain and R. Srivastava, "Enhanced eeg-based alzheimer's disease detection using synchrosqueezing transform and deep transfer learning," *Neuroscience*, 2025.

[245] M. A. Maito, H. Santamaría-García, S. Moguilner, K. L. Possin, M. E. Godoy, J. A. Avila-Funes, M. I. Behrens, I. L. Brusco, M. A. Bruno, J. F. Cardona, *et al.*, "Classification of alzheimer's disease and frontotemporal dementia using routine clinical and cognitive measures across multicentric underrepresented samples: a cross sectional observational study," *The Lancet Regional Health–Americas*, vol. 17, 2023.

[246] S. Wu, P. Zhan, G. Wang, X. Yu, H. Liu, and W. Wang, “Changes of brain functional network in alzheimer’s disease and frontotemporal dementia: a graph-theoretic analysis,” *BMC neuroscience*, vol. 25, no. 1, p. 30, 2024.

[247] J. Bang, S. Spina, and B. L. Miller, “Frontotemporal dementia,” *The Lancet*, vol. 386, no. 10004, pp. 1672–1682, 2015.

[248] G. Musa, A. Slachevsky, C. Muñoz-Neira, C. Méndez-Orellana, R. Villagra, C. González-Billault, A. Ibáñez, M. Hornberger, and P. Lillo, “Alzheimer’s disease or behavioral variant frontotemporal dementia? review of key points toward an accurate clinical and neuropsychological diagnosis,” *Journal of Alzheimer’s Disease*, vol. 73, no. 3, pp. 833–848, 2020.

[249] A. Miltiadous, K. D. Tzimourta, T. Afrantou, P. Ioannidis, N. Grigoriadis, D. G. Tsalikakis, P. Angelidis, M. G. Tsipouras, E. Glavas, N. Giannakeas, and A. T. Tzallas, “"a dataset of eeg recordings from: Alzheimer’s disease, frontotemporal dementia and healthy subjects",” 2024.

[250] A. Miltiadous, K. D. Tzimourta, T. Afrantou, P. Ioannidis, N. Grigoriadis, D. G. Tsalikakis, P. Angelidis, M. G. Tsipouras, E. Glavas, N. Giannakeas, *et al.*, “A dataset of scalp eeg recordings of alzheimer’s disease, frontotemporal dementia and healthy subjects from routine eeg,” *Data*, vol. 8, no. 6, p. 95, 2023.

[251] J. Bruna and S. Mallat, “Invariant scattering convolution networks,” *IEEE transactions on pattern analysis and machine intelligence*, vol. 35, no. 8, pp. 1872–1886, 2013.

[252] Y. Si, R. He, L. Jiang, D. Yao, H. Zhang, P. Xu, X. Ma, L. Yu, and F. Li, “Differentiating between alzheimer’s disease and frontotemporal dementia based on the resting-state multilayer eeg network,” *IEEE Transactions on Neural Systems and Rehabilitation Engineering*, 2023.

[253] A. K. Ho, R. Iansek, C. Marigliani, J. L. Bradshaw, and S. Gates, “Speech impairment in a large sample of patients with parkinson’s disease,” *Behavioural neurology*, vol. 11, no. 3, pp. 131–137, 1998.

[254] R. L. Albin, A. B. Young, and J. B. Penney, "The functional anatomy of basal ganglia disorders," *Trends in neurosciences*, vol. 12, no. 10, pp. 366–375, 1989.

[255] G. Dimauro and F. Girardi, "Italian parkinson's voice and speech," 2019.

[256] V. V. Moca, H. Bârzan, A. Nagy-Dăbâcan, and R. C. Mureșan, "Time-frequency super-resolution with superlets," *Nature communications*, vol. 12, no. 1, pp. 1–18, 2021.

[257] A. Kumar, M. Kumar, R. Komaragiri, *et al.*, "Stsr: Spectro-temporal super-resolution analysis of a reference signal less photoplethysmogram for heart rate estimation during physical activity," *IEEE Transactions on Instrumentation and Measurement*, vol. 71, pp. 1–10, 2022.

[258] P. M. Tripathi, A. Kumar, M. Kumar, and R. Komaragiri, "Multilevel classification and detection of cardiac arrhythmias with high-resolution superlet transform and deep convolution neural network," *IEEE Transactions on Instrumentation and Measurement*, vol. 71, pp. 1–13, 2022.

[259] P. M. Tripathi, A. Kumar, M. Kumar, and R. S. Komaragiri, "Automatic seizure detection and classification using super-resolution superlet transform and deep neural network-a preprocessing-less method," *Computer Methods and Programs in Biomedicine*, p. 107680, 2023.

[260] A. Kumar, R. Komaragiri, M. Kumar, *et al.*, "A novel cs-net architecture based on the unification of cnn, svm and super-resolution spectrogram to monitor and classify blood pressure using photoplethysmography," *Computer Methods and Programs in Biomedicine*, vol. 240, p. 107716, 2023.

[261] P. Srikanth and C. Koley, "An intelligent algorithm for autorecognition of power system faults using superlets," *Sustainable Energy, Grids and Networks*, vol. 26, p. 100450, 2021.

[262] R. M. Cichy and D. Kaiser, "Deep neural networks as scientific models," *Trends in cognitive sciences*, vol. 23, no. 4, pp. 305–317, 2019.

[263] X. Wan, F. Ren, and D. Yong, "Using inception-resnet v2 for face-based age recognition in scenic spots," in *2019 IEEE 6th International Conference on Cloud Computing and Intelligence Systems (CCIS)*, pp. 159–163, IEEE, 2019.

[264] K. A. Tanjaya, M. F. Naufal, and H. Arwoko, "Pilates pose classification using mediapipe and convolutional neural networks with transfer learning," *Jurnal Ilmiah Teknik Elektro Komputer dan Informatika (JITEKI)*, vol. 9, no. 2, pp. 212–222, 2023.

[265] K. Simonyan and A. Zisserman, "Very deep convolutional networks for large-scale image recognition," *arXiv preprint arXiv:1409.1556*, 2014.

[266] Y. Guo, J. Yang, Y. Liu, X. Chen, and G.-Z. Yang, "Detection and assessment of parkinson's disease based on gait analysis: A survey," *Frontiers in Aging Neuroscience*, vol. 14, p. 916971, 2022.

[267] Y. Guo, L. Wang, Y. Li, L. Guo, and F. Meng, "The detection of freezing of gait in parkinson's disease using asymmetric basis function tv-arma time–frequency spectral estimation method," *IEEE Transactions on Neural Systems and Rehabilitation Engineering*, vol. 27, no. 10, pp. 2077–2086, 2019.

[268] M. Delrobaei, N. Baktash, G. Gilmore, K. McIsaac, and M. Jog, "Using wearable technology to generate objective parkinson's disease dyskinesia severity score: Possibilities for home monitoring," *IEEE Transactions on Neural Systems and Rehabilitation Engineering*, vol. 25, no. 10, pp. 1853–1863, 2017.

[269] G. Yogev, N. Giladi, C. Peretz, S. Springer, E. S. Simon, and J. M. Hausdorff, "Dual tasking, gait rhythmicity, and parkinson's disease: which aspects of gait are attention demanding?," *European journal of neuroscience*, vol. 22, no. 5, pp. 1248–1256, 2005.

[270] J. M. Hausdorff, J. Lowenthal, T. Herman, L. Gruendlinger, C. Peretz, and N. Giladi, "Rhythmic auditory stimulation modulates gait variability in parkinson's disease," *European Journal of Neuroscience*, vol. 26, no. 8, pp. 2369–2375, 2007.

[271] S. Frenkel-Toledo, N. Giladi, C. Peretz, T. Herman, L. Gruendlinger, and J. M. Hausdorff, "Treadmill walking as an external pacemaker to improve gait rhythm and stability in parkinson's disease," *Movement disorders: official journal of the Movement Disorder Society*, vol. 20, no. 9, pp. 1109–1114, 2005.

[272] S. V. Perumal and R. Sankar, "Gait and tremor assessment for patients with parkinson's disease using wearable sensors," *Ict Express*, vol. 2, no. 4, pp. 168–174, 2016.

[273] C. Zhong and W. W. Ng, "A robust frequency-domain-based graph adaptive network for parkinson's disease detection from gait data," *IEEE Transactions on Multimedia*, 2022.

[274] C. Dong, Y. Chen, Z. Huan, Z. Li, G. Gao, and B. Zhou, "An "optical flow" method based on pressure sensors data for quantification of parkinson's disease characteristics," *Biomedical Signal Processing and Control*, vol. 81, p. 104377, 2023.

[275] J. S. Perlmutter, "Assessment of parkinson disease manifestations," *Current protocols in neuroscience*, vol. 49, no. 1, pp. 10–1, 2009.

[276] S. Veeraragavan, A. A. Gopalai, D. Gouwanda, and S. A. Ahmad, "Parkinson's disease diagnosis and severity assessment using ground reaction forces and neural networks," *Frontiers in physiology*, vol. 11, p. 587057, 2020.